

## JRC TECHNICAL REPORT

# Integrating dispersion modelling and experimental approach to optimize indoor/outdoor detection of airborne agents

## Mimicking the exposure of an infrastructure

*ERNCIP Detection of Indoor Airborne Chemical and Biological Agents Thematic Group*

Karakitsios, S.  
Maggos, T.  
Busker, R.  
Armand, P.  
Bartzis, J.G.

Cardarilli, M. (Ed.)

2022



The research leading to these results has received funding from the European Union as part of the European Reference Network for Critical Infrastructure Protection (ERNCIP) project

This publication is a technical report by the Joint Research Centre (JRC), the European Commission's science and knowledge service. It aims to provide evidence-based scientific support to the European policymaking process. The scientific output expressed does not imply a policy position of the European Commission. Neither the European Commission nor any person acting on behalf of the Commission is responsible for the use that might be made of this publication. For information on the methodology and quality underlying the data used in this publication for which the source is neither Eurostat nor other Commission services, users should contact the referenced source. The designations employed and the presentation of material on the maps do not imply the expression of any opinion whatsoever on the part of the European Union concerning the legal status of any country, territory, city or area or of its authorities, or concerning the delimitation of its frontiers or boundaries.

#### Contact information

Name: Rainer JUNGWIRTH  
Address: Via E. Fermi 2749, 21027, Ispra (VA), Italy  
Email: [rainer.jungwirth@ec.europa.eu](mailto:rainer.jungwirth@ec.europa.eu)  
Tel.: +39 0332785648

EU Science Hub  
<https://ec.europa.eu/jrc>

JRC129051

EUR 31172 EN

PDF

ISBN 978-92-76-55599-5

ISSN 1831-9424

doi:10.2760/48622

Luxembourg: Publications Office of the European Union, 2022

© European Union, 2022



The reuse policy of the European Commission is implemented by the Commission Decision 2011/833/EU of 12 December 2011 on the reuse of Commission documents (OJ L 330, 14.12.2011, p. 39). Except otherwise noted, the reuse of this document is authorised under the Creative Commons Attribution 4.0 International (CC BY 4.0) licence (<https://creativecommons.org/licenses/by/4.0/>). This means that reuse is allowed provided appropriate credit is given and any changes are indicated. For any use or reproduction of photos or other material that is not owned by the EU, permission must be sought directly from the copyright holders.

All content © European Union, 2022

How to cite this report: Karakitsios, S., Maggos, T., Busker, R., Armand, P. and Bartzis, J.G., Integrating dispersion modelling and experimental approach to optimize indoor/outdoor detection of airborne agents, Cardarilli, M., ed., EUR 31172 EN, Publications Office of the European Union, Luxembourg, 2022, ISBN 978-92-76-55599-5, doi:10.2760/48622, JRC129051.

# Contents

<b>Acknowledgements .....</b>	<b>1</b>
<b>Abstract .....</b>	<b>2</b>
<b>1. Introduction.....</b>	<b>3</b>
1.1. Context.....	3
1.2. Purpose of the Piloting Activity.....	4
1.3. Content and structure of this document .....	4
<b>2. Experimental Activity.....</b>	<b>5</b>
2.1. The Building Mock-Up .....	5
2.1.1 Layout Design .....	5
2.1.2 Construction.....	5
2.1.3 Shipping .....	6
2.2. Detection Experiments.....	7
2.2.1 Experimental set-up .....	8
2.2.2 Scenario Design.....	12
2.2.3 Analysis of results.....	18
2.3. Results of Detection Experiments .....	32
2.3.1 Conclusions of experimental trials .....	33
<b>3. Modelling Activity .....</b>	<b>34</b>
3.1. Computation Approach (Code_Saturne) .....	34
3.1.1 The Pre-Experimental Phase.....	34
3.1.1.1 Implementation of the aeraulic simulations .....	36
3.1.1.2 Dispersion simulation of chemical releases.....	43
3.1.2 The Post-Experimental Phase .....	51
3.1.2.1 Implementation of aeraulic simulations .....	52
3.1.2.2 Simulation of the experimental releases .....	61
3.1.3 Conclusions of Code_Saturne simulations.....	77
3.2. Computation Approach (ADREA-HF) .....	79
3.2.1 The Pre-Experimental Phase.....	81
3.2.1.1 The external source .....	81
3.2.1.2 The internal source .....	85
3.2.2 The Post-Experimental Phase .....	87
3.2.2.1 The external source .....	88
3.2.2.2 The internal source .....	91
3.2.3 Conclusions of ADREA-HF simulations.....	93
3.2.4 Conclusions of CFD simulations.....	94
<b>4. Conclusions.....</b>	<b>98</b>
<b>References .....</b>	<b>100</b>
<b>List of abbreviations.....</b>	<b>101</b>
<b>List of figures .....</b>	<b>102</b>
<b>List of tables.....</b>	<b>105</b>

## **Acknowledgements**

This work has received funding from the European Union's Horizon 2020 research and innovation programme under grant agreement No 775989, as part of the European Reference Network for Critical Infrastructure Protection project.

## **Authorship credit**

*T. MAGGOS - Experimental activity, The building mock-up; general review;*

*R. BUSKER, J. VAN DER MEER, A. VAN WUIJCKHUIJSE - Experimental Activity, Detection experiments;*

*P. ARMAND - Modelling activity, Computational approach with Code\_Saturne;*

*J. BARTZIS - Modelling activity, Computational approach with ADREA-HF;*

*T. TJÄRNHAGE - Experimental Activity, Detection experiments (provision of Photo Ionization Detector);*

*S. KARAKITSIOS – Group coordination, integration of chapters, contribution to drafting, general review.*

## **Authors**

*Spyros KARAKITSIOS, Aristotle University of Thessaloniki, Greece*

*Thomas MAGGOS, National Center for Scientific Research Demokritos (NCSR), Greece*

*Ruud BUSKER, Netherlands Organisation for Applied Scientific Research (TNO), The Netherlands*

*Patrick ARMAND, Atomic and alternative Energies Commission (CEA), France*

*John BARTZIS, University of Western Macedonia, Greece*

## **Contributors**

*Jeroen VAN DER MEER, Netherlands Organisation for Applied Scientific Research (TNO), The Netherlands*

*Arjan VAN WUIJCKHUIJSE, Netherlands Organisation for Applied Scientific Research (TNO), The Netherlands*

*Tjorbörn TJÄRNHAGE, Swedish Defence Research Agency (FOI), Sweden*

## **Editor**

*Monica CARDARILLI, European Commission, Joint Research Centre, Italy*

## Abstract

The overarching objective of the ERNCIP "Detection of Indoor Airborne Chemical & Biological Agents" Thematic Group (TG) is to strengthen resilience of critical infrastructure against airborne CB threats by improvement of detection capabilities. The subsidiary aim of the research described in this technical report is to develop knowledge on the behaviour of chemical releases, given some likely attack scenarios, and to propose ways to optimally detect those inside buildings. Making use of a combined approach consisting of experiments and dispersion modelling is considered a strong endeavour towards this aim.

To provide input for dispersion model development a series of medium-scale experiments with representative simulant chemical has been designed. The study made use of controlled release of simulant chemicals in an ambient breeze tunnel (AMB). In the AMB a mock-up of a simple building was installed (scale 1:5). The experiments involved three mimicked attack scenarios: i) focal release from within the mimicked building and external release of agent approaching the mock-up from the outside from a ii) short and iii) a larger distance. Tri-ethylphosphate (TEP) was selected as simulant (for nerve gases). The detector used was an ion mobility spectrometry (IMS) instrument.

Release of TEP was successful in all three exposure scenarios, it resulted in reproducible detection signals from 6 IMS instrument placed in 6 rooms of the building mock-up. The speed and magnitude in which TEP levels were recorded in the respective rooms showed a clear and reproducible picture in the sense that some of the rooms appeared to be better reachable for the externally released TEP than others. Subsequent 2 different dispersion modelling approaches were undertaken to understand and describe those differences:

- I. the Code\_Saturne<sup>1</sup> has been used to perform the simulations both before and after the experiments. Pre-trials computations illustrate the differences in the dispersion pattern when an internal versus an external released is considered. Post-trials computations are fully consistent with the pre-trials computations and the physical phenomena enlightened in the different trials;
- II. The ADREA-HF code<sup>2</sup> has been used to perform the simulations utilizing the CFD RANS approximation and the standard  $k-\epsilon$  turbulence model. The results show that rooms concentrations time profiles can be quite different. The room specific location with respect to the source and the associated ambient air pattern plays an important role to this differentiation. The poorly ventilated rooms are associated with relatively long residence and arrival times. The poorly ventilated rooms tend to lower the peak concentrations.

---

<sup>1</sup> <https://www.code-saturne.org/cms/web/>

<sup>2</sup> <http://www2.ipta.demokritos.gr/pages/ADREA-HF.html>

# 1. Introduction

## 1.1. Context

In case critical infrastructure is subject to a deliberate release of toxic chemical agents, it is of utmost importance to be able to provide early warning messages signalling presence of hazardous chemicals serving as triggers to activate protective countermeasures (Karakitsios S., 2016). In reverse, in case of a hoax attack, it is needed to be able to disprove suspected danger as soon and as firm as possible. In both cases, to generate corresponding early warning signals, detection systems should be in place. These must respond fast enough to allow life-saving protective measures such as evacuation, seeking shelter and applying personal protective equipment.

Moreover, these detection systems should also be highly reliable, meaning having low false alarm rates. More specifically this means having a low false negative alarm rate in order to avoid missing actual attacks as well as having a low false positive alarm rate to classify an event as a hoax and then to avoid unnecessary discontinuation of the critical infrastructure functionality. The forthcoming sensor requirements thus need to include high response rates, high sensitivity and coverage of a broad spectrum of chemical agents (Busker R., 2016).

Selecting adequate detection system is challenging. First of all, responsible authorities need to have insight into the threat the critical infrastructure may be subject to. Next, is needed to know which sensor(s) respond to the critical chemicals. In addition, one must be able to place sensors throughout the critical infrastructure in an effective and affordable manner. This requires the ability to identify those spots in critical infrastructures that are best equipped to deploy sensors at. These must be the locations that, depending on the way an agent is released, are most likely to become hot-spots in the sense of agent concentration. This now, obviously, requires insight into agent distribution. This in turn is highly dependent on the way hazardous chemicals have been / might be released, on the physical properties of the agents, on the functionality of the critical infrastructure and the geometry and air circulation of the building itself.

On top of this complexity, the challenge is that little is known about indoor behaviour of a released toxic agent, let alone how to optimally detect it. In complex buildings, such as transportation hubs, concentration levels of released chemical vary dramatically depending on the agent properties, on local ventilation, on design of the building and so on. Therefore, there is an urgent need to gain more insight into behaviour of dispersed chemical inside buildings and into the interaction of detection equipment (Karakitsios S. et al., 2020). Such insight would be used to develop optimal detection deployment strategies.

Ultimately there is a need for advanced modelling and simulation tools that are able to predict chemical agent distribution throughout a typical building, thereby providing guidance to sensor deployment and detailed placement. This requires knowledge of agent characteristics, of agent distribution mechanisms, of response properties of qualifying sensors, of feasible attack scenarios, of building geometry and of the resulting likelihood that early warning signals are timely and justly generated. Although a substantial amount of knowledge of the distinct elements of this complex challenge is available, integration of these elements into applicable insight is lacking (Karakitsios S., 2019). The European Commission therefore launched a combined piloting experimental and computational study, as part of the European Reference Network for Critical Infrastructure Protection program (ERNICIP - more particularly the Detection of Indoor Airborne Chemical and Biological Agents Thematic Group) to address mentioned shortcomings.

## **1.2. Purpose of the Piloting Activity**

The piloting research activity aimed to apply knowledge on chemical releases and to implement ways to detect contaminant dispersions inside buildings, including the interaction of indoor/outdoor environments through an agent-based dispersion analysis. This activity included mid-scale experiments with controlled release of simulant chemicals to analyse the impact on critical infrastructure as well as secondary effects to surrounding open areas due to the release of the chemical agent.

In particular, the purpose of the piloting activity was to develop knowledge on the behaviour of chemical releases, given some likely attack scenarios, and to propose ways to optimally detect those inside buildings. Making use of a combined approach consisting of experiments and dispersion modelling is considered a strong endeavour towards this aim. In that respect, this study was set up to let the modelling support the experimental design and subsequently have the experimental data feed into the dispersion models to validate and refine those.

The pilot activity was run from February to July 2021 under pandemic restrictions and mobility limitations. All organizational issues and technical details were planned, coordinated and managed among the TG members via remote meetings only. This study is the result of an outstanding effort, unique and continuous support given by the TG members committed to it.

The combined and scaled approach is considered to be a good compromise between feasibility and realism which requires mimicking a building through a mock-up (Karakitsios S. et al. (2020); Karakitsios, S. e. (2016); COST Action ES1006 (2012)).

## **1.3. Content and structure of this document**

This document describes the experimental and modelling activity carried out by the TG during the pilot activity. In particular, it is structured according to the various steps carried out, from mock-up design to comparison of modelling studies with experimental results, which in turn correspond to the timeline of the piloting activity.

**Chapter 2** — Experimental activity

**Chapter 3** — Modelling activity

**Chapter 4** — Conclusions

Each chapter can be considered complementary in the fields of application and for scenario release conditions. Chapters narrative has a modular structure which can adapt to different operational and technical needs as well as task objectives.

This document moves the TG work towards a broader investigation on how the knowledge gained during the previous years can be applied in practice. It also contributes to strengthening the resilience of critical infrastructures against airborne threats by improving detection capabilities of chemical-biological release, feeding into recommendations for sensors placement and policy-making.

## 2. Experimental Activity

### 2.1. The Building Mock-Up

To enable experiments that provide input for dispersion model development, within constraints of time, budget and experimental safety, it was proposed to perform mid-scale experiments with representative simulant chemicals. The proposed approach was making use of controlled release of simulant chemicals in a mid-sized facility such as an ambient breeze tunnel (AMB). Within the project constraints this was considered the optimal compromise between feasibility and realism. Release of smartly selected chemicals in the ABM is feasible and permitted. This approach allows, for example, experimental variations: choice of agents, controlled wind speed and direction, distance and angle of agent release, choice and tuning of detectors and design of the target. Estimated environmental damage and experimental risks are minimal and known in advance. Obviously, this approach requires mimicking a building. For that purpose, a scaled (1:5) mock-up of a simple building was delivered in this project and the design and construction phase are described in the following paragraphs.

#### 2.1.1 Layout Design

A detailed design of a simple building at 1:5 scale making an approximate volume of 7 m<sup>3</sup> and a total surface of 36 m<sup>2</sup> was delivered. The building has two levels each divided in two connected rooms with stairs in between. The building has inlet and outlet openings and it is designed to enable installing sensors inside the rooms. The design is such that the physical presence of the sensors including accessory cables and tubing has not influence on the dispersion behaviour of vaporous agent as the sensors are located in a 'closed room'. All rooms are accessible from the outside of the building to facilitate the installation of sensor tubing etc. Also, all joints are sealed to prevent leakage to other rooms. To minimize interaction of chemical agent with the mock-up material, 6 mm Plexiglas® was used for the construction.

#### 2.1.2 Construction

The mock-up is constructed from 6 mm Plexiglas®. It consists of 13 rooms which are connected through internal openings (doors, corridors, staircases). Only room 7 is isolated from the rest as it is dedicated for sensors installation. All rooms are accessible from the outside of the building through windows which are closed tightly during the experiments. Pictures from the construction phase of the mock-up are shown below (Figures 1-3).

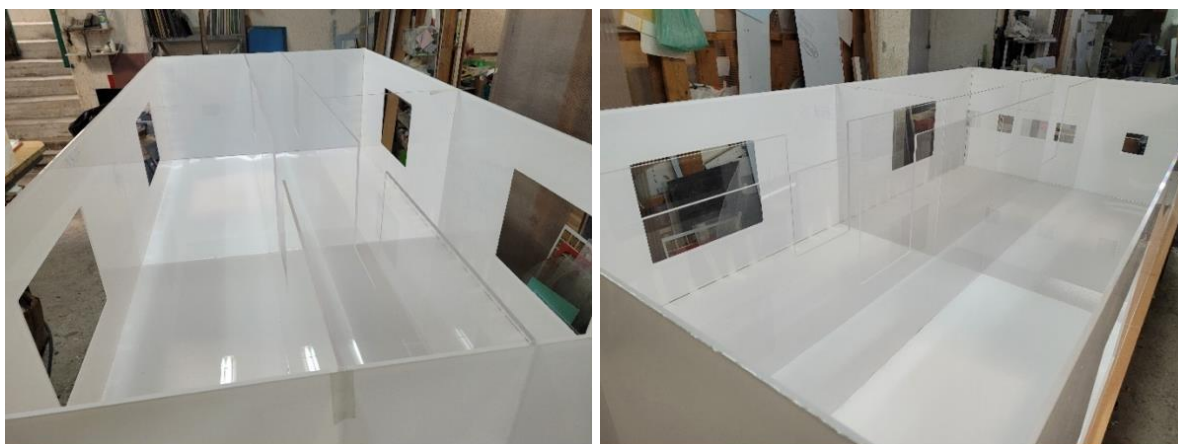


**Figure 1.** Internal details and subdivision of the mock-up



**Figure 2.** External details and openings of the mock-up



**Figure 3.** External view and levels of the mock-up

### 2.1.3 Shipping

The entire mock-up was constructed in Athens (Greece) and subsequently shipped to the experimental site (TNO, The Netherlands). The mock-up was sent on the 2<sup>nd</sup> of April 2021 (Figures 4) and arrived at TNO premises, in The Netherlands, on the 8<sup>th</sup> of April 2021 (Figure 5).



**Figure 4.** Details of the mock-up shipment in NCSR Demokritos, Greece



**Figure 5.** The mock-up at TNO, The Netherlands

## 2.2. Detection Experiments

Several options can be considered to design experiments that provide insight into indoor chemical agent behaviour and detection of agents. Large scale real-building experiments obviously most closely mimic realistic scenarios, but take a very long time to prepare, they are costly and require a suitable building in which chemicals can be released without repercussions. Furthermore, experiments using real toxic agents may have advantages from the perspective of sensor response prediction. In addition, it would in practice mean that experiments can only be done at small (laboratory fume-hood) scale.

All considered, to enable experiments that provide input for dispersion model development, within constraints of time, budget and experimental safety, it was decided

to perform mid-scale experiments with representative simulant chemicals. This approach makes use of controlled release of simulant chemicals in a mid-sized facility, more particularly an ambient breeze tunnel (AMB). To mimic a critical infrastructure building a scaled (roughly 1:5) mock-up of a simple building has been designed and delivered as described in the previous paragraphs.

The experimental design involves three simulated attack scenarios:

1. Focal release from within the target critical infrastructure building (simulated as point release from within the building mock-up);
2. External release of agent approaching the target building from the outside from a 'short distance' (simulated as a point release of agent from distance of 3 m from mock-up);
3. External release from 'far way' as a semi-largescale attack (simulated by a release throughout the AMB).

The measurements include recording sensor responses to agents released according to the three scenarios. Sensors have been in several chambers of the mock-up to monitor agent concentration as well as sensor response to thereupon. They also include ground truth concentration level measurements by analytical chemical methods. Wind flows were measured at several locations within the AMB. All results were subsequently used as input parameters to modelling efforts.

### **2.2.1 Experimental set-up**

The experimental set-up obviously is, highly simplified, downscaled, restricted by safety-considerations and in some aspects inevitably artificial. The need to install chemical and physical sensors and forthcoming tubing and cabling to enable measurements definitely disturbs agent distribution to some extent. Several precautions have been taken to minimize the influence of the experimental necessities on the level of realism of the experiments.

Essentially the experimental set-up involved the following step-wise approach:

- Endorsing the most relevant and experimentally achievable exposure scenarios;
- Installing the building mock-up built;
- Establishing a facility in which the experiments can be performed in an almost realistic and controlled manner;
- Selecting relevant simulant agents that have physical chemical properties resembling real agents;
- Selecting commercially available sensors that reasons to the agents of choice;
- Providing a detailed description of the facility's geometry and the position of the building mock-up therein;
- Generating volatile chemicals according to the three attack scenarios thereby exposing the building mock-up;
- Describing and measuring the parameters that influence agent distribution such as wind speed, ambient temperature, ground truth level of chemical agent, agent generation rate;
- Recording of sensor response to agent release inside the mock-up.

The following sections describe the subsequent experimental details.

#### **Ambient Breeze Tunnel**

The TNO Ambient Breeze Tunnel is a rectangular building which measures 6 meters wide, 6 meters high and 20 meters long (Figures 6-7). The back side is open, allowing vapor to freely flow out. The front side is equipped with a series of 25 (distributed as 5x5) 1 m diameter ventilators to generate the required wind speed.



**Figure 6.** AMB front side view



**Figure 7.** AMB back side view

Immediately in front of the ventilators on the AMB inside a system of 6 horizontal aluminium tubes is mounted to enable uniform vapor distribution (Figure 8). Each of those tubes has many perforations through which vapor is released. The facility enables to generate chemical clouds in a range of 0.01-10 mg/m<sup>3</sup> in windspeeds of 0-5 m/s.



**Figure 8.** View from inside the ABM showing the 6 tubes that distribute vapor

### Sensors and chemicals

Commercially available and actually in-service chemical sensors have been selected to ensure a desired level of realism.

The first detector used was the LCD 3.3 of Smiths Detection Company, UK (Figure 9); this is based on ion mobility spectroscopy. The LCD 3.3 is able to detect relevant agents in the concentration range of 10 µg/m<sup>3</sup> Ion Mobility Spectrometry (IMS). Data collection rate 1 Hz. The sensor has a sample flow of 100 mL/min. The other a Photo Ionization Detector (PID) designed and supplied by FOI<sup>3</sup> (Sweden).



**Figure 9.** LCD 3.3 detector (left) and Young Anemometer (right)

<sup>3</sup> <https://www.foi.se/en/foi.html>

Sensors have been placed such that they sample from spots inside the mock-up (one sensor in a room) while influencing the air flows and thus the agent dispersion inside the mock-up as little as possible. This holds for the physical presence of sensors, cables and tubing as well as for the sampling flow of the sensors. It should however be realized that a certain minimal sampling flow is needed for the sensors (0.1-1 L/min for a typical detector) to sample levels of agents exceeding the limit of detection. To prevent active pumping of air through the mock-up the detectors were installed in the rooms.

Before, during and shortly after each release of agent the mounted sensors have been read-out and recorded. For ground truth agent level measurements, the widely used Tenax sampling with subsequent chemical analysis has been applied.

Wind speed inside the AMB as well as inside (selected spots of) the mock-up has been monitored using anemometers. Two different brands have been applied. The first sensor was a Young anemometer (see Figure 9). This sensor has an acquisition rate of 30 Hz. The second sensor was a Gill anemometer and has an acquisition rate of 1 Hz. The datafiles have been converted into files (.txt), containing three columns. Those columns describe respectively the windspeed in xyz-directions in m/s. Ambient temperature and humidity were recorded.

### Characteristics of chemicals

The chemicals (simulants for toxic threat agents) selected for use in the experiments were:

- Tri-ethylphosphate (TEP); simulant for nerve agents (Figure 10):
  - boiling point: 215 °C;
  - density: 1,07 g/cm<sup>3</sup>.
- Toluene simulant for a volatile TIC:
  - boiling point: 111 °C;
  - density: 0,867 g/cm<sup>3</sup>.

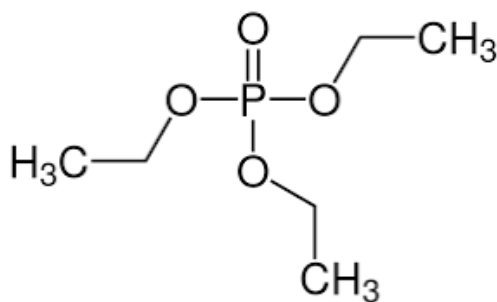


**Figure 10.** Tri-ethylphosphate (TEP)

To make the experiments as realistic as possible, a number of related parameters were taken into consideration. First of all, the amount of toxic agent - a perpetrator is likely to be able to apply - was taken into consideration. This obviously depends on many factors, such as availability of toxic agent in a relevant amount, the aggregation form (in scope of the project: limited to more or less volatile liquids only), the inherent toxicity, the agent dispersion, the size, geometry and function of the target building, the attackers' intentions etc.

In short: to achieve an 'effective' dosage, the agent needs to be delivered at the target location at least at a concentration (C) for a given duration of time (t) such that their product. The exposure dosage (concentration x time) and the inherent toxicity are the dominant factors determining whether or not a realistic attack is at stake. When the 'desired' concentration for a given time has been established, the agent release rate at

the source is then automatically determined. The experimental phase has been performed at the TNO premises. The following (combinations of) parameters have been varied:

- Release type Scenario 1, 2 or 3;
- Exposure dosage.

### **2.2.2 Scenario Design**

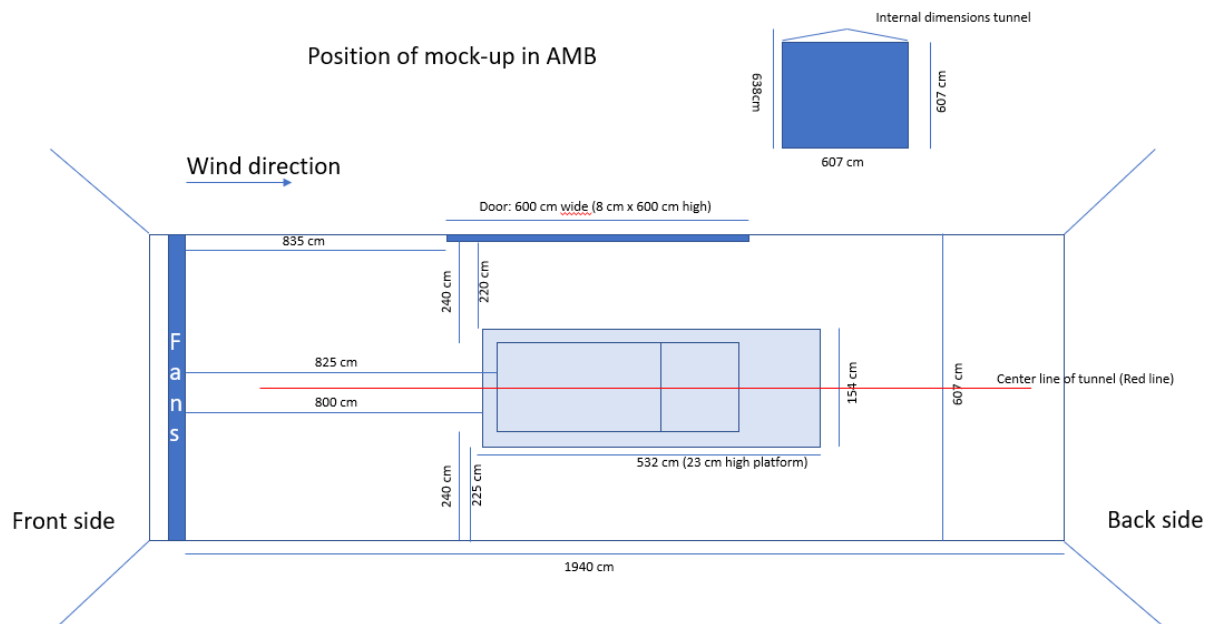
The mock-up was assembled and installed in the Breeze Tunnel facility at TNO, in the Netherlands. The exact location of the mock-up is schematically displayed in Figure 11. Prior to assembly some transport damage had to be repaired in order to enable installation. The mock-up was installed in the Breeze tunnel on its own transport platform (Figure 12).

All LCD 3.3 detectors were placed inside the mock-up on the bottom with its inlet head in the middle of the room (Figures 13-14).

All cables were taped into the corners of the rooms as much as possible. Some openings had to be drilled in order to feed cables through walls. the aim was always to use the least intrusive route towards the 'sensor' room where the laptop for data acquisition was placed. Only a single UTP and laptop power cable were exiting through the bottom of this room to enable charging of the laptop and viewing of the live signals on an external screen positioned in the control room. The location of the wind speed sensors is described for the individual experimental configurations.

All 25 wind fans were frequency-controlled during all experiments and kept at 28Hz (resulting in a wind-speed of approximately 3 m/s). The tunnel was emptied to such level that only the most essential parts of the test facility were present to avoid unwanted disturbance of the air stream.

For sampling a series of 4 sampling lines (tubes) were positioned in front of the mock-up for reference of the source concentration and inside the mock-up for quantifying TEP concentration in the mock-up. A sampling point was positioned between rooms 11 and 13 as a reference for the incoming vapor, in room 1 as reference for the exiting vapor and room 8 as reference for the lowest concentration in the 'building'. All sampling points were positioned next to the detector sampling head in the middle of the room. Sampling was performed using a vacuum pump from outside the Breeze Tunnel preventing the need to enter the facility during an experiment. The whole setup was controlled from a control room enabling remote control of wind speed and source conditions.



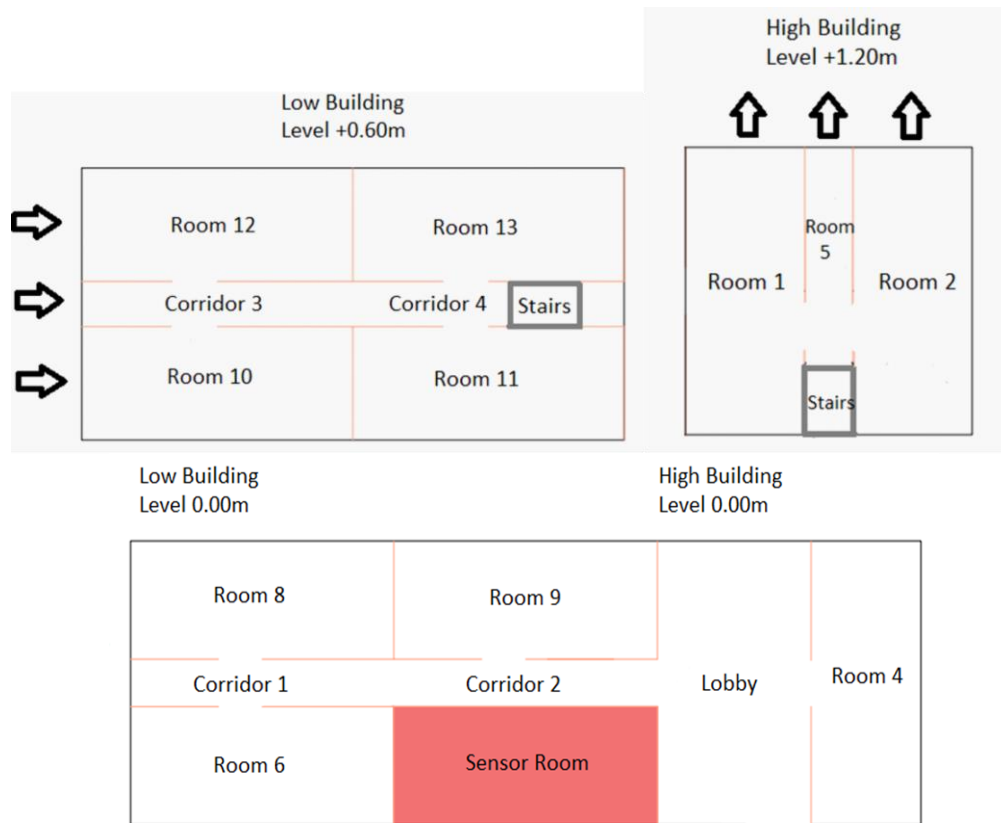


**Figure 13.** Arrangement of the rooms in the mock-up

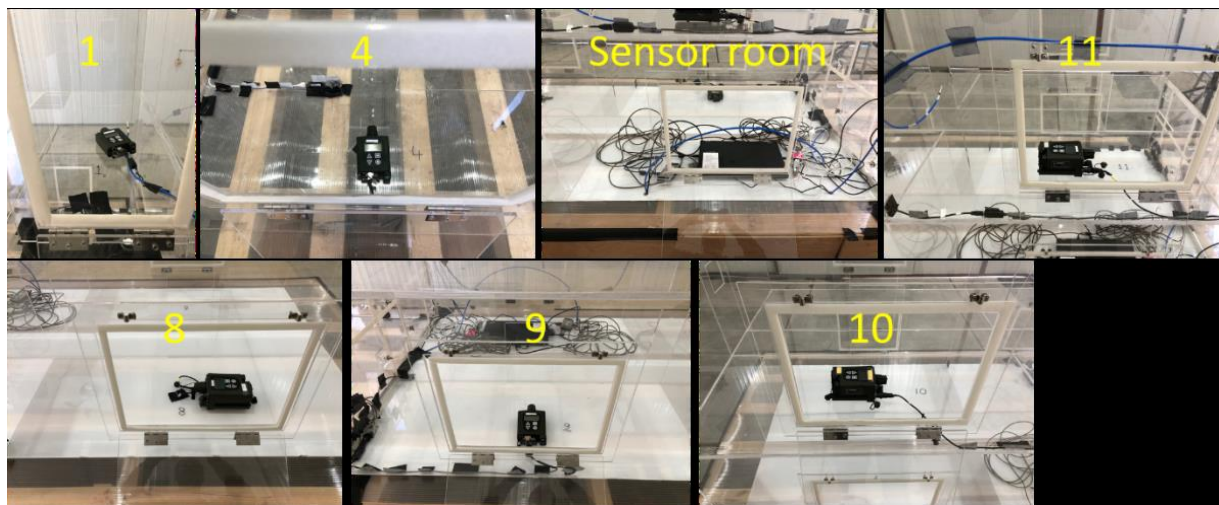


**Figure 14.** Six LCD 3.3 detectors installed in the mock-up rooms indicated with numbers

In total **three release scenarios** have been used for the experiments. In particular:

- The first scenario executed (**Scenario 3**) was a series of three experiments used to simulate a distant cloud ("**low cloud**") passing the building. These experiments were mainly used to determine the release amounts needed for the upcoming scenarios and as a means of testing the complete setup with all equipment installed. A series of low hanging clouds were created across the whole width of the tunnel where the maximum height of the cloud was approximately 2 meters.
- The second scenario (**Scenario 2**) was an **external release** at short distance.

The aim was to create a point source cloud that would pass the inlets of the building. The release location was tested prior to the actual experiments with a smoke generator. It was clear that smoke entered the mock-up and passed through rooms. The release location was then fitted with a long piece of tubing leading to the vapor generator setup placed at remote location to not disturb the air flow towards the mock-up. The long tubing proved to promote condensation during the first experiments which resulted in trying another approach. It was decided to place the vapor source inside the tunnel despite the influence on the air flow towards the mock-up. With this setup a total of 4 experiments were performed.

- The last scenario (**Scenario 1**) was the simulation of an **internal release** in room '8'. This room was chosen because it was the most 'remote' room in the building that had very little air circulation. In room 8 a release point was positioned by fitting a piece of tubing in the middle of the room close to floor level. Also, a series of PID sensors were placed in a number of rooms to measure Toluene distribution. Testing with Toluene resulted in the conclusion that the PID sensors did not function as expected. Contact with the supplier did not result in a quick fix. Therefore, it was decided to switch to TEP that could be measured with the already installed LCD 3.3 detectors. Using an external evaporator TEP was evaporated and fed into room 8 via the tubing. In total three experiments were performed in this configuration varying both source strength and duration of release.

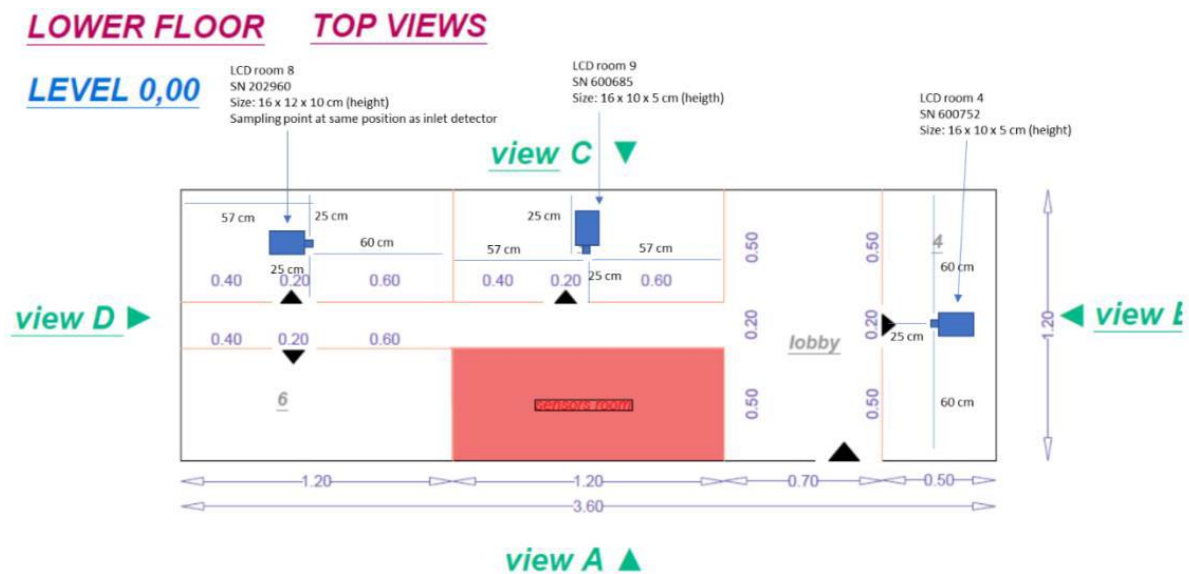


**Figure 15.** Ground Floor level detector/sampling positions



			concentration release
1	10	Internal point release	
	11		
	12		TEP in room 8
	13		TEP in room 8, replicate with preconditioning of syringe

Experiments 4,5, and 10 were try-outs that did not result in follow-up therefore no results have been reported.

**Table 2.** Detailed overview of experiments performed (agents and releases)

Experiment number	Agent	Scenario; Rationale	Remark	Release rate (gram / hour)	Release duration (min)
1	TEP neat	Scenario 3; Low cloud from distance		70	10
2	TEP neat	Scenario 3; Low cloud from distance		35	10
3	TEP neat	Scenario 3; Low cloud from distance		35	10
4	TEP 4% in H2O	Scenario 2; External release at short distance (3 m)	Try-out failed due to condensation in tubing; results not presented		
5	TEP 4% in H2O	Scenario 2; External release at short distance (3 m)	Try-out failed due to condensation in tubing; results not presented		
6	TEP 4% in H2O	Scenario 2; External release at short distance (3 m)		140	10
7	TEP 4% in H2O	Scenario 2; External release at short distance (3 m)		140	10
8	TEP 4% in H2O	Scenario 2; External release at short distance (3 m)		420	210
9	TEP 4% in H2O	Scenario 2; External release at short distance (3 m)		47	30
10	Toluene	Scenario 1; Release from within (room 8)	Try-out failed due to lacking PID response; no further attempts; results not presented		
11	TEP neat	Scenario 1; Release from within (room 8)			2
12	TEP neat	Scenario 1; Release from within (room 8)			2
13	TEP neat	Scenario 1; Release from within (room 8)			4

## 2.2.3 Analysis of results

### Scenario 3

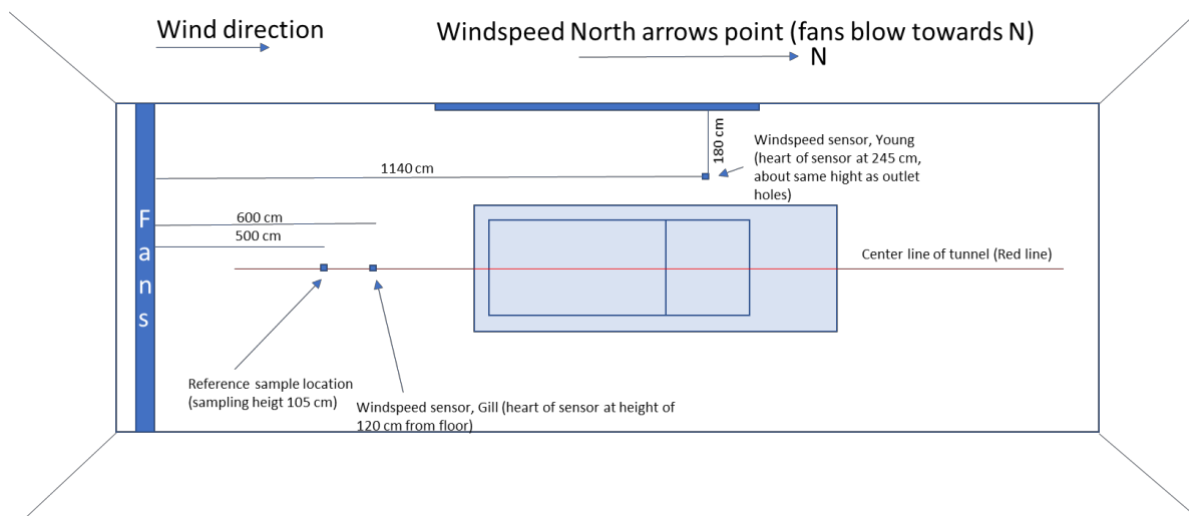


**Figure 18.** Scenario 3 - schematic overview of position of windspeed sensors and reference sample location around mock-up

### **Experiment #1: Confidence test with cloud over full width of the tunnel (distant release)**

Experiment Time:

- Date: 19-04-2021
- Source start: 14:23:00
- Sampling start: 14:28:00
- Source Stop: 14:33:00

Experimental parameters:

- **Chemical released:** TEP (neat).
- **Dimensions cloud:** approximately 2-meter-high, 6-meter-wide (only bottom two release tubes of tunnel are used). These are not exact dimensions since the vapor is released from two horizontal tubes in front of the wind fans in a turbulent air stream.
- **Windspeed:** 28 Hz resulting in  $\pm 3$  m/s (measured with anemometers in tunnel).
- **Target concentration in cloud:**  $0.5 \text{ mg/m}^3$  (calculated by a cloud front ( $\sim 2$  m high,  $\sim 6$  meterwide)  $12 \text{ m}^2 \times 3 \text{ m/s} = 36 \text{ m}^3/\text{s}$ ).
- **Release amount** 70 g/h (duration 10 minutes) = 11.7 gram total (calculated by  $70 \text{ gram}/(36 \text{ m}^3 \times 3600 \text{ s}) = 0.5 \text{ mg/m}^3$ ).
- Chemical is evaporated using a Controlled Evaporator Mixer that uses heat ( $180^\circ\text{C}$ ) and nitrogen gas (80 L/min) to evaporate TEP liquid. This vapor is injected in a tubular transport system that transports the mixed vapor to the inlet tubes of the tunnel using a small amount of additional transport air ( $10.000 \text{ m}^3/\text{hour}$ ). This airstream leaves the horizontal inlet tubes via small holes that result in a mixing effect with the wind stream through the tunnel (bottom tube: 55 cm (center), 2nd tube 125 cm (center) both measured from floor level).
- LCD Sensor data is recorded using the central laptop in the mock-up.

### **Results:**

Data recorded with the LCD's was plotted in a graph displaying the response-time graph (Figure 19). The response is an arbitrary scale. Reference concentration measurements drawn by a number of Tenax failed due to a problem with the sampling.

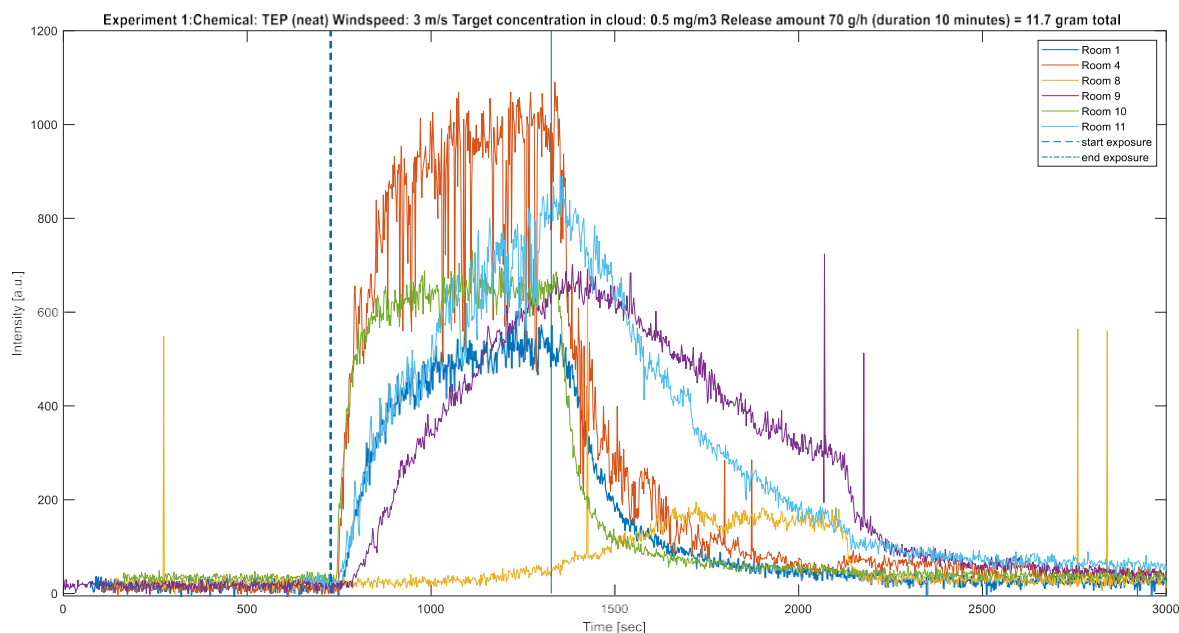


**Figure 19.** Experiment #1 - LCD 3.3 signals plotted against time

### **Experiment #2: Confidence test with cloud over full width of the tunnel (distant release)**

Experiment Time:

- Date: 19-04-2021
- Source start: 15:10:00
- Sampling start: 15:15:00
- Source Stop: 15:20:00

Experimental parameters:

- **Chemical released:** TEP (neat).
- **Dimensions cloud:** approximately 1-2 meters high, 6-meter-wide (only bottom release tube of tunnel is used) (bottom tube: 125 cm (distance centerline tube to floor level, diameter tube 32 cm). These are not exact dimensions since the vapor is released from one horizontal tube in front of the wind fans in a turbulent air stream.
- **Windspeed:** 28 Hz resulting in  $\pm 3$  m/s (measured with anemometers in tunnel).
- **Target concentration in cloud:** 0.5 mg/m<sup>3</sup> (calculated by a cloud front ( $\sim 1$  m high,  $\sim 6$ -meter-wide)  $6 \text{ m}^2 \times 3 \text{ m/s} = 18 \text{ m}^3/\text{s}$ . (Lower concentration anticipated due to use of a single release tube instead of all release tubes at the entrance of the tunnel).
- **Release amount** 35 g/h (duration 10 minutes) = 5.85-gram total (calculated by  $35 \text{ gram}/(18 \text{ m}^3 \times 3600 \text{ s}) = 0.5 \text{ mg/m}^3$ ).
- Chemical is evaporated using a Controlled Evaporator Mixer that uses heat (180 °C) and nitrogen gas (80L/min) to evaporate TEP liquid. This vapor is injected in a tubular transport system that transports the mixed vapor to the inlet tubes of the tunnel using a small amount of additional transport air (7.000 m<sup>3</sup>/hour). This airstream leaves the horizontal inlet tube via small holes that result in a mixing effect with the wind stream through the tunnel (bottom tube: 55 cm (distance centerline tube to floor level, diameter tube 32 cm).
- LCD Sensor data is recorded using the central laptop in the mock-up.

### **Results:**

Data recorded with the LCD's was plotted in a graph displaying the response-time graph

(Figure 20). The response is an arbitrary scale. The concentration was determined by a series of reference samples. Each sample was drawn by pumping 100mL of air onto a Tenax tube during approximately 20 seconds with a manual air pump. The concentrations are listed in Table 3.

**Table 3.** Experiment #2 - Sampling start time

Date	Location	Time	Result (mg/m <sup>3</sup> )	Comments
19-4-2021	Reference	15:15:30	0,097	
19-4-2021	Corridor	15:16:12	0,211	
19-4-2021	Room 1	14:29:44	nd	sample tube broken
19-4-2021	Room 8	14:30:20	nd	problem with sampling

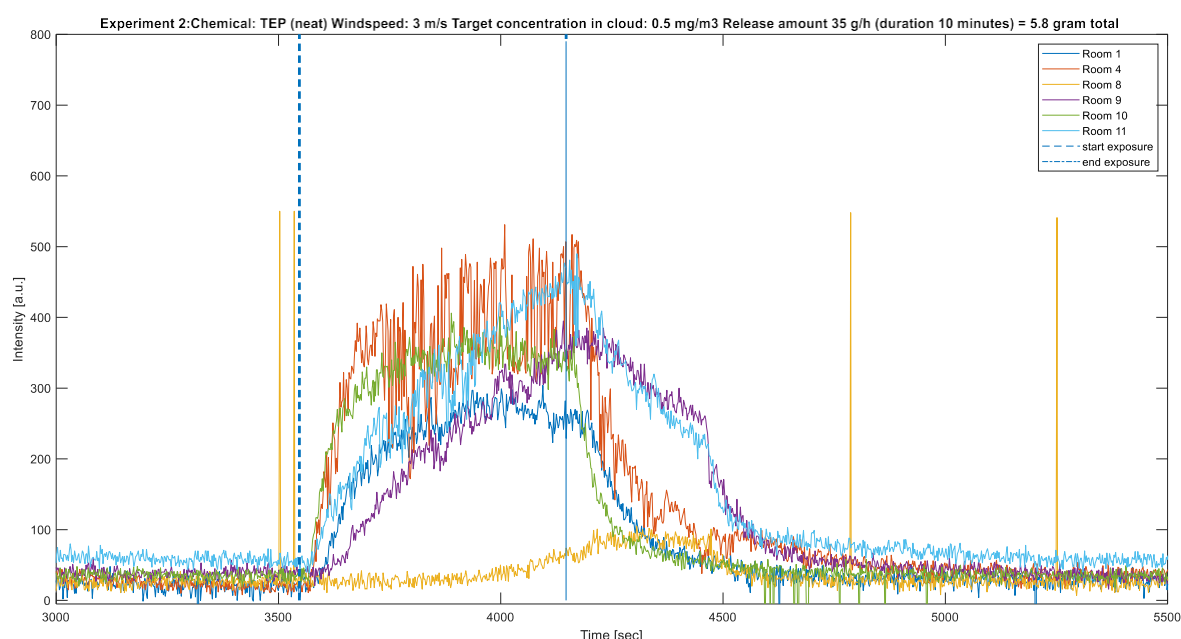


**Figure 20.** Experiment #2 - LCD 3.3 signals plotted against time

**Experiment #3: Confidence test with cloud over full width of the tunnel (distant release)**

Experiment Time:

- Date: 19-04-2021
- Source start: 15:50:00
- Sampling start: 15:55:00
- Source Stop: 16:00:00

Experimental parameters:

- **Chemical released:** TEP (neat).
- **Dimensions cloud:** approximately 1-2 meters high, 6 meter wide (only bottom

release tube of tunnel is used). These are not exact dimensions since the vapor is released from one horizontal tube in front of the wind fans in a turbulent air stream.

- Windspeed: 28 Hz resulting in  $\pm 3$  m/s (measured with anemometers in tunnel).
- **Target concentration in cloud:**  $0.5 \text{ mg/m}^3$  (calculated by a cloud front ( $\sim 1$  m high,  $\sim 6$  meter wide)  $6 \text{ m}^2 \times 3 \text{ m/s} = 18 \text{ m}^3/\text{s}$ ).
- **Release amount**  $35 \text{ g/h}$  (duration 10 minutes) = 5.85 gram total (calculated by  $35 \text{ gram}/(18 \text{ m}^3 \times 3600 \text{ s}) = 0.5 \text{ mg/m}^3$ ).
- Chemical is evaporated using a Controlled Evaporator Mixer that uses heat ( $180^\circ\text{C}$ ) and nitrogen gas ( $80\text{L/min}$ ) to evaporate TEP liquid. This vapor is injected in a tubular transport system that transports the mixed vapor to the inlet tubes of the tunnel using a small amount of additional transport air ( $7.000 \text{ m}^3/\text{hour}$ ). This airstream leaves the horizontal inlet tube via small holes that result in a mixing effect with the wind stream through the tunnel (bottom tube: 125 cm (distance centerline tube to floor level, diameter tube 32 cm).
- LCD Sensor data is recorded using the central laptop in the mock-up.

### **Results:**

Data recorded with the LCD's was plotted in a graph displaying the response-time graph (Figure 21). The response is an arbitrary scale. The concentration was determined by a series of reference samples. Each sample was drawn by pumping 100 mL of air onto a Tenax tube during approximately 20 seconds with a manual air pump. The concentrations are listed in Table 4.

**Table 4.** Experiment #3 - Sampling start time

Date	Location	Time	Result ( $\text{mg/m}^3$ )	Comments
19-4-2021	Reference	15:55:32	0,196	
19-4-2021	Corridor	15:56:13	0,182	
19-4-2021	Room 1	15:56:55	0,192	
19-4-2021	Room 8	15:57:45	nd	Below detection limit

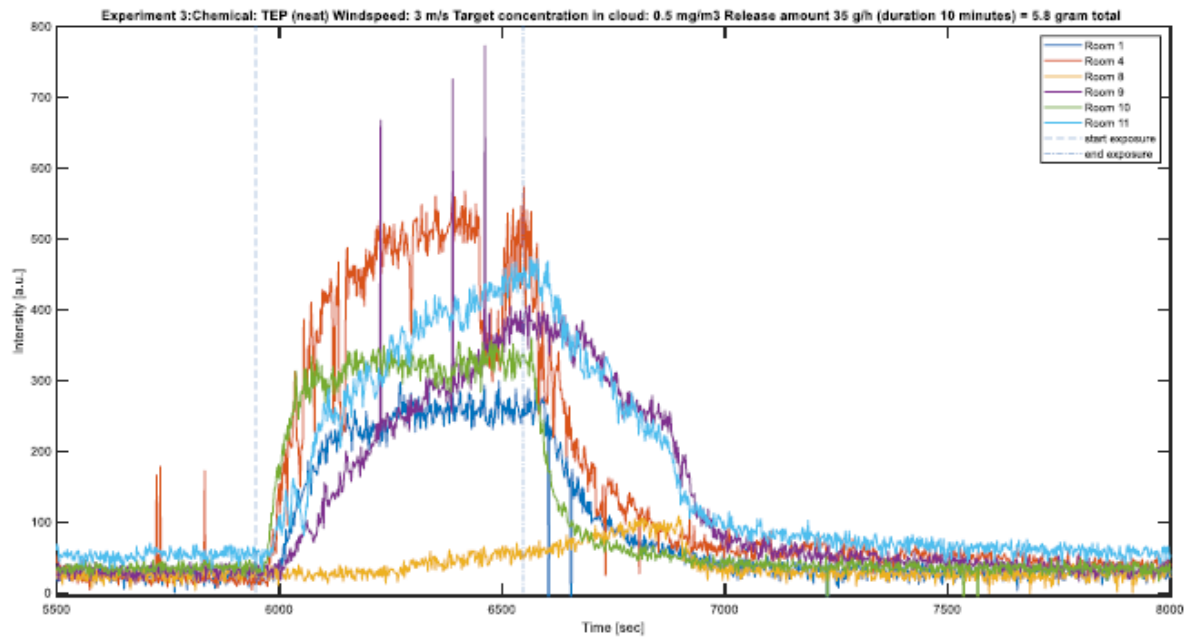


**Figure 21.** Experiment #3 - LCD 3.3 signals plotted against time

## Scenario 2

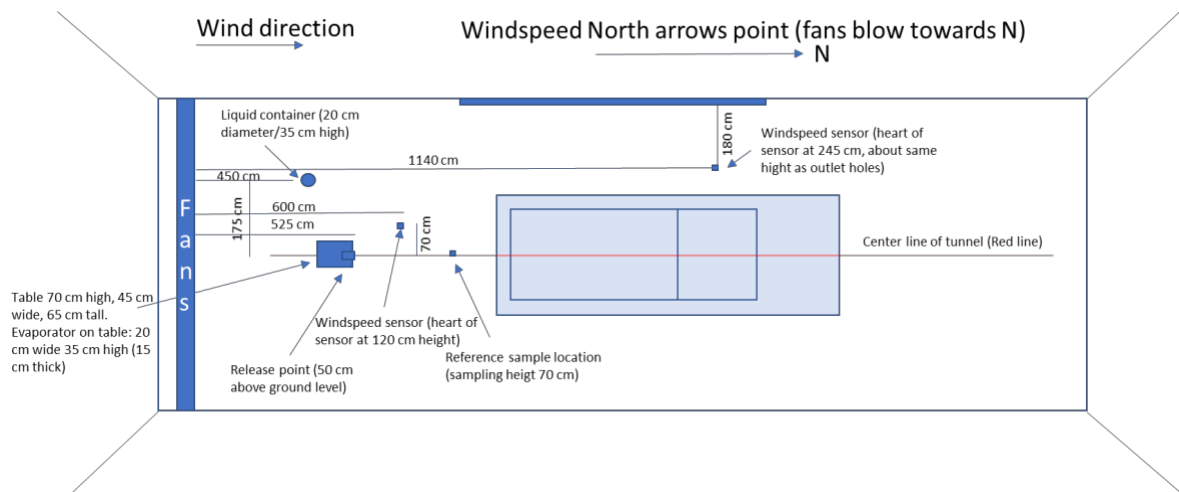


**Figure 22.** Scenario 2 - schematic overview of position of windspeed sensors, reference sample and source location around mock-up

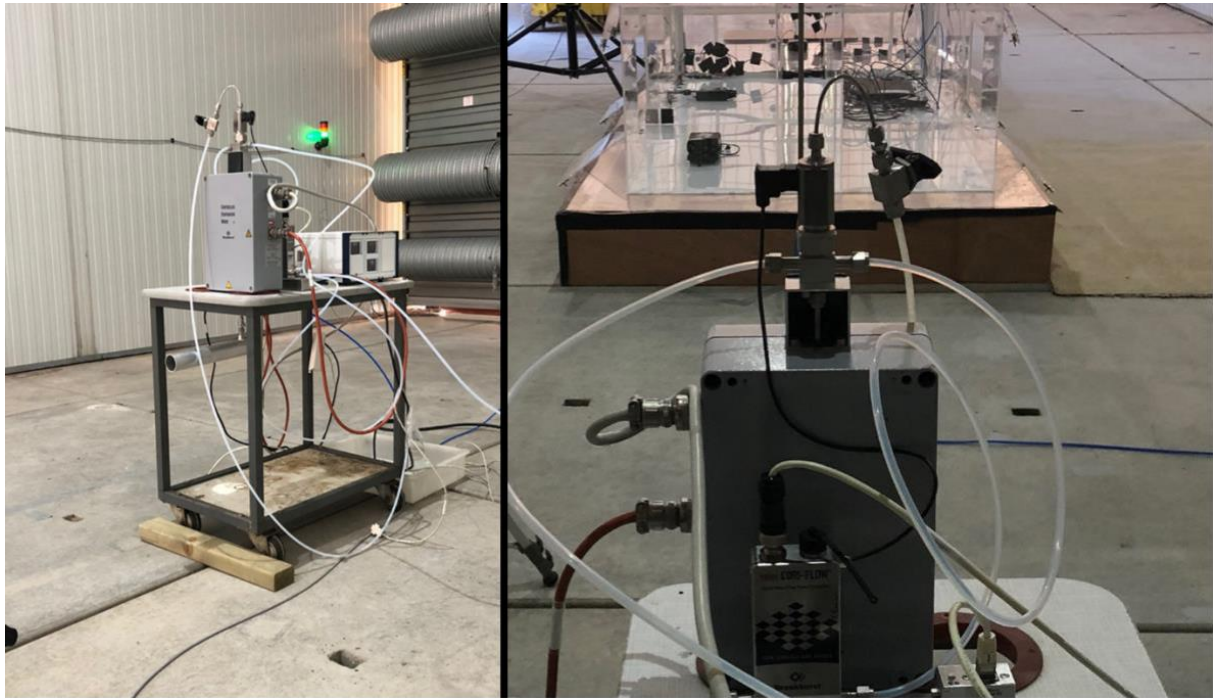


**Figure 23.** Scenario 2 - Release apparatus used as point source (right) in front of mock-up (left)

**Experiment #6: External point release close to mock-up with evaporator in tunnel**

Experiment Time:

- Date: 22-04-2021
- Source start: 09:58:00
- Sampling start: 10:03:00
- Source Stop: 10:08:00

Experimental parameters:

- **Chemical released:** TEP (4% solution in mq water).
- **Dimensions cloud:** the source was a CEM (description below) that was positioned at 50cm above floor level. From this point the vapor spreads towards the mock-up.
- Windspeed: 28 Hz resulting in  $\pm 3$  m/s (measured with anemometers in tunnel).
- **Target concentration in cloud:**  $0.5 \text{ mg/m}^3$  (calculated by a cone shaped cloud front (length 3 m, radius 0.57 m at front of building)  $1.02\text{m}^2 \times 3 \text{ m/s} = 3.1 \text{ m}^3/\text{se} \times 0.5 \text{ mg/m}^3 = 1.7 \text{ mg/s} = 5.6 \text{ gram/h}$  (neat).
- **Release amount** 140 g/h, 4 % solution (duration 10 minutes) = 0.93 gram total TEP.
- Chemical is evaporated using a Controlled Evaporator Mixer, positioned in the tunnel, that uses heat (180 °C) and nitrogen gas (80 L/min) to evaporate TEP liquid. This vapor released in the tunnel using a horizontal outlet tube pointing towards the mock-up. The outer diameter of the tube is 4.1 cm and the inner diameter is 3.9 cm. The height of the tube is 50 cm, the length is 25 cm.
- LCD Sensor data is recorded using the central laptop in the mock-up.

**Results:**

Data recorded with the LCD's was plotted in a graph displaying the response-time graph (Figure 24). The response is an arbitrary scale. The concentration was determined by a series of reference samples. Each sample was drawn by pumping 100 mL of air onto a Tenax tube during approximately 20 seconds with a manual air pump. The

concentrations are listed in Table 5.

**Table 5.** Experiment #6 - Sampling start time

Date	Location	Time	Result (mg/m <sup>3</sup> )	Comments
22-4-2021	Reference	10:03:18	0,86	
22-4-2021	Corridor	10:03:48	0,49	
22-4-2021	Room 1	10:04:15	0,53	
22-4-2021	Room 8	10:04:46	0,062	

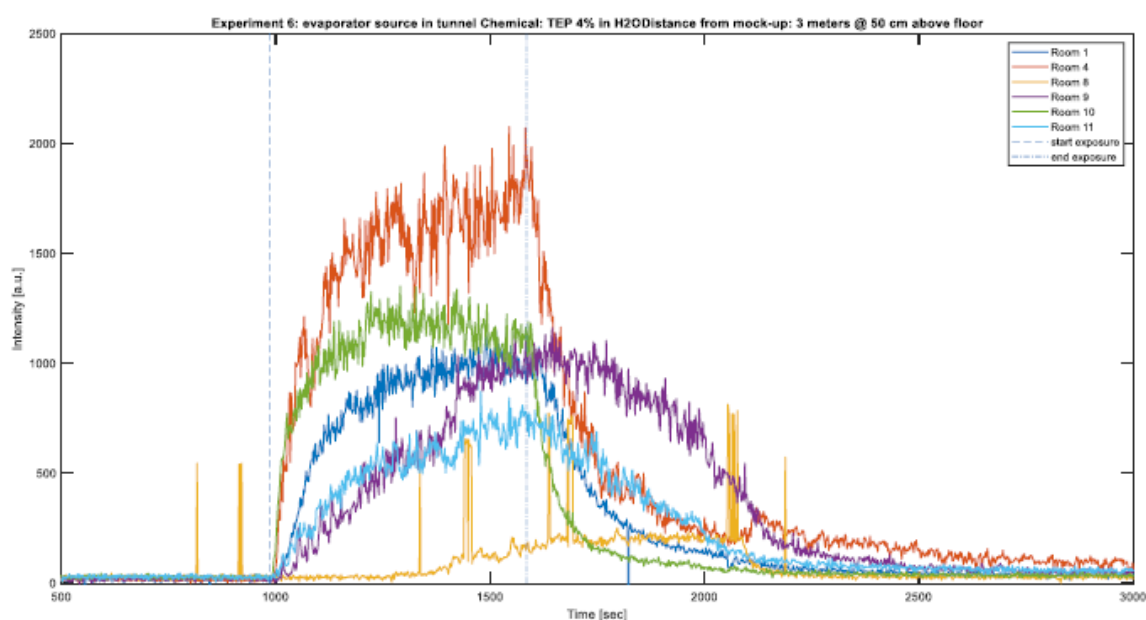


**Figure 24.** Experiment #6 - LCD 3.3 signals plotted against time

**Experiment #7: External point release close to mock-up with evaporator in tunnel (replicate)**

Experiment Time:

- Date: 22-04-2021
- Source start: 10:38:50
- Sampling start: 10:43:00
- Source Stop: 10:49:00

Experimental parameters:

- **Chemical released:** TEP (4% solution in mq water).
- **Dimensions cloud:** the source was a CEM (description below) that was positioned at 50cm above floor level. From this point the vapor spreads towards the mock-up.
- **Windspeed:** 28 Hz resulting in  $\pm 3$  m/s (measured with anemometers in tunnel).
- **Target concentration in cloud:** 0.5 mg/m<sup>3</sup> (calculated by a cone shaped cloud

front (length 3 m, radius 0.57 m at front of building)  $1.02 \text{ m}^2 \times 3 \text{ m/s} = 3.1 \text{ m}^3/\text{s}$   
 $\times 0.5 \text{ mg/m}^3 = 1.7 \text{ mg/s} = 5.6 \text{ gram/h (neat)}$ .

- **Release amount** 140 g/h, 4 % solution (duration 10 minutes) = 0.93 gram total TEP.
- Chemical is evaporated using a Controlled Evaporator Mixer, positioned in the tunnel, that uses heat (180 °C) and nitrogen gas (80 L/min) to evaporate TEP liquid. This vapor released in the tunnel using a horizontal outlet tube pointing towards the mock-up. The outer diameter of the tube is 4.1 cm and the inner diameter is 3.9 cm. The height of the tube is 50 cm, the length is 25 cm.
- LCD Sensor data is recorded using the central laptop in the mock-up.

### Results:

Data recorded with the LCD's was plotted in a graph displaying the response-time graph (Figure 25). The response is an arbitrary scale. The concentration was determined by a series of reference samples. Each sample was drawn by pumping 100mL of air onto a Tenax tube during approximately 20 seconds with a manual air pump. The concentrations are listed in Table 6.

**Table 6.** Experiment #7 - Sampling start time

Date	Location	Time	Result (mg/m <sup>3</sup> )	Comments
22-4-2021	Reference	10:44:33	0,77	
22-4-2021	Corridor	10:45:35	0,5	
22-4-2021	Room 1	10:46:16	0,49	
22-4-2021	Room 8	10:47:00	0,18	

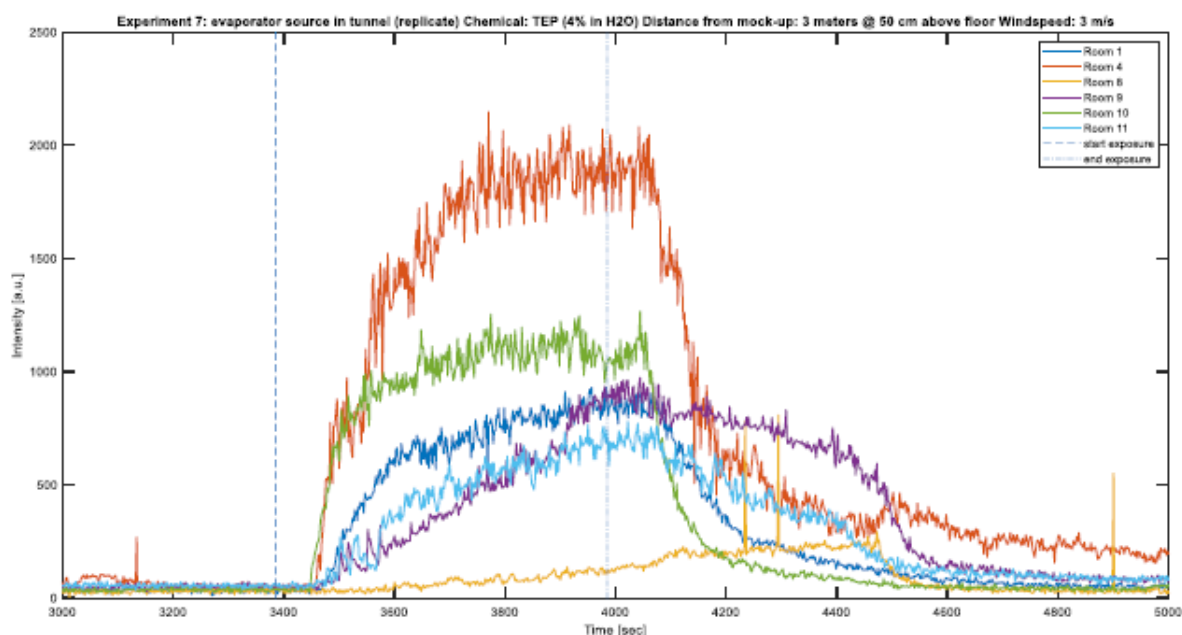


**Figure 25.** Experiment #7 - LCD 3.3 signals plotted against time

**Experiment #8: External point release close to mock-up with evaporator in tunnel (short intense release)**

Experiment Time:

- Date: 22-04-2021
- Source start: 14:52:25
- Sampling start: 10:53:25 (only reference short release)
- Source Stop: 14:55:45

Experimental parameters:

- **Chemical released:** TEP (4% solution in mq water).
- **Dimensions cloud:** the source was a CEM (description below) that was positioned at 50cm above floor level. From this point the vapor spreads towards the mock-up.
- **Windspeed:** 28 Hz resulting in  $\pm 3$  m/s (measured with anemometers in tunnel).
- **Target concentration in cloud:**  $1.5 \text{ mg/m}^3$  (calculated by a cone shaped cloud front (length 3 m, radius 0.57 m at front of building)  $1.02 \text{ m}^2 \times 3 \text{ m/s} = 3.1 \text{ m}^3/\text{s} \times 1.5 \text{ mg/m}^3 = 4.6 \text{ mg/s} = 16.5 \text{ gram/h}$  (neat). The concentration is 3 times higher and the release time is 3 times shorter than experiment 7 resulting in an equal released amount.
- Release amount 140 g/h, 4 % solution (duration 3:20 minutes) = 0.93 gram total TEP.
- Chemical is evaporated using a Controlled Evaporator Mixer, positioned in the tunnel, that uses heat (180 °C) and nitrogen gas (80 L/min) to evaporate TEP liquid. This vapor released in the tunnel using a horizontal outlet tube pointing towards the mock-up. The outer diameter of the tube is 4.1 cm and the inner diameter is 3.9 cm. The height of the tube is 50 cm, the length is 25 cm.
- LCD Sensor data is recorded using the central laptop in the mock-up.

**Results:**

Data recorded with the LCD's was plotted in a graph displaying the response-time graph (Figure 26). The response is an arbitrary scale. The concentration was determined by a series of reference samples. Each sample was drawn by pumping 50 mL of air onto a Tenax tube during approximately 10 seconds with a manual air pump. The concentration is given in Table 7.

**Table 7.** Experiment #8 - Sampling start time

Date	Location	Time	Result (mg/m <sup>3</sup> )	Comments
22-4-2021	Reference	14:53:26	2,22	only reference sampled (short release)

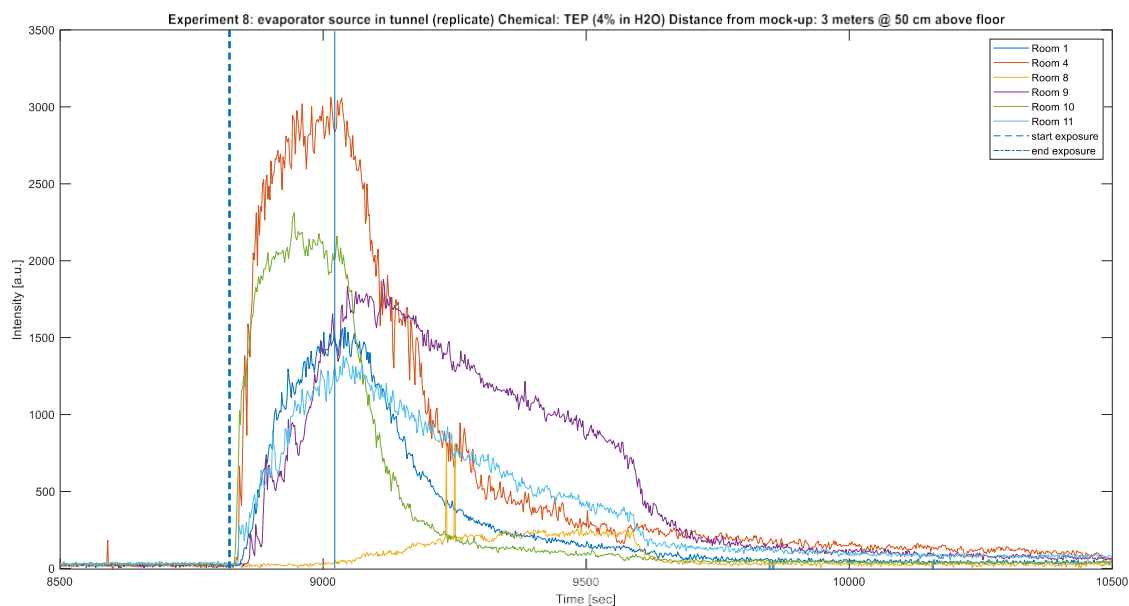


**Figure 26.** Experiment #8 - LCD 3.3 signals plotted against time

***Experiment #9: External point release close to mock-up with evaporator in tunnel (long low concentration release)***

Experiment Time:

- Date: 22-04-2021
- Source start: 15:25:00
- Sampling start: 15:35:00
- Source Stop: 15:55:00

Experimental parameters:

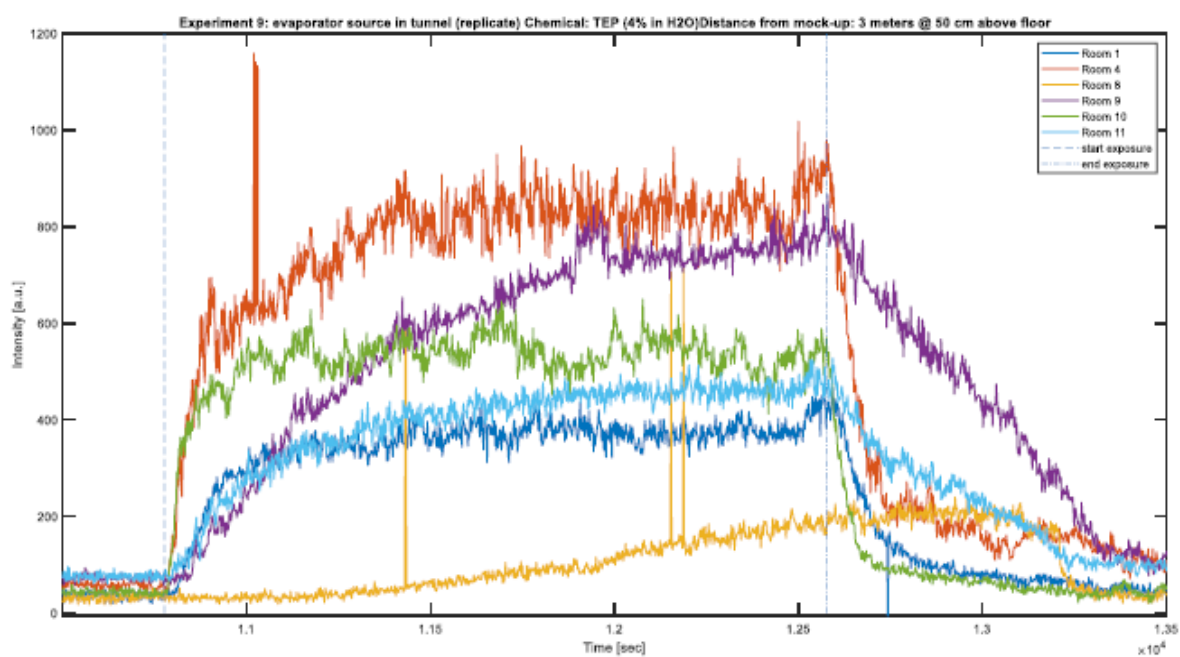
- **Chemical released:** TEP (4% solution in mq water).
- **Dimensions cloud:** the source was a CEM (description below) that was positioned at 50cm above floor level. From this point the vapor spreads towards the mock-up.
- **Windspeed:** 28 Hz resulting in  $\pm 3$  m/s (measured with anemometers in tunnel).
- **Target concentration in cloud:**  $0.167 \text{ mg/m}^3$  (calculated by a cone shaped cloud front (length 3 m, radius 0.57 m at front of building)  $1.02 \text{ m}^2 \times 3 \text{ m/s} = 3.1 \text{ m}^3/\text{s} \times 0.167 \text{ mg/m}^3 = 0.5 \text{ mg/s} = 1.86 \text{ gram/h}$  (neat). The concentration is 3 times lower and the release time is 3 times longer than experiment 7 resulting in an equal released amount.
- **Release amount** 140 g/h, 4 % solution (duration 30 minutes) = 0.93 gram total TEP.
- Chemical is evaporated using a Controlled Evaporator Mixer, positioned in the tunnel, that uses heat ( $180^\circ\text{C}$ ) and nitrogen gas (80 L/min) to evaporate TEP liquid. This vapor released in the tunnel using a horizontal outlet tube pointing towards the mock-up. The outer diameter of the tube is 4.1 cm and the inner diameter is 3.9 cm. The height of the tube is 50 cm, the length is 25 cm.
- LCD Sensor data is recorded using the central laptop in the mock-up.

***Results:***

Data recorded with the LCD's was plotted in a graph displaying the response-time graph (Figure 27). The response is an arbitrary scale. The concentration was determined by a series of reference samples. Each sample was drawn by pumping 50-100 mL of air onto a Tenax tube during approximately 10 seconds with a manual air pump. The concentration is listed in Table 8.

**Table 8.** Experiment #9 - Sampling start time

Date	Location	Time	Result (mg/m <sup>3</sup> )	Comments
22-4-2021	Reference	15:35:14	0,67	
22-4-2021	Corridor	15:35:44	0,24	
22-4-2021	Room 1	15:36:12	0,23	
22-4-2021	Room 8	15:36:50	0,062	

**Figure 27.** Experiment #9 - LCD 3.3 signals plotted against time

## **Scenario 1**

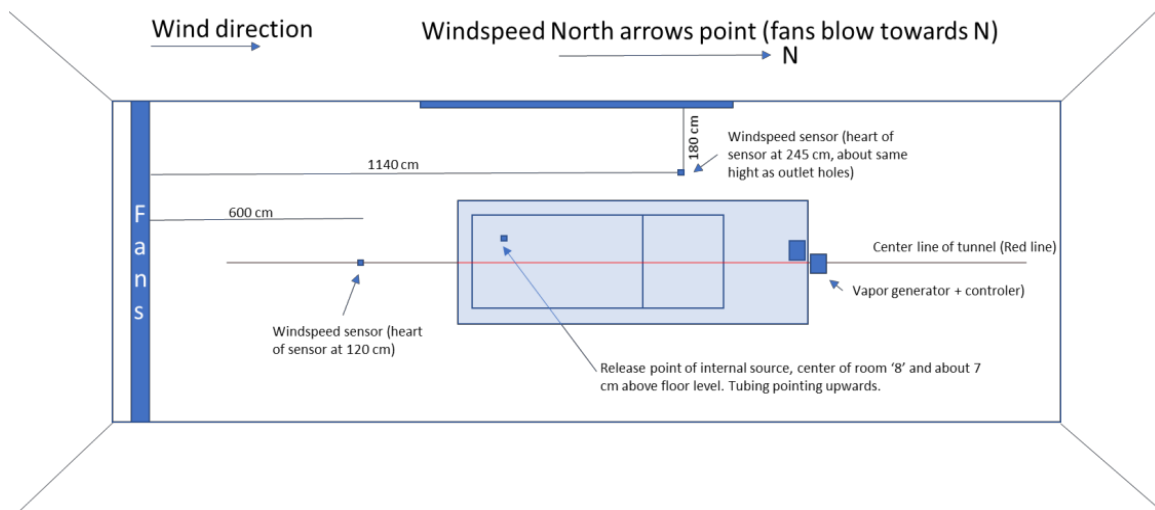


**Figure 28.** Scenario 1 - Schematic overview of position of windspeed sensors and source location around mock-up

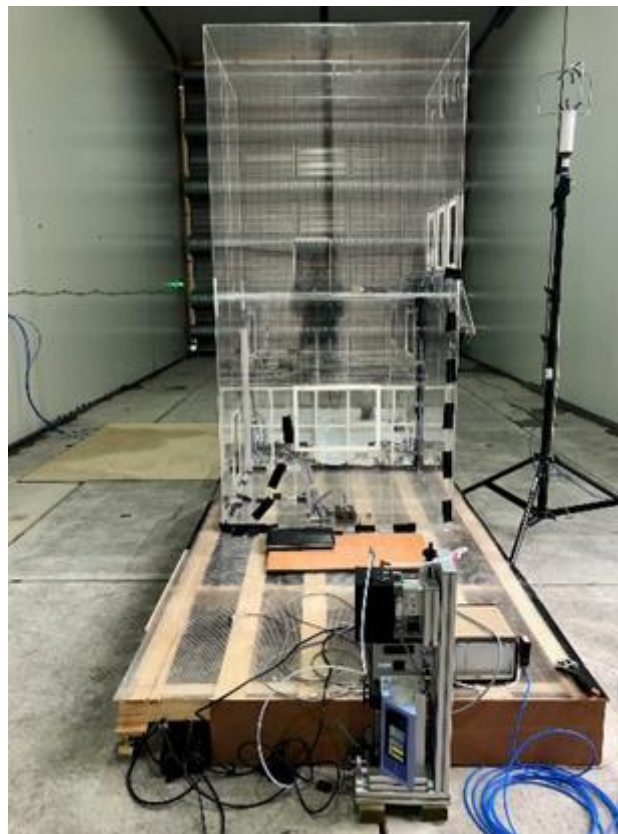


**Figure 29.** Scenario 1 - Evaporator positioned behind the mock-up

### ***Experiment #11: Internal point release (TEP in room 8)***

Experiment Time:

- Date: 29-04-2021
- Source start: 15:07:00
- Sampling start: no reference sample

- Source Stop: 15:09:00
- All windows open: 15:20:00 (venting mock-up)

Experimental parameters:

- **Chemical released:** TEP (neat).
- TEP was released in room '8' in the center of the room close to ground level (7 cm above floor).
- **Windspeed:** 28 Hz resulting in  $\pm 3$  m/s (measured with anemometers in tunnel).
- **Target concentration**  $1.5 \text{ mg/m}^3$ . Vapor was created by evaporating 235 nL/min (duration 2 minutes) of TEP and transporting it to room 8 with a volume of approximately  $0.4 \text{ m}^3$ .
- Chemical is evaporated using a Controlled Evaporator Mixer that uses heat ( $150^\circ\text{C}$ ) and nitrogen gas ( $1.3 \text{ L/min}$ ) to evaporate TEP liquid. This vapor released in using a piece of tubing that end in room 8 in the center of the room at 7 cm above floor level. The tubing dimension is 6 mm outside, 4 mm inside and points upward.
- LCD Sensor data is recorded using the central laptop in the mock-up.
- No reference samples were taken due to high concentration. The high concentration measurement would result in a saturation of the sampling devices and thereby underestimation of the actual concentration.
- After release all windows were opened (see time table for exact time) to vent the rooms.

### Results:

The response of the LCD in room 8 is saturated due to high concentration.

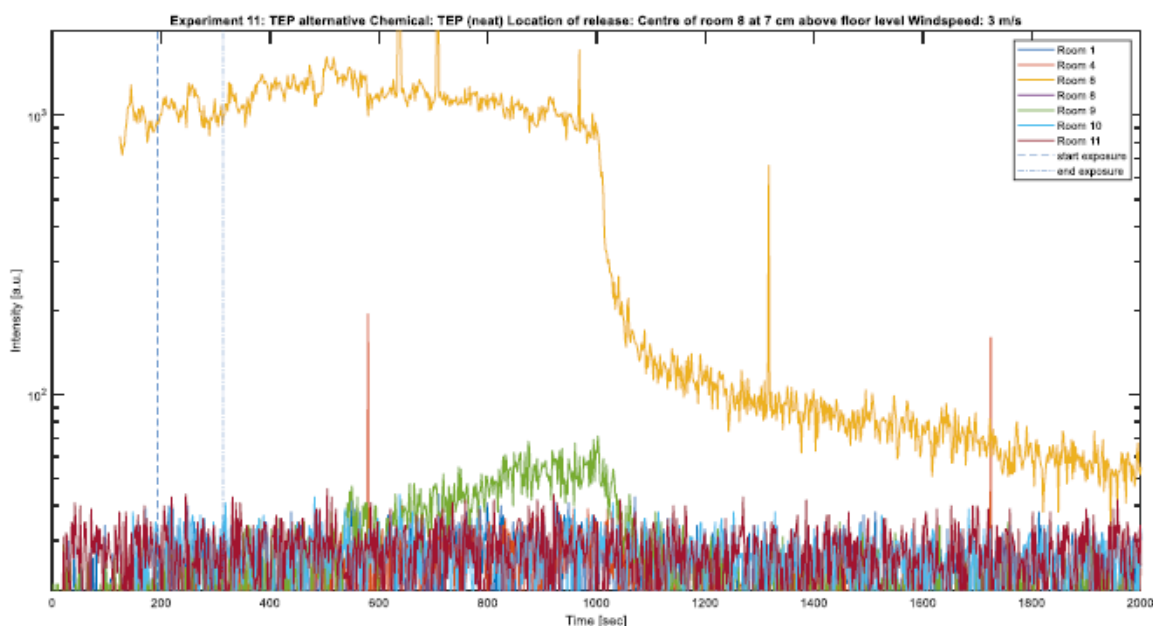


**Figure 30.** Experiment #11 - LCD signals plotted against time

### Experiment #12: Internal point release (TEP in room 8)

Experiment Time:

- Date: 29-04-2021
- Source start: 15:39:00
- Sampling start: no reference sample
- Source Stop: 15:41:00
- All windows open: 15:50:00 (venting mock-up)

Experimental parameters:

- **Chemical released:** TEP (neat).
- TEP was released in room '8' in the center of the room close to ground level (7 cm above floor).
- **Windspeed:** 28 Hz resulting in  $\pm 3$  m/s (measured with anemometers in tunnel).
- Target concentration  $6 \text{ mg/m}^3$ . Vapor was created by evaporating  $1 \text{ }\mu\text{L/min}$  (duration 2 minutes) of TEP and transporting it to room 8 with a volume of approximately  $0.4 \text{ m}^3$ .
- Chemical is evaporated using a Controlled Evaporator Mixer that uses heat ( $150^\circ\text{C}$ ) and nitrogen gas ( $1.3\text{L/min}$ ) to evaporate TEP liquid. This vapor released in using a piece of tubing that end in room 8 in the center of the room at 7 cm above floor level. The tubing dimension is 6 mm outside, 4 mm inside and points upward.
- LCD Sensor data is recorded using the central laptop in the mock-up.
- No reference samples were taken due to high concentration.
- After release all windows were opened to vent the rooms.

### Results:

The response of the LCD in room 8 is saturated due to high concentration.

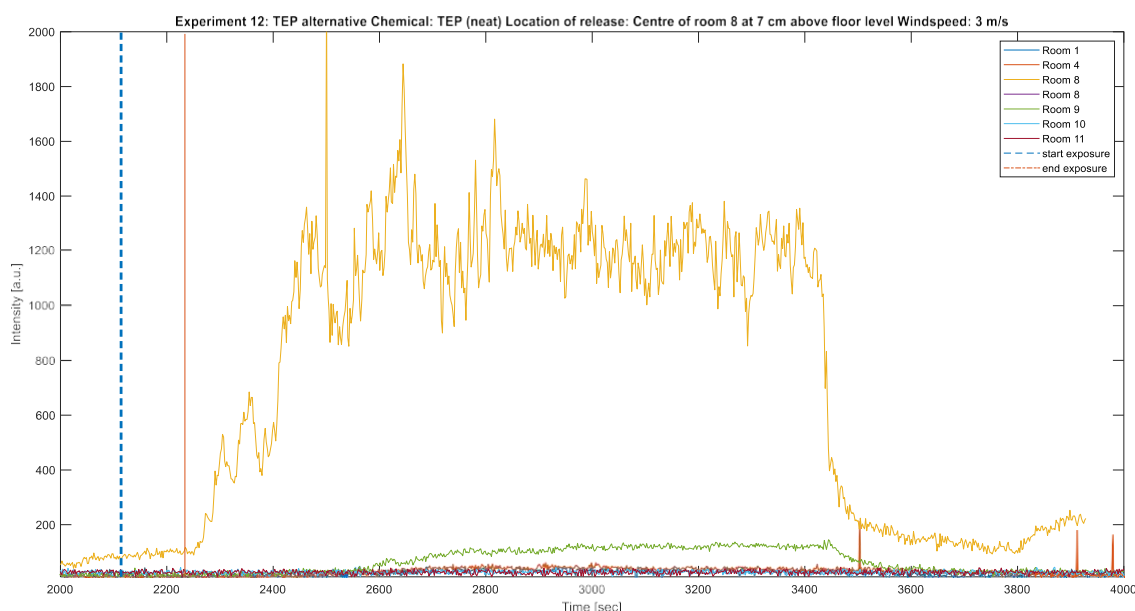


**Figure 31.** Experiment #12 - LCD signals plotted against time

### **Experiment #13: Internal point release (TEP in room 8, replicate with preconditioning of syringe)**

Experiment Time:

- Date: 29-04-2021
- Source start: 16:15:00
- Sampling start: no reference sample
- Source Stop: 16:19:00
- All windows open: 16:24:00 (venting mock-up)

Experimental parameters:

- **Chemical released:** TEP (neat).
- TEP was released in room '8' in the center of the room close to ground level (7 cm above floor).

- **Windspeed:** 28 Hz resulting in  $\pm 3$  m/s (measured with anemometers in tunnel).
- **Target concentration** 6 mg/m<sup>3</sup>. Vapor was created by evaporating 1  $\mu$ L/min (duration 2 minutes) of TEP and transporting it to room 8 with a volume of approximately 0.4 m<sup>3</sup>.
- Chemical is evaporated using a Controlled Evaporator Mixer that uses heat (150 °C) and nitrogen gas (1.3 L/min) to evaporate TEP liquid. The vapor was released in the center of room 8 at 7 cm above floor level by using a piece of tubing. The tubing dimension is 6 mm outside, 4 mm inside and points upward. Prior to release the syringe used was preconditioned. This is why the release took longer to start (less control).
- LCD Sensor data is recorded using the central laptop in the mock-up.
- No reference samples were taken due to high concentration.
- After release all windows were opened (see 'Experiment time' for exact time) to vent the rooms.

### Results:

The response of the LCD in room 8 is saturated due to high concentration.

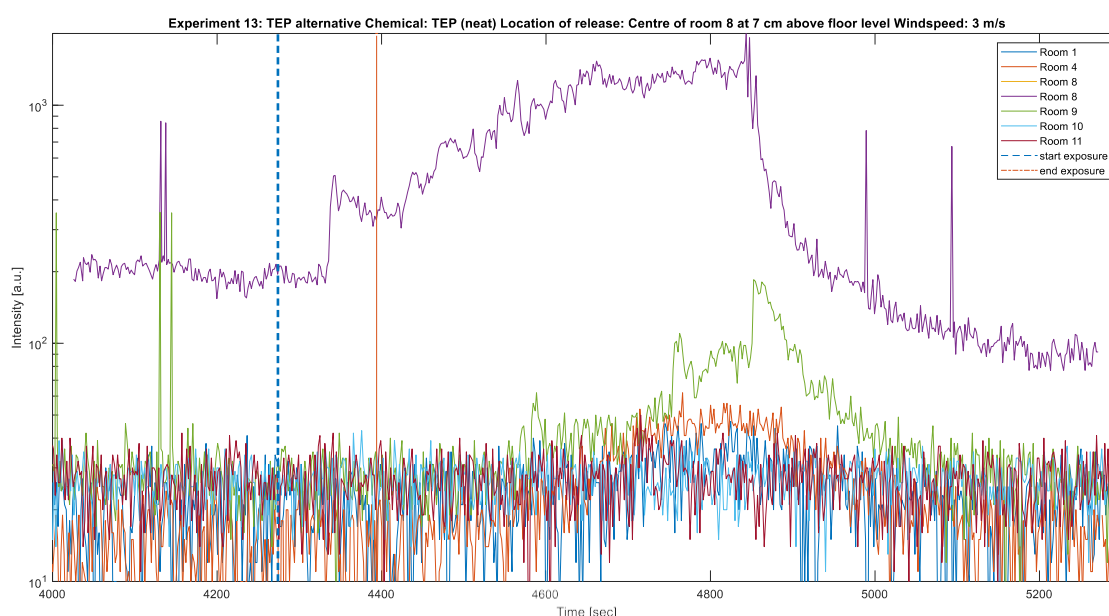


**Figure 32.** Experiment #13 - LCD signals plotted against time

## 2.3. Results of Detection Experiments

As shown by the analysis of results, the experimental study only had a small number of parameters that varied. Only one chemical has been used, TEP; only one detector has been applied (LCD 3.3) and only one windspeed setting was used (3 m/s). Reflecting on the experimental approach many parameters could have been chosen to allow a broader variation of relevant circumstances.

As stated in the previous chapters, three attack scenarios have been mimicked: release of agent from within the building mock-up; release of agents at short distance (3 m) from outside the mock-up; release of a cloud of agents from 'far away' by exposing the entire AMB and the mock-up therein.

Numerous simulants for toxic agents could have been selected. Obviously, prerequisites were detectability by the sensors at hand, favourable physical chemical properties and

low toxicity. Due to the limited resources in budget and time, only TEP was used. This might be regarded as a shortcoming, but for achieving the study objective, it turned that the substantial amount of data obtained from the TEP studies have been useful and fulfilling.

Many chemical sensors could have been used. The attempts to apply PID detectors (kindly made available by FOI) for detecting toluene as a model Toxic Industrial Chemical sadly failed. Then it was decided to continue (Scenario 1) experiments just with TEP and the LCD 3.3 detectors which proved excellently able to detect that substance.

Range of TEP concentrations might have been studied, however, the most essential part of the range finding efforts was to achieve levels that resulted in actual LCD signals with successful TEP generation and some level of realism.

Due to the high demands regarding information on the local turbulence and wind speed within the AMB, it was decided to limit to wind speed applied in the AMB to just one setting (3 m/s).

The actual time to execute the experiments (including time needed to repair the damage to the mock-up arisen during transport; range finding and facility cleaning) was limited to 2 working weeks. Still, the short duration combined with the variety of prerequisites and the high level of uncertainty of the particular experimental approach did not prohibit the delivery of an impressive data set and interesting findings.

### 2.3.1 Conclusions of experimental trials

The experiments, the results of which have been described in the previous section, had as essential objective to serve as input for subsequent modelling of agent dispersion. Overarching conclusions need to draw on the basis of the combination and integration of experiments and modelling. A more comprehensive overview of conclusions is given based on the modelling executed before and after the experiments. However, some observations can be made:

- Release of TEP was successful in all three exposure scenarios:
  - **Scenario 1** resulted in substantial TEP concentration in the room 8 it was released in;
  - **Scenario 2** (after some failed attempts) resulted in clear and reproducible TEP releases;
  - **Scenario 3** resulted in clear and reproducible TEP releases.
- Ground truth measurements of TEP by Tenax sampling and subsequent GC-MS analysis were (apart from some missing data) successful;
- The LCD 3.3 detector was well able to detect offered levels of TEP;
- Efforts to apply the PID system to detect toluene failed;
- The detectors inside the mock-up responded well;
- Clear, significant and reproducible differences of sensor response between sensors placed in different mock-up rooms have been recorded:
  - **Scenario 1** (experiments 11, 12, 13):
    - Apart from room 8 itself TEP was detected in room 9.
  - **Scenario 2** (experiments 6, 7, 8, 9):
    - Ranking room that showed to fastest response: 4=10>1>11>9>8;
    - Ranking room that showed highest level: 4>10>9>1>11>8.
  - **Scenario 3** (experiments 1, 2, 3):
    - Ranking room that showed to fastest response: 4=10>11=1>9>8;
    - Ranking room that showed highest level: 4>11>9>10=1>8.

Release of TEP was successful in all three exposure scenarios, it resulted in reproducible detection signals from 6 IMS instrument placed in 6 rooms of the building mock-up. The speed and magnitude in which TEP levels were recorded in the respective rooms showed a clear and reproducible picture in the sense that some of the rooms appeared to be better reachable for the externally released TEP than others. Subsequent dispersion modelling will be undertaken to understand and describe those differences.

### 3. Modelling Activity

3D simulations were performed with Code\_Saturne and ADREA-HF CFD models with the aim to firstly pre-compute, and secondly reproduce, the flow and dispersion of the chemical in the above-described mock-up.

#### 3.1. Computation Approach (Code\_Saturne)

A Computational Fluid Dynamics (CFD) work was applied on the spatial and temporal distribution of chemicals inside a mock-up placed in a wind tunnel where vapours are transported and dispersed by a turbulent flow generated by large fans.

The objective of the experimental trials was to mimic the exposure of a building undergoing an attack from the outside in a near-by release location. The situation of a release occurring inside the mock-up is also considered.

In general, as in this particular project, 3D modelling and simulation based on CFD have a double use regarding experiments:

- The first one relates to the **design** of the trials before they are performed;
- the second one relates to the **replication** of the trials after they are carried out.

Thus, simulations have been carried out with Code\_Saturne both before and after the experiments. **Pre-trials computations** illustrate the differences in the dispersion pattern when an internal versus an external released is considered. **Post-trials computations** are fully consistent with the pre-trials computations and the physical phenomena enlightened in the different trials.

Preparatory CFD simulations have the great interest to predictionally and reliably inform about what will be encountered in the experiments. CFD simulations for replicating experimental trials generally provide a good estimate of the concentrations where sensors were set up in the wind tunnel and building mock-up. Moreover, they give a full space and time knowledge of the flow and dispersion patterns, while experiments only exploit a very limited number of sensors measuring at a limited number of instants.

##### 3.1.1 The Pre-Experimental Phase

As a first step, the preparatory simulation work based on the trials conditions is presented hereafter.

Figure 33 shows the principle of the experimental assembly. While the flow in the wind tunnel should be essentially one-directional, it is anticipated that a complex 3D flow was established in and around the mock-up placed in the wind tunnel (Figure 34).

Indeed, there are three openings in the mock-up wall facing the incident air flow from the blower fans (these openings are at the second floor of the lower part of the mock-up). There are also three openings for air extraction located on one of the mock-up side walls (these openings are at the second floor of the upper part of the mock-up).

Two successive releases were planned, one upstream of the flow outside the mock-up (Figure 35), the other in the mock-up on the ground floor of the lower part (Figure 36).

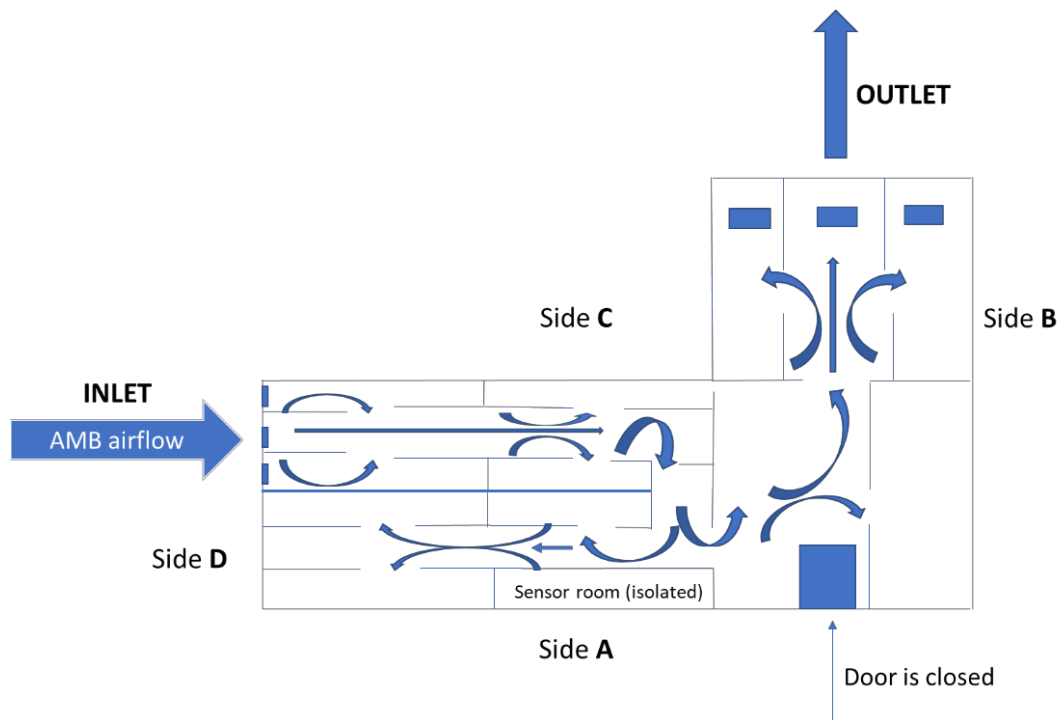


**Figure 33.** Principle of the experiment

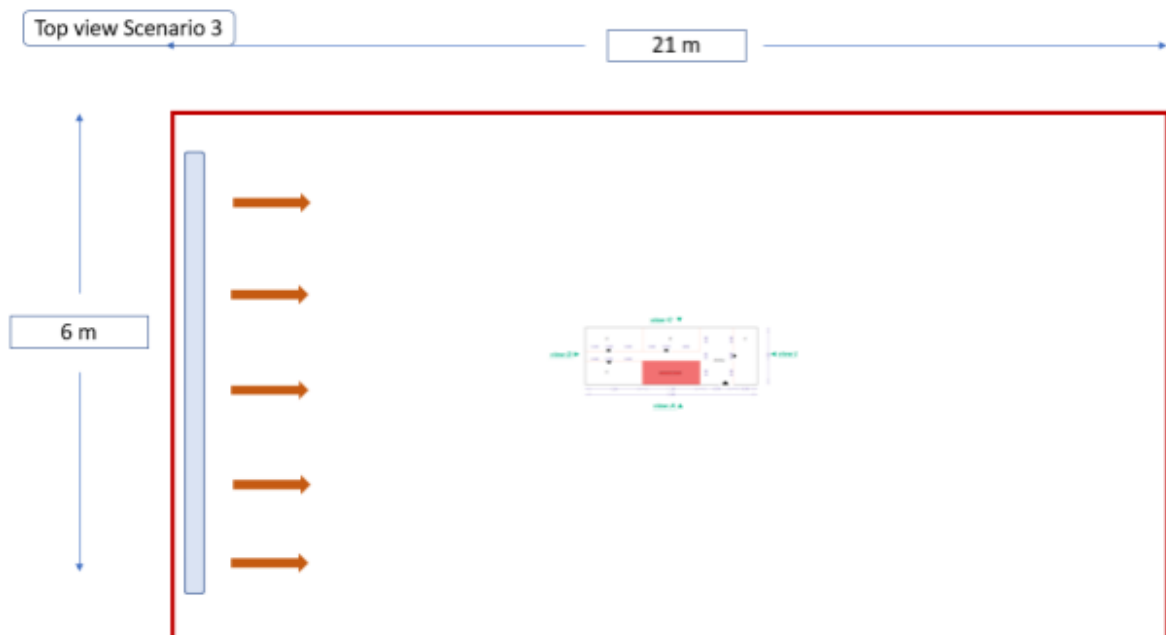


**Figure 34.** Positioning of the mock-up in the wind tunnel

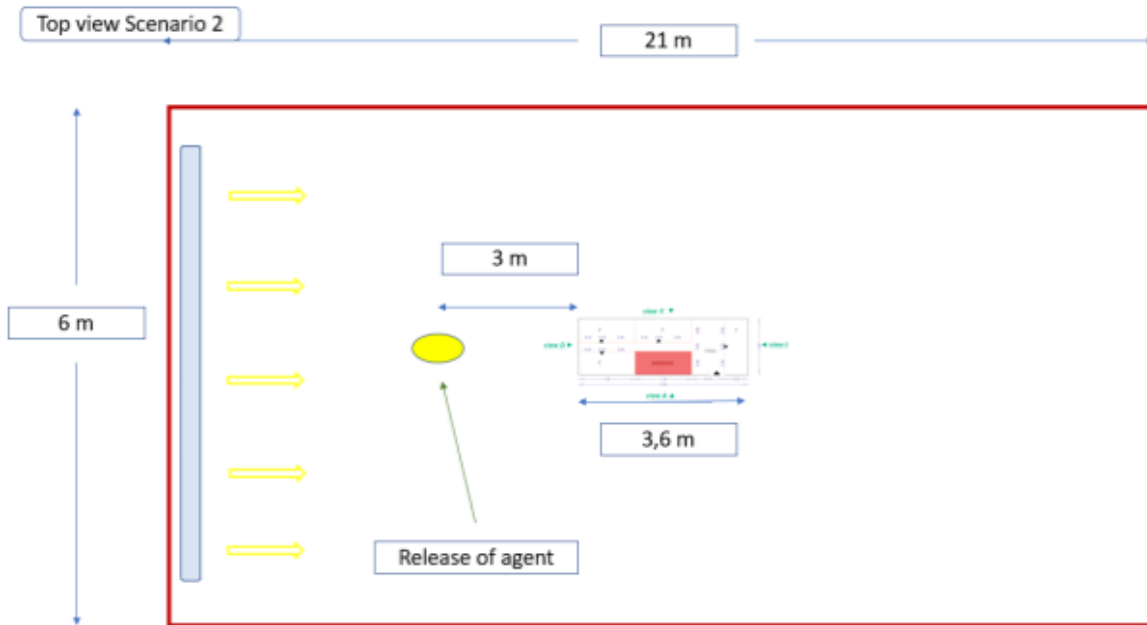


**Figure 35.** Positioning of the external release in the wind tunnel

## LOWER FLOOR    TOP VIEWS

### LEVEL 0,00

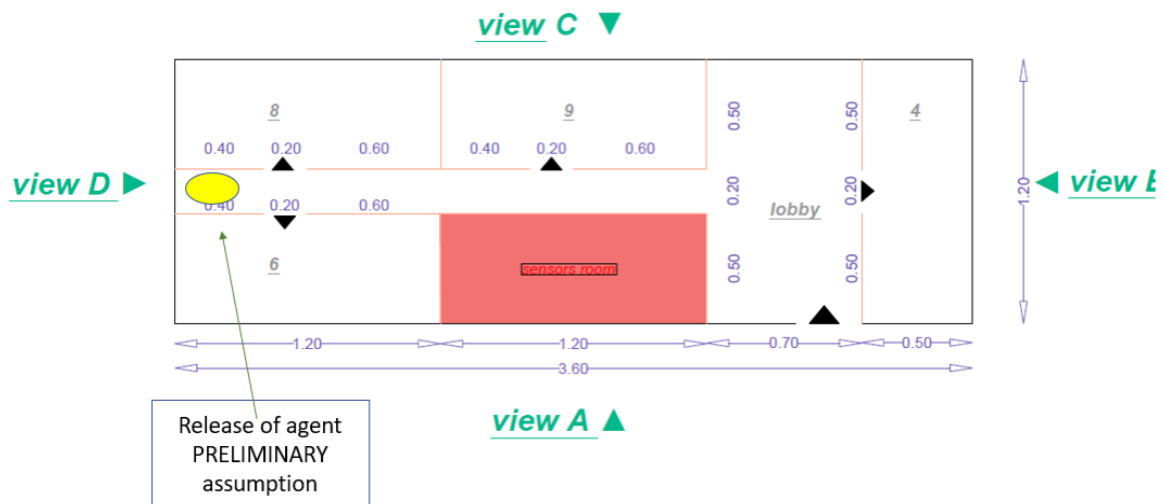


**Figure 36.** Positioning of the internal release

### **3.1.1.1 Implementation of the aeraulic simulations**

As mentioned above, the CFD simulations have been implemented using the open-source software Code\_Saturne that is developed by the R&D of EDF (the French electricity board) and the CEREa at the "École des Ponts-et-Chaussées" (Paris, France). The elaboration of the geometry and mesh has been performed with Ansa<sup>4</sup> software and the

<sup>4</sup> <https://www.ansa-usa.com/software/ansa/>

post-processing of the results with Paraview<sup>5</sup> software.

In order to evaluate the sensitivity of the flow numerical solution to the mesh type and the spatial discretization, several meshes were tested and compared. Then, the mesh considered as the most suitable for the problem was selected and used in the rest of the numerical study.

### **Generation of the 3D digital mock-up**

The 3D geometry of the mock-up was elaborated from the 2D plans provided to the modelers. It is conformed to the Plexiglas® mock-up. The small building mock-up consists of an upper part and a lower part (Figure 37).

In the low-rise building, there is a ground floor and a second floor with four rooms per level, one of which, on the ground floor, is condemned to place sensor equipment. One corridor per level serves the different rooms. The two levels communicate by a staircase represented by a hole in the floor in the digital mock-up as in the Plexiglas® mock-up. The air inlets are located in the two upstairs rooms facing the incident flow and in the central corridor.

In the high-rise building, the rooms are twice as high as in the low-rise building. There are also two levels communicating by a staircase represented by a hole in the floor in the digital mock-up as in the Plexiglas® mock-up. On the ground floor, there is a lobby and a room. Upstairs, two large rooms on either side of the stairwell and a much smaller central room take up the space.

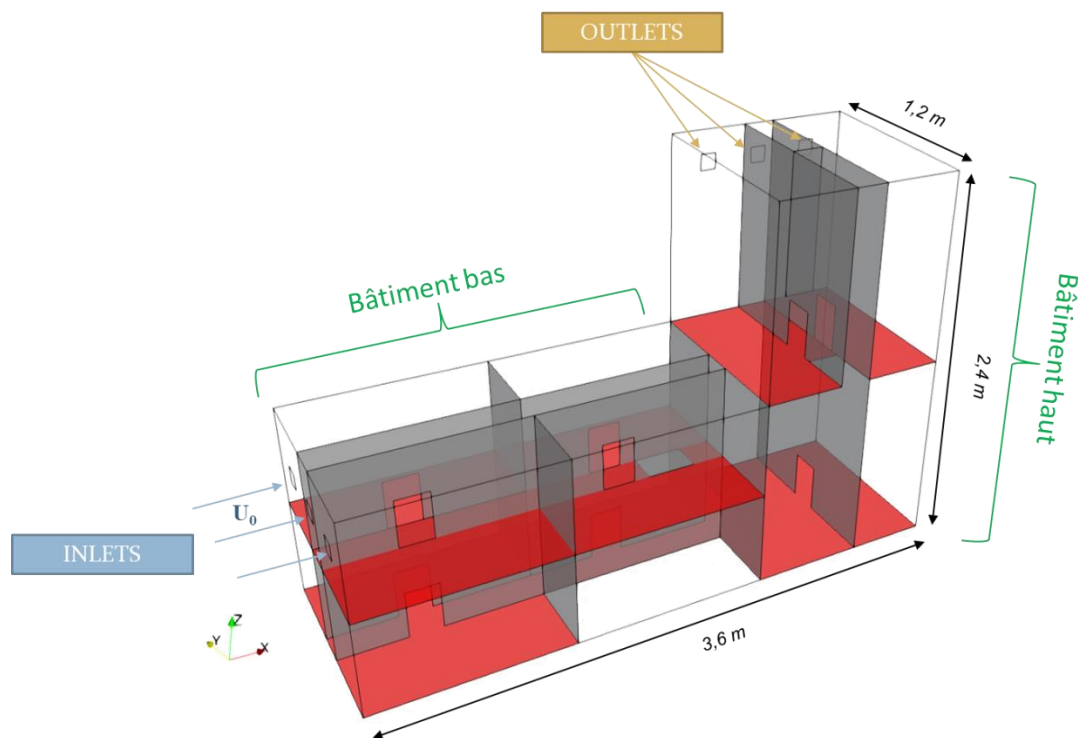


**Figure 37.** Geometry of the mock-up consisting in a low-rise building and a high-rise building

### **Boundary conditions, solvers and meshing options**

Without preliminary knowledge on the part of the experimenters of the air flow in the wind tunnel, it was decided not to consider it and to perform simulations of the flow only inside the mock-up. Thus, it was necessary to set the boundary conditions for the entry

<sup>5</sup> <https://www.paraview.org/>

of air into the mock-up. The outlets were considered to be in direct contact with the outside atmosphere.

For the simulations presented below, the following boundary conditions were defined:

- The air velocity at the inlets is  $V_{\text{inlet}} = U_0 = 1.0 \text{ m.s}^{-1}$ ;
- The static pressure at the outlets is  $P_{\text{outlet}} = P_{\text{atm}}$ .

First of all, it has to be pointed out that 3D flow in the mock-up (as the flow in a full-scale building) may not admit a stationary solution. It is even more likely that the 3D flow is unsteady. Yet, a steady simulation is easier to handle and its results are easier to present and compare with measurements. It is also anticipated that even if the “real” flow in the mock-up is unsteady, the stationary solution should be representative of the flow pattern in the mock-up. Thus, for the sake of simplicity, it was decided to seek for a stationary flow solution.

A Computational Fluid Dynamics problem implies a mathematical solver for the numerical resolution of the Navier-Stokes equations. It implies an iterative process that requires a stop criterion when the converged state of the solution is reached. In case of a stationary flow, the velocity and pressure fields no longer change with additional iterations of the solver. In the mock-up study, two stationary solvers of Code\_Saturne were implemented and their parameters adapted.

The turbulence was evaluated using a RANS  $k-\epsilon$  model as it generally quickly produces correct results for fluid mechanics problems in confined environments. Yet, it is worth noticing that more precise and informative turbulence models could have been used for a higher computational cost.

Four meshes (Figure 38) were generated with different cell types and sizes (Table 9). The study related to the meshes had the main objective to calculate a converged stationary flow solution with a mesh having a moderate number of cells.

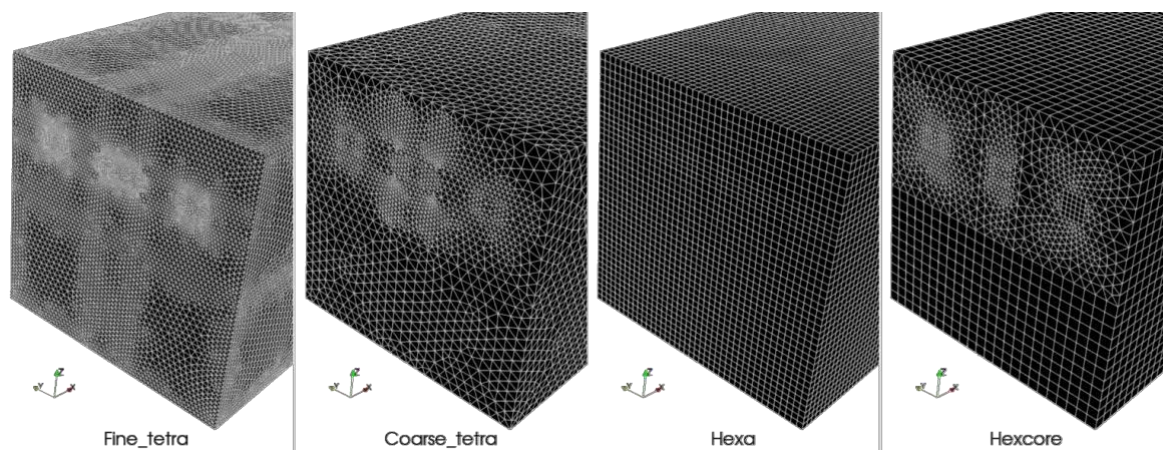


**Figure 38.** View of the four tested meshes

**Table 9.** Characteristics of the four tested meshes

Name of the mesh	Fine_tetra	Coarse_tetra	Hexa	Hexcore
Type of the cells	Tetrahedra	Tetrahedra	Hexahedra	Tetra / hexahedra

<b>Average cell size</b>	1-4 cm	2-6 cm	3 cm	2-5 cm
<b>Total number of cells</b>	2,146,518	457,853	252,080	71,259

Thereafter, the velocity fields computed on the different meshes are shown in a 2D vertical section plane of the mock-up (Figure 39). In first intention, the stationary solver "by default" of Code\_Saturne was used with a relaxation coefficient of the equations equal to 0.7. The velocity in the 2D vertical section plane is presented for the four meshes (Figure 40).

It is noticeable in Figure 40 that the overall results are similar with more marked numerical diffusion effects on the air jets for the coarsest mesh (Hexcore). However, the results are relatively different in the lower velocity zones such as the recirculation zones created by the shears with the fast jets.

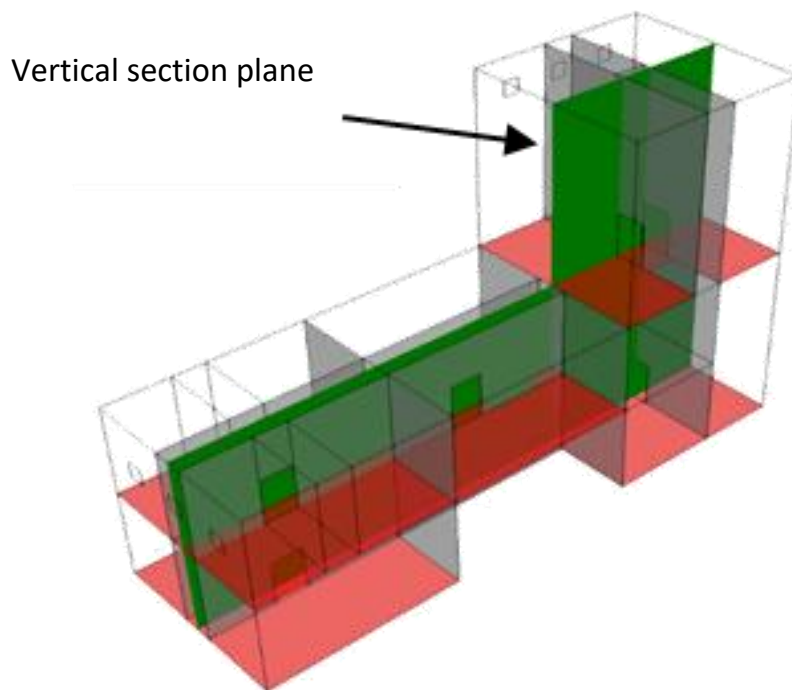


**Figure 39.** View of the vertical section plane across the mock-up

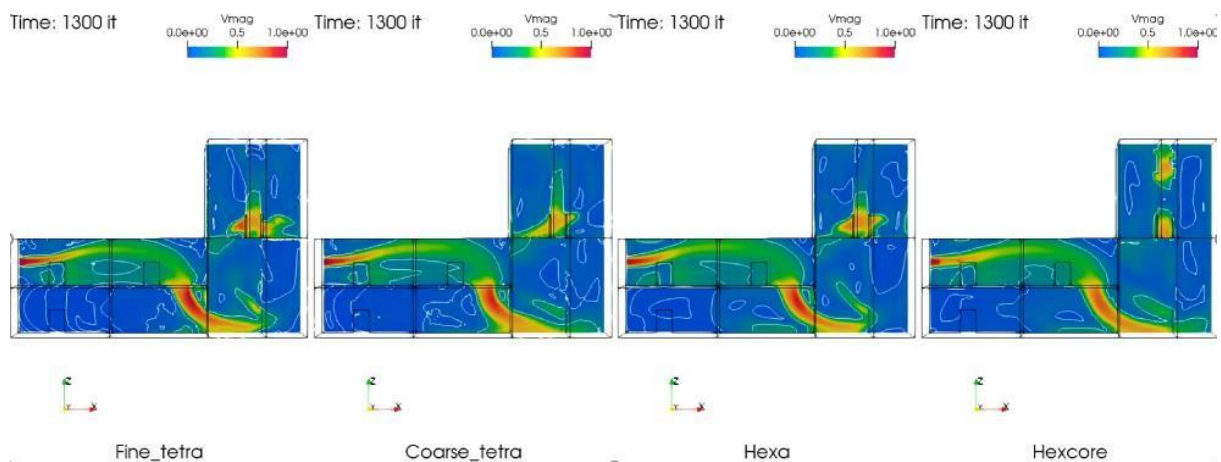


**Figure 40.** 2D velocity fields in a vertical section plane. Results for the four meshes

When the velocity results are visualized dynamically along with the numerical iterations, it becomes apparent that the chosen solver leads to an unstable solution whatever the mesh used, in particular in the corridor of the ground floor, which is the zone envisaged to perform the internal to the mock-up release. These instabilities are unsteady turbulent phenomena inherent in the geometry, which make the robust convergence of the flow to a stationary solution difficult. Thus, to stabilize the CFD calculations and make them converge towards a mean stationary solution, we used another solver of Code\_Saturne adapted to a “quasi-stationary” resolution. With this solver, the time step varies in time and space around a reference ( $dt_{ref} = 0.05$  s) while respecting a criterion of numerical stability ( $CFL < 5$ ). Moreover, the time step is relaxed until the convergence towards a numerically stable solution.

Using the quasi-stationary solver, an overall stabilization of the air flow is observed, in particular in the previously unstable zone of the corridor on the ground floor (Figure 41).

The four meshes produce very similar results, the two tetrahedral meshes still exhibiting instabilities with the chosen parameters. It is probable that the search for suitable sets of parameters would stabilize these two calculations as well. Two of the meshes, Hexa and Hexcore, converge towards almost stationary solutions in the sense that the velocity no longer changes in almost the entire domain. The two solutions are quite close to each other, the Hexcore mesh being more subject to numerical diffusion than the Hexa mesh. This is an expected effect of the relatively low resolution in space, in particular at the level of the jets coming from the air inlets.

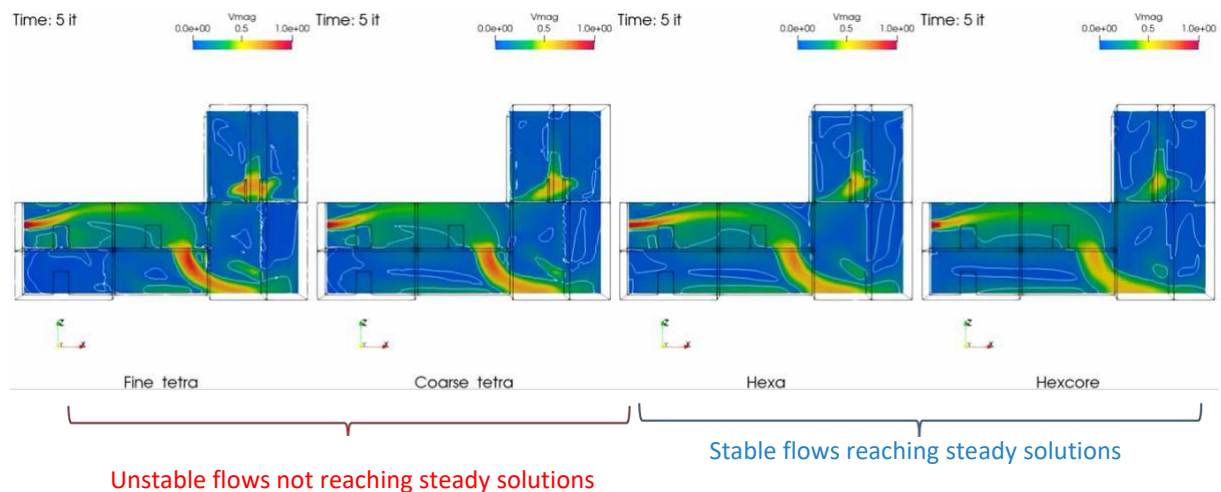


**Figure 41.** Influence of the four meshes on the convergence of the velocity field

Finally, the hexahedral mesh (Hexa case) was kept and numerical parameters were fitted to obtain a stable stationary flow solution in view of the dispersion simulations to be carried out. In these conditions, the velocity field and the velocity vectors are shown in different section planes in Figure 42, Figure 43 and Figure 44. The streamlines are also presented in Figure 45. It is interesting to note that the air jets coming from the openings in the mock-up upstream wall generate high-velocity recirculation in the rooms and the corridor at the second floor of the low-rise building. The area on the ground floor of the low-rise building is generally much less ventilated than the upper floor of this building and the high-rise building.

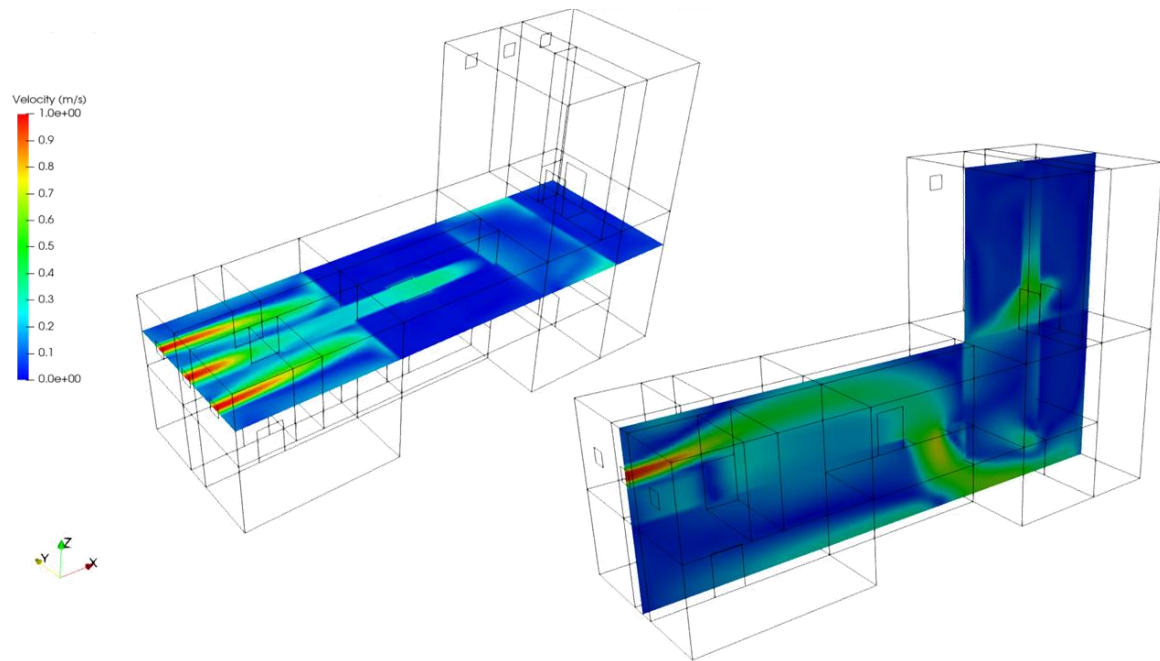


**Figure 42.** Velocity field in two section planes across the mock-up

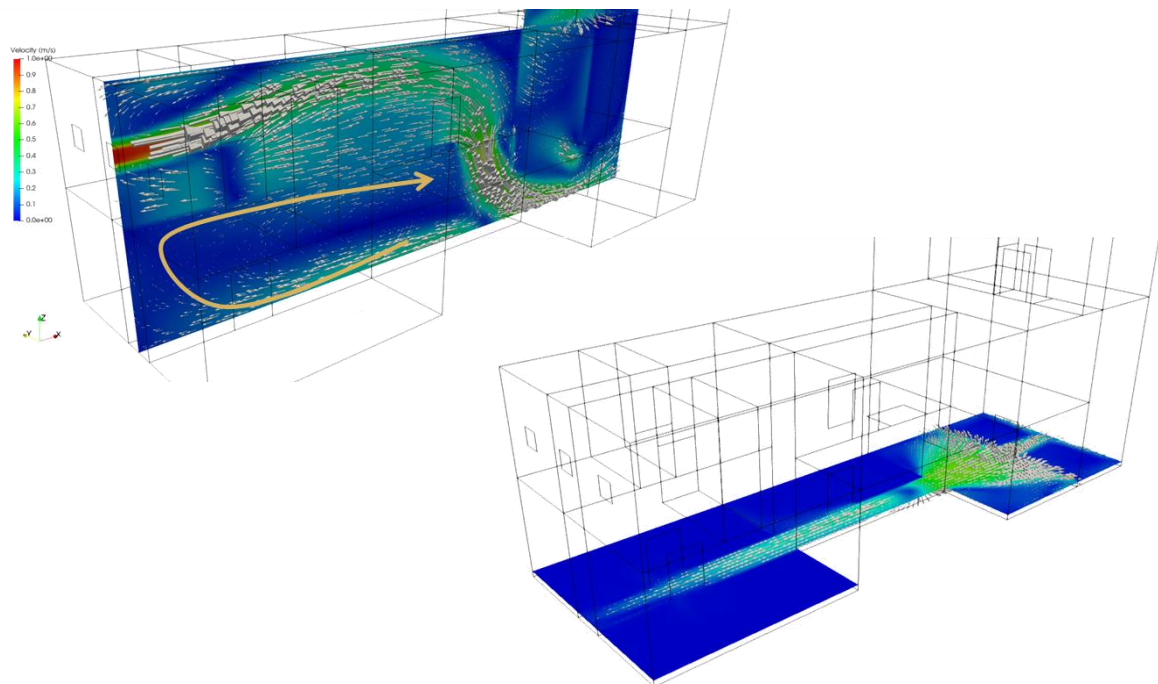


**Figure 43.** Velocity field and velocity vectors in two section planes of the lower building

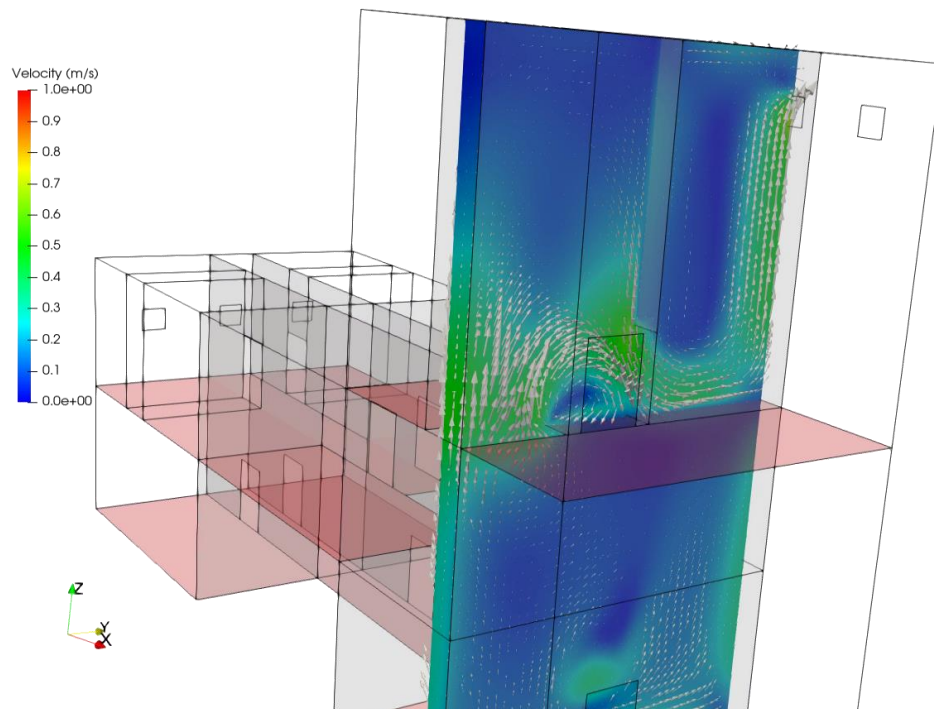


**Figure 44.** Velocity field and velocity vectors in a section plane of the higher building

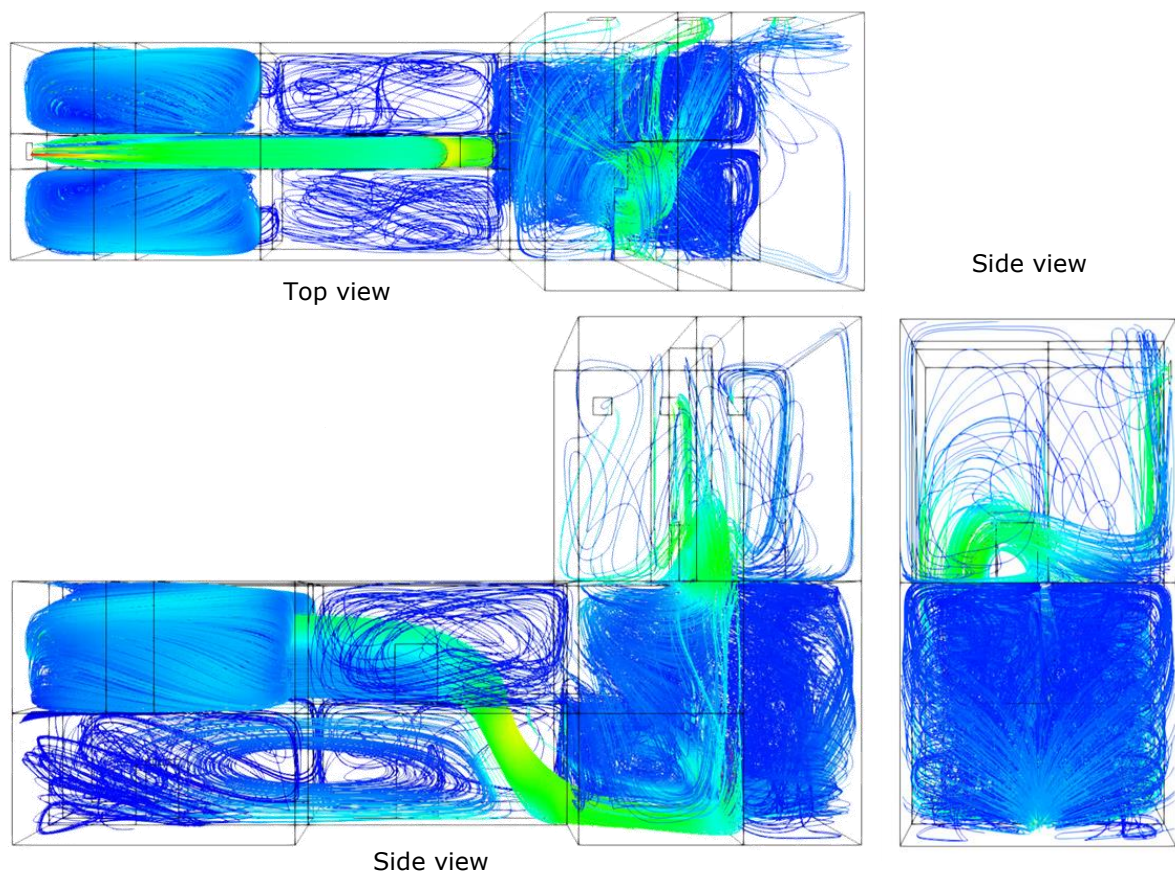


**Figure 45.** Streamlines in the mock-up

### 3.1.1.2 Dispersion simulation of chemical releases

#### *Case-studies for the releases*

Thereafter, two test-cases of dispersion simulations internal to the mock-up are considered:

- The **first test-case** is associated with a release located **outside** the mock-up upstream of the flow;
- the **second test-case** with a release located **inside** the mock-up.

The parameters of these 3D simulations, namely the air inlet velocity and the characteristics of the release (amplitude and duration) could be changed according to the experimental conditions.

#### **Release from the exterior of the mock-up (First test-case)**

The first test-case corresponds to the dispersion of a chemical released out of the mock-up upstream of the flow at a sufficient distance so that the concentration of the chemical entering the mock-up is supposed to be uniform.

An unsteady transport equation is solved for a scalar "C" representing the volumetric concentration of the chemical. The stationary velocity field computed previously is used for this simulation.

The initial concentration of the chemical is zero in the whole simulation domain. At  $t = 0$ , it becomes non-zero on the three air inlets (Figure 46). The boundary condition for the scalar C takes the value  $C_0 = 1$  for 60 seconds before returning to zero. The evolution of the concentration in the mock-up is computed for 1,400 seconds.

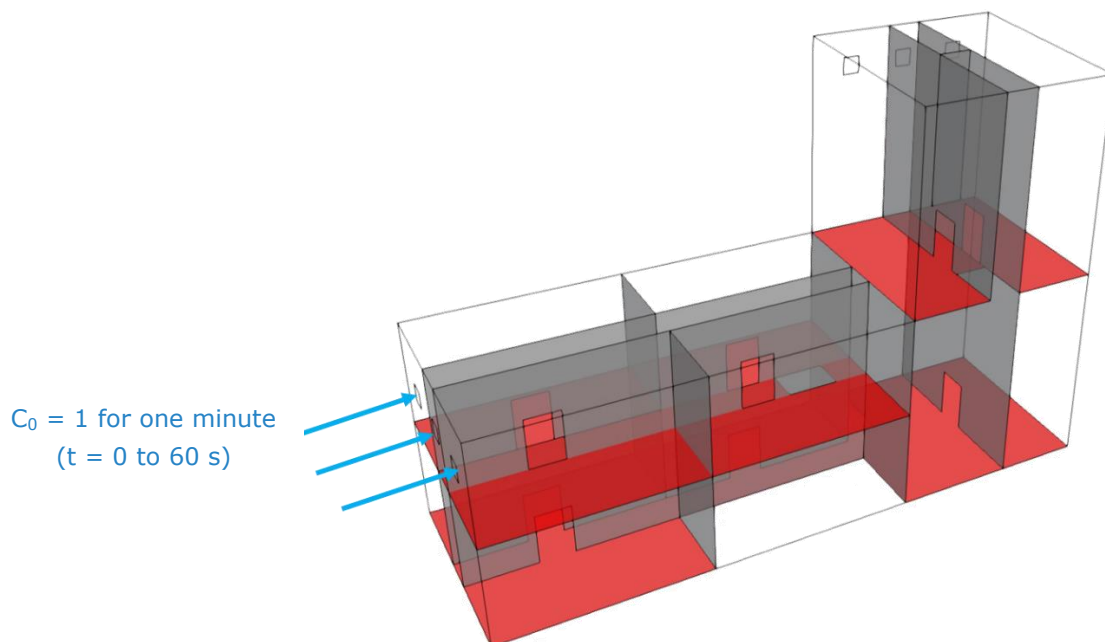


**Figure 46.** First test-case – Boundary condition for the concentration at the mock-up inlets  $C_0 = 1$  for one minute ( $t = 0$  to 60 s)

As the dispersion simulation is unsteady by nature, the 3D results must be analysed dynamically. Two successive phases in the simulation may be highlighted: the actual dispersion for 60 seconds then the purging of the system.

The following Figures show the concentration of the chemical at different times:

- Figure 47 presents the chemical plume delimited by the concentration  $C = 0.1$  at  $t = 8$  s, i.e. at the start of the dispersion process; the upstairs side rooms fill up first as the plume moves faster down the hall;
- Figure 48 presents the chemical concentration in a vertical section plane across the mock-up at  $t = 53.2$  s; the filling process and the preferential path taken by the chemical are clearly visualized;
- Figure 49 presents the chemical concentration in a vertical section plane across the mock-up at  $t = 74.2$  s; the mock-up is purged by the injection of fresh air into the small building.

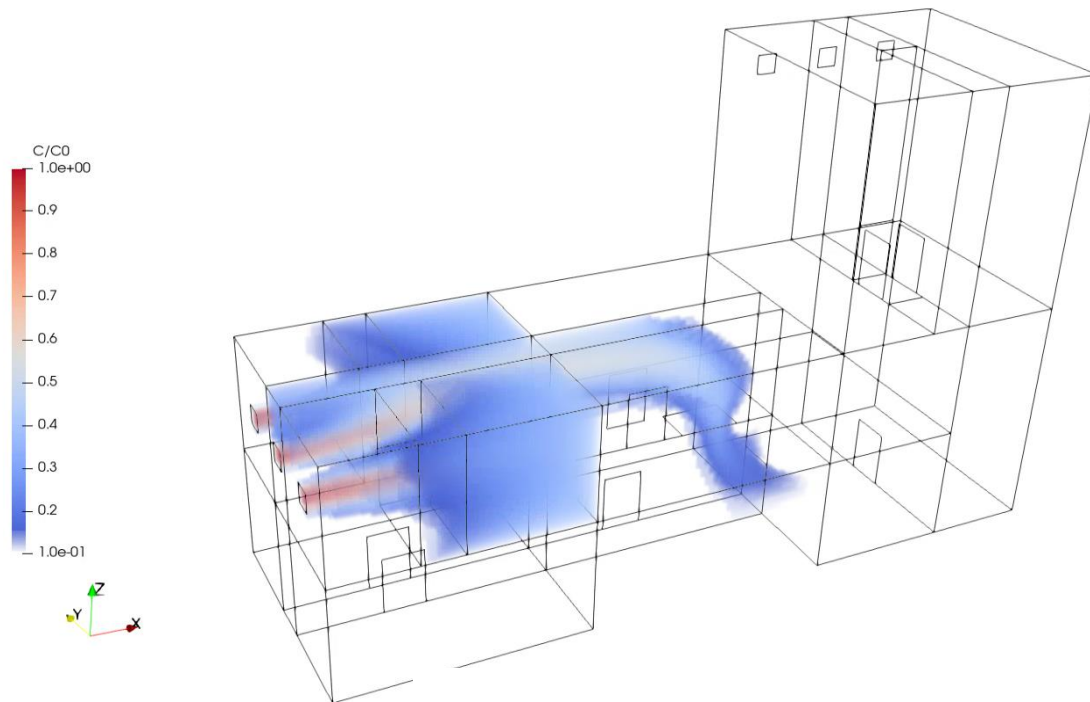


**Figure 47.** First test-case – Chemical cloud delimited by the concentration  $C = 0.1$  at  $t = 8$  s

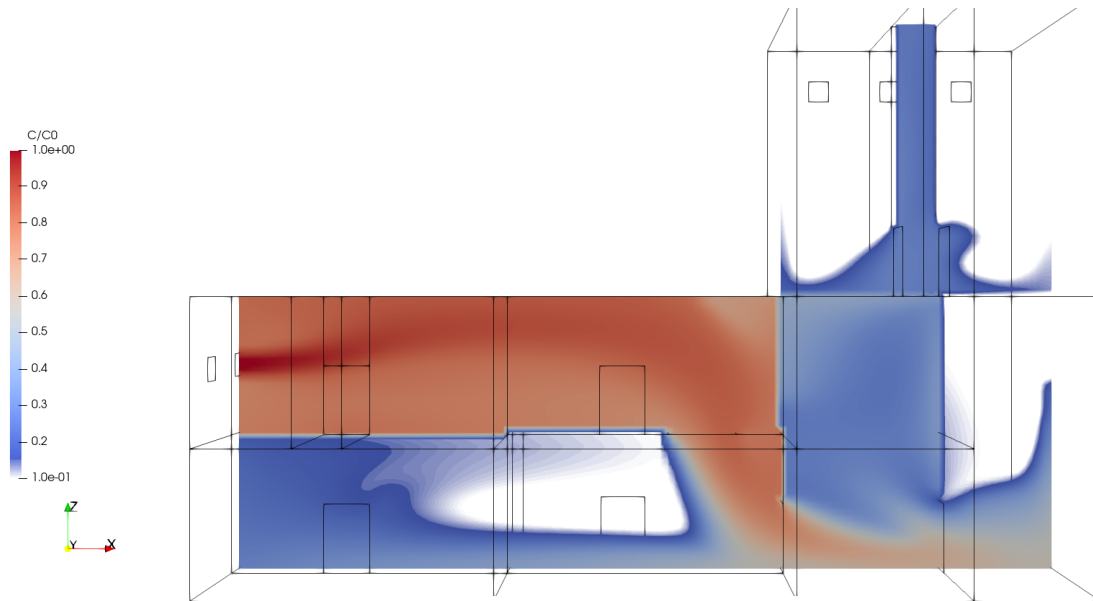


**Figure 48.** First test-case – Chemical volume concentration in a vertical section plane at  $t = 53.2$  s

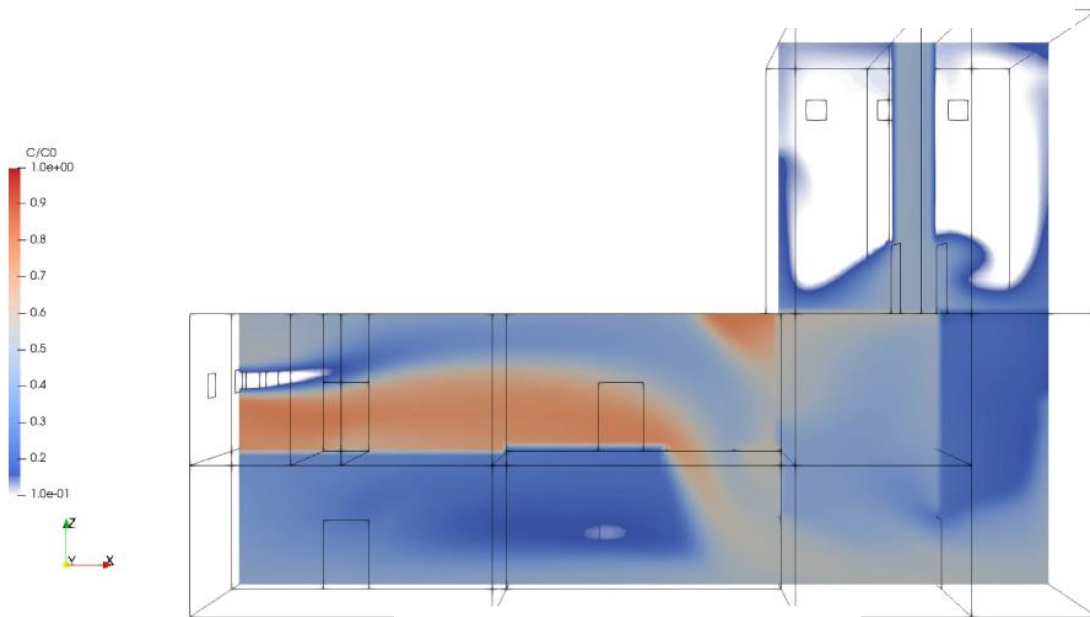


**Figure 49.** First test-case – Chemical volume concentration in a vertical section plane at  $t = 74.2$  s

Figure 50 shows the quantity of the chemical remaining in the mock-up (in blue) and the average concentration of the chemical in the mock-up (in orange, logarithmic scale) over time.

It can be observed that 90% of the chemical is evacuated from the mock-up in 400 seconds, while there are still some cells in the mesh with positive concentrations at the end of the simulation ( $t = 1,400$  s). Likewise, the average concentration does not reach zero, even if it becomes very low at the end of the simulation.

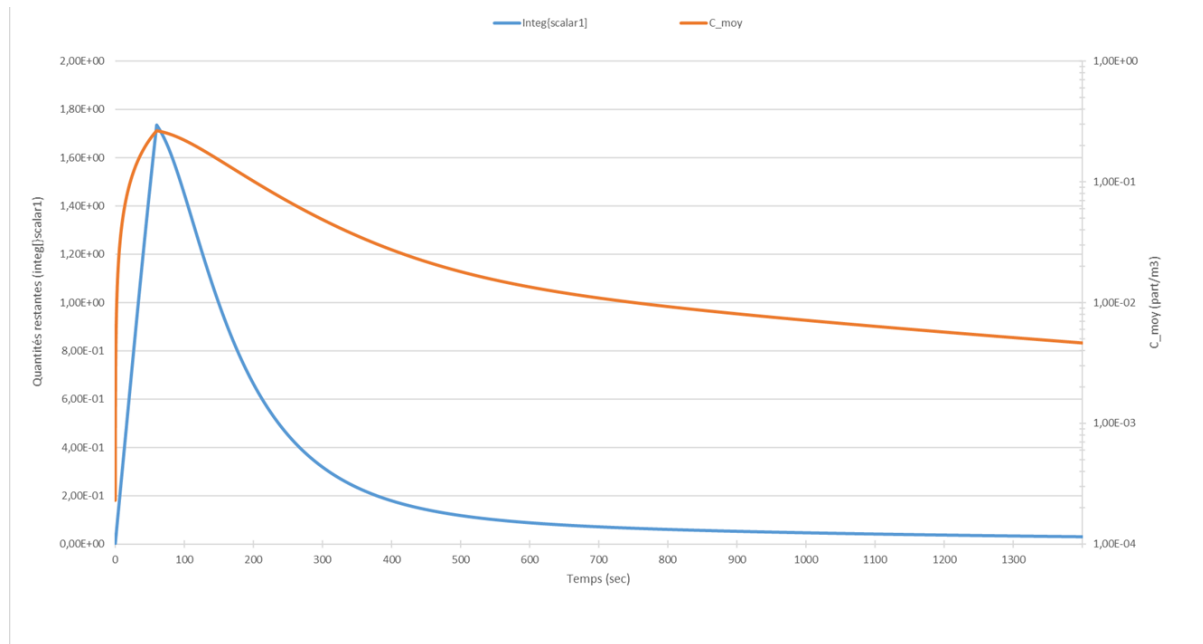


**Figure 50.** First test-case – Quantity of the chemical in the mock-up (in blue) and average concentration of chemical in the mock-up (in orange, logarithmic scale) over time

### ***Release from inside the building (Second test-case)***

The second test-case corresponds to the dispersion of a chemical from inside the mock-up, and more precisely from the corridor of the ground floor.

As previously, an unsteady transport equation is solved for a scalar “C” representing the volumetric concentration of the chemical emitted from a volume source. Again, the stationary velocity field is used for this simulation.

The initial concentration of the chemical is zero in the whole simulation domain. At  $t = 0$ , it becomes non-zero in a cell of the mesh (Figure 51). A unit source term is considered: it could be a unit of mass (e.g. 1 mg). The source term is dispersed for 60 seconds, that is to say  $1.67 \cdot 10^{-2}$  unit per second. The evolution of the concentration in the mock-up is computed for 1,400 seconds.

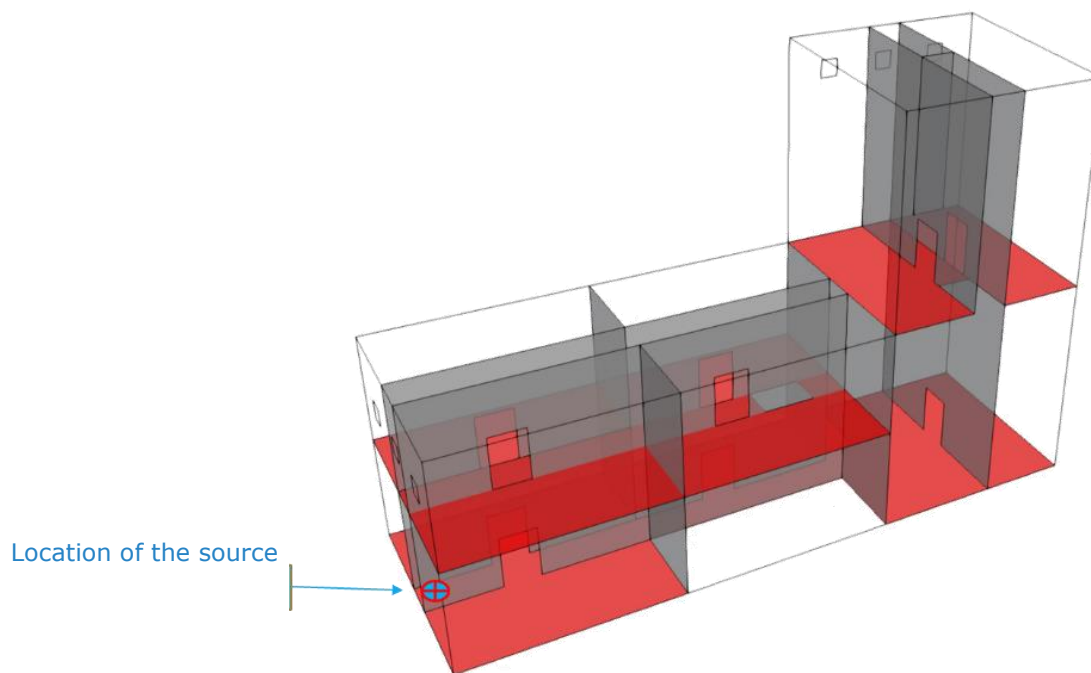


**Figure 51.** Second test-case – Location of the source inside the mock-up in the corridor of the ground floor

As for the first test-case, the dispersion of the chemical plume is unsteady by nature and the results have to be analysed dynamically through animations.

The following Figures show the concentration of the chemical at different times:

- Figure 52 presents the chemical plume delimited by the concentration  $C = 0.01$  at  $t = 43.0$  s; the filling of the corridor of the ground floor in the low-rise building precedes the transfer of the chemical to the lobby of the high-rise building; the side rooms of the ground floor and the first floor of the low-rise building are only slightly or not impacted by dispersal;
- Figure 53 presents the chemical concentration in a vertical section plane across the mock-up at  $t = 51.0$  s; the plume rises above the source and it is entrained into the recirculation cell created in the corridor by the shear with the air jet coming from the floor; this recirculation is represented by the arrow in Figure 43.

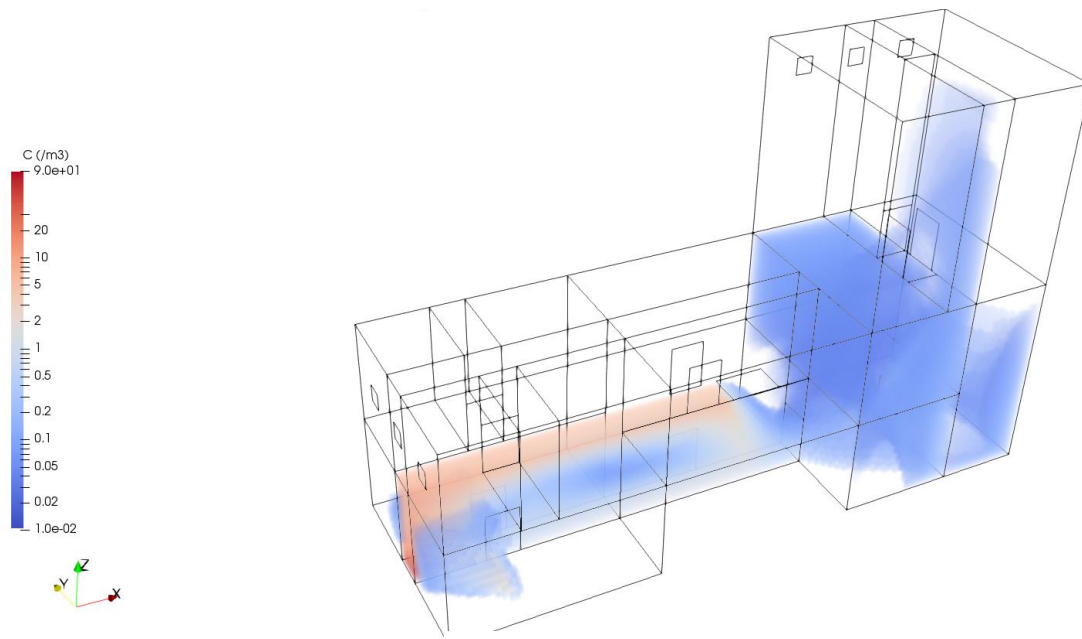


**Figure 52.** Second test-case – Chemical cloud delimited by the concentration  $C = 0.01$  at  $t = 43,0$  s

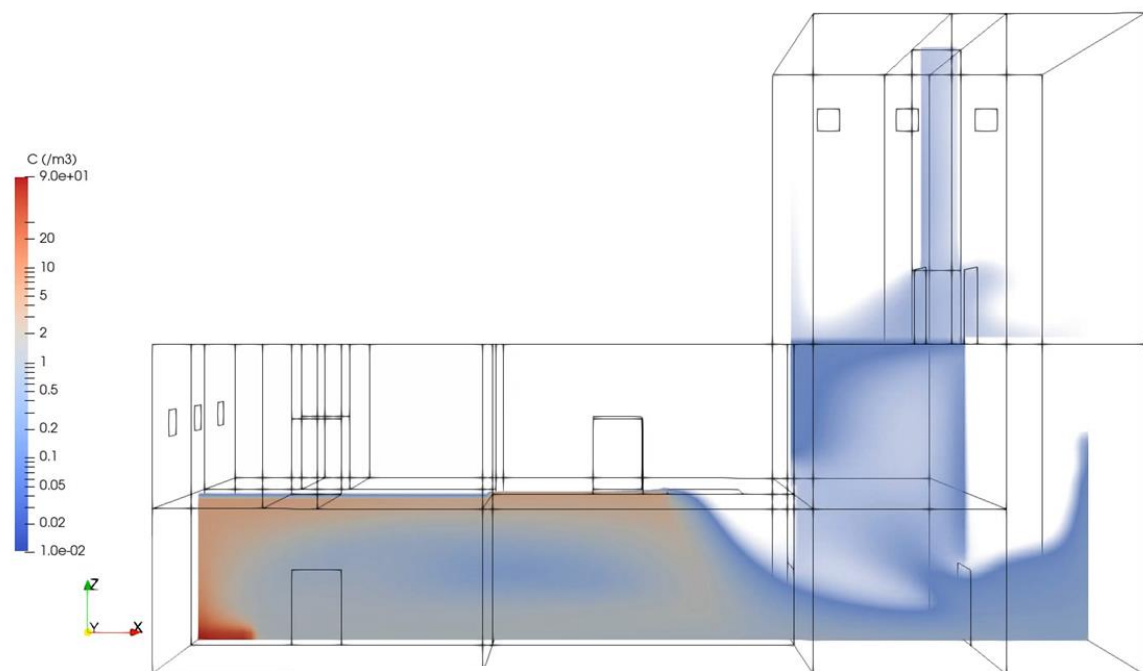


**Figure 53.** Second test-case – Chemical volume concentration in a vertical section plane at  $t = 51,0$  s

Figure 54 shows the quantity of the chemical remaining in the mock-up (in blue) and the average concentration of the chemical in the mock-up (in orange, logarithmic scale) over time. It can be observed that 80% of the chemical is evacuated from the mock-up in 550 seconds, while a significant amount of the chemical remains in the mock-up,

approximately 10% of the total released quantity, at the end of the simulation ( $t = 1,400$  s).

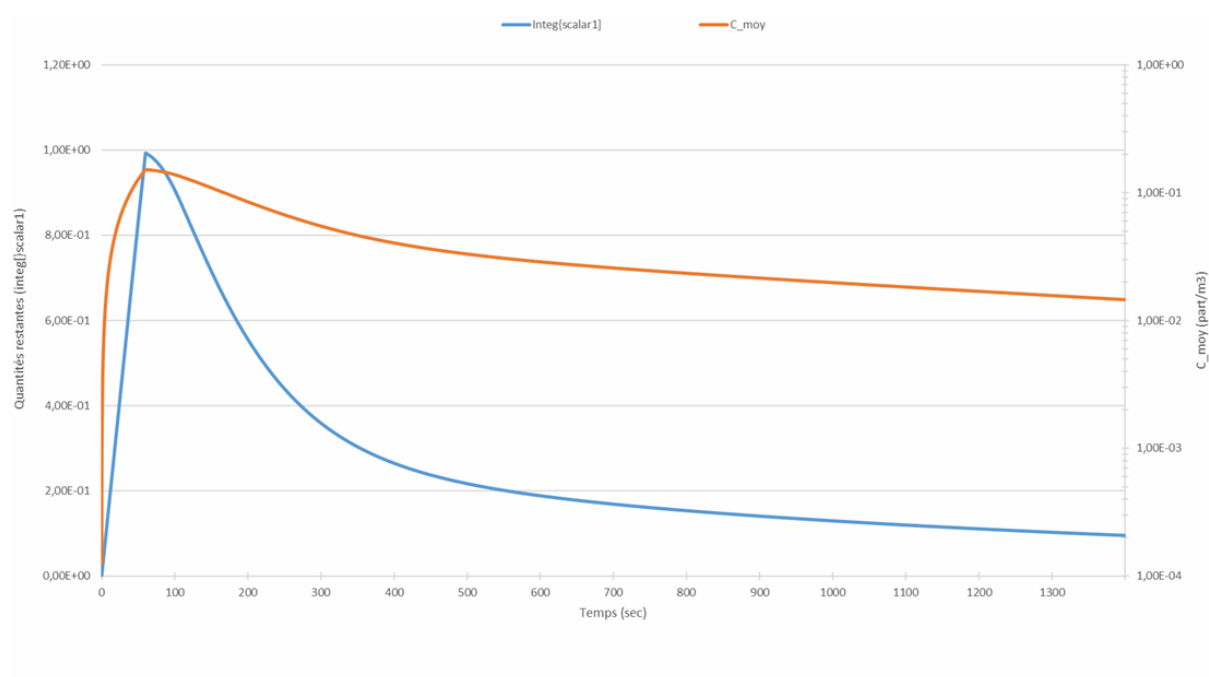


**Figure 54.** Second test-case – Quantity of the chemical remaining in the mock-up (in blue) and average concentration of the chemical in the mock-up (in orange, logarithmic scale) over time

Figure 55 and Figure 56 show the average concentrations over time in the different parts of the mock-up as they are identified in Figure 13.

The highest average concentrations are located in the Corridor 1 and Corridor 2 and in the stairwell on the ground floor of the low-rise building since Corridor 1 is the area where the release takes place. This area has a small volume, what results in a high concentration at this location. The other rooms of the low-rise building impacted by the chemical are Room 6, Room 8 and Room 9. In the high-rise building, all rooms behave similarly and achieve comparable average concentrations.

The comments are identical for the maximum concentrations reached over time in the different parts of the mock-up as presented in Figure 57 and Figure 58.

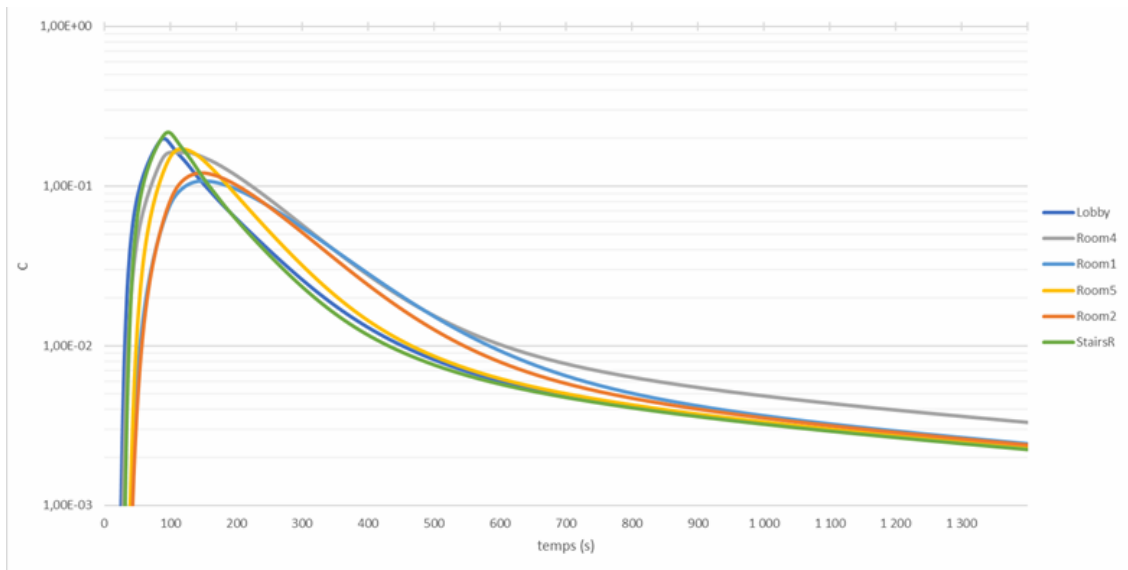


**Figure 55.** Second test-case – Average concentrations in the different rooms of the upper part of the mock-up

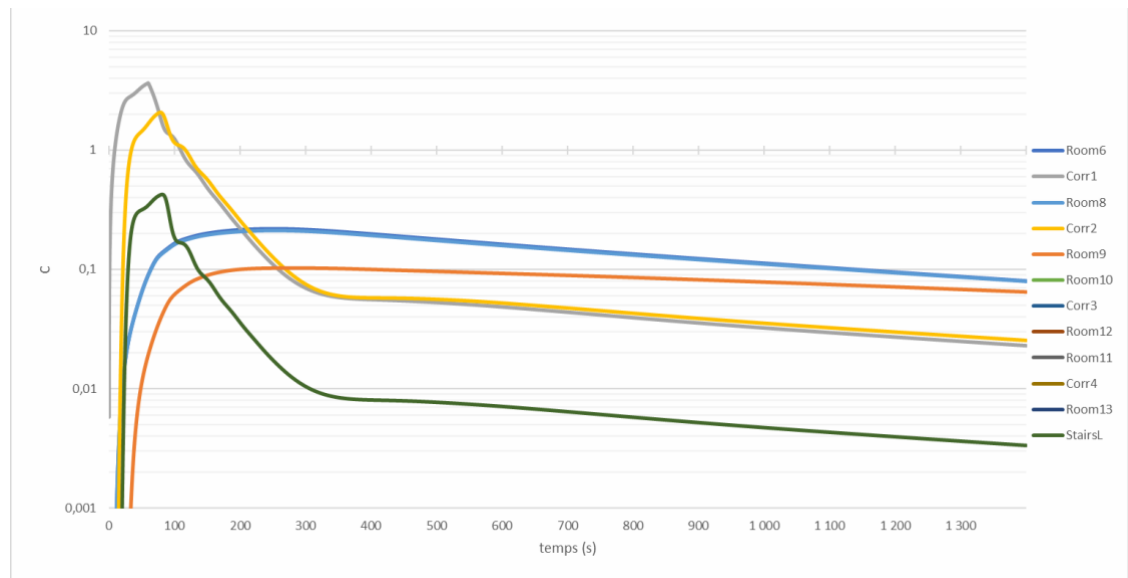


**Figure 56.** Second test-case – Average concentrations in the different rooms of the lower part of the mock-up

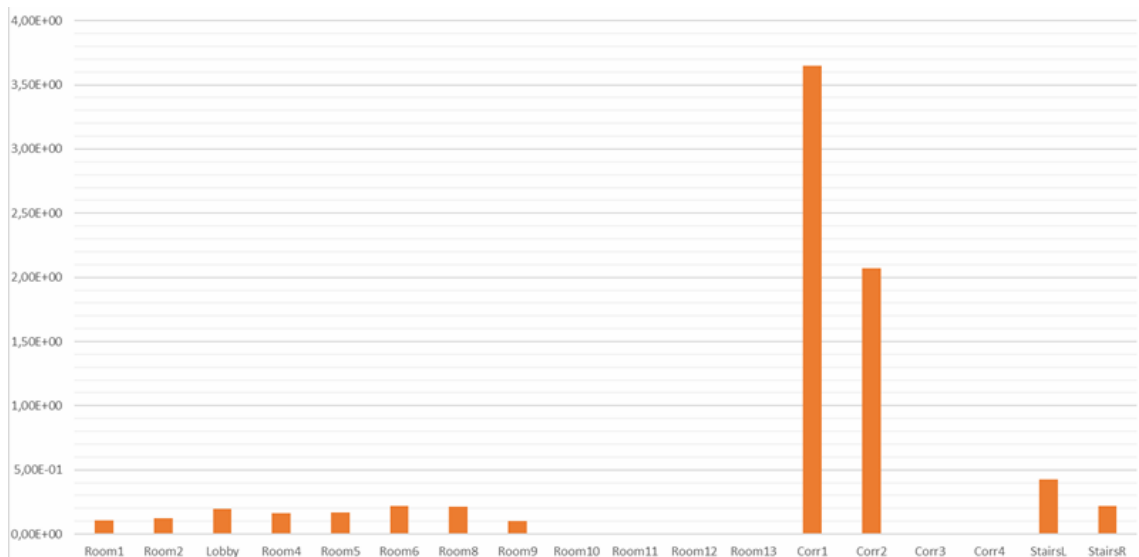


**Figure 57.** Second test-case – Maximum concentrations in the different rooms of the mock-up

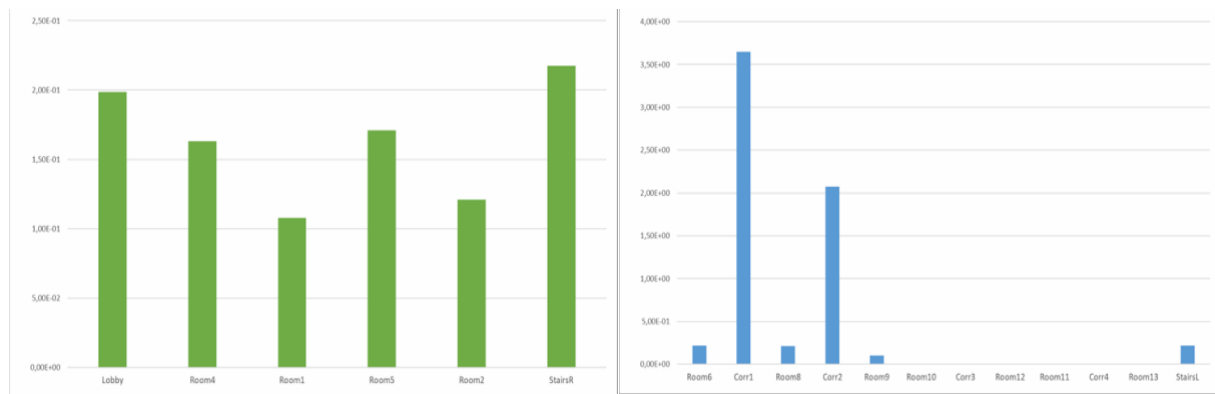


**Figure 58.** Second test-case – Maximum concentrations in the different rooms of the mock-up (on the left: upper part; on the right: lower part)

### 3.1.2 The Post-Experimental Phase

This section presents the second part of the 3D modelling and simulation work carried out after the realization of the experimental trials in the wind tunnel (by TNO in April 2021). As for the preparation of the experiments, the simulations of the actual trials were performed with Code\_Saturne. However, there is a difference as in the following of the report, the digital 3D mock-up includes both the wind tunnel and the small building, itself immersed in the wind tunnel used during the tests (Figure 59).



**Figure 59.** Installation of the small building mock-up in the wind tunnel

### **3.1.2.1 Implementation of aerodynamic simulations**

#### ***Generation of the 3D digital mock-up for the trials***

Both geometries (wind tunnel and small building) were accounted for in the same calculations, with the same overall mesh therefore. The geometry of the small building is shown in Figure 60. The mesh is the same as which was retained for the simulations of the flow and releases in the "indoor only" configuration.

Unlike the simulations carried out to prepare for the experiments, the simulations of the trials couple the inside and outside of the small building. Thus, the inlets and outlets of the previous calculations (small building only) are replaced by openings towards the environment of the wind tunnel.

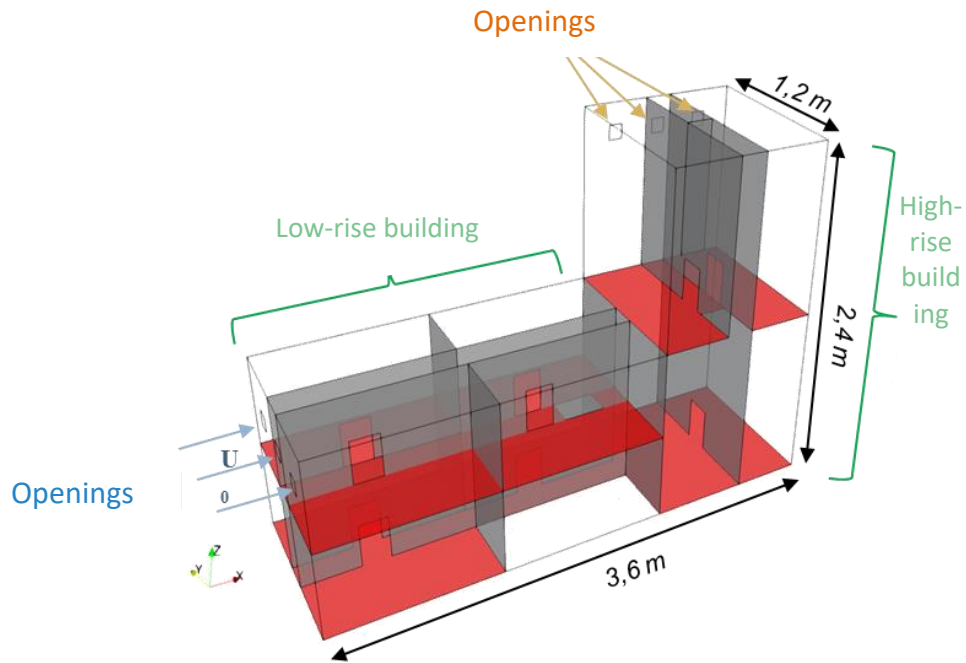
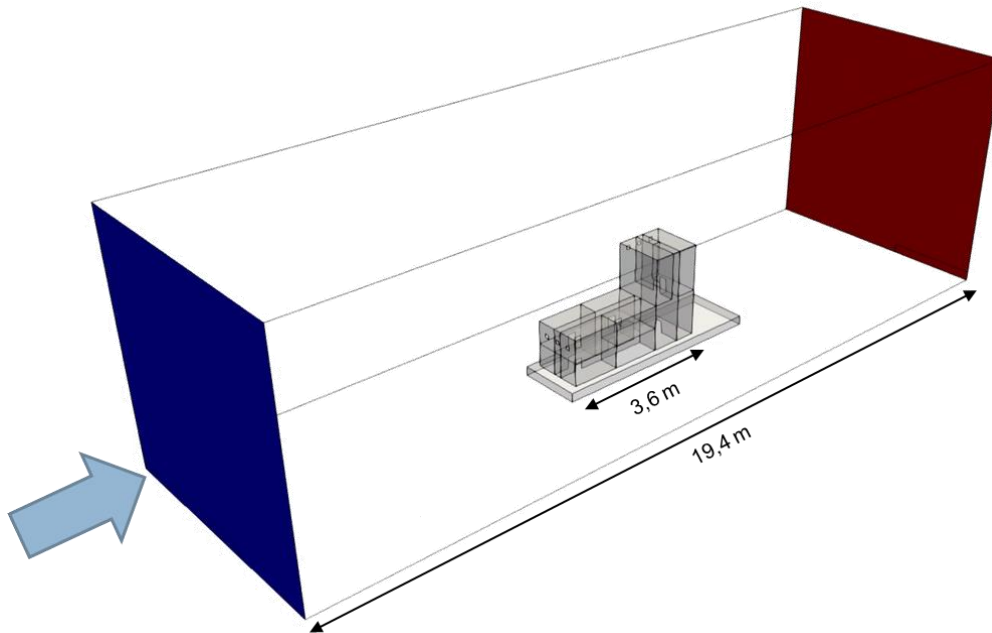


**Figure 60.** Geometry of the small building in the coupled indoor/outdoor configuration

**Table 10.** Characteristics of the small building in the coupled indoor/outdoor configuration

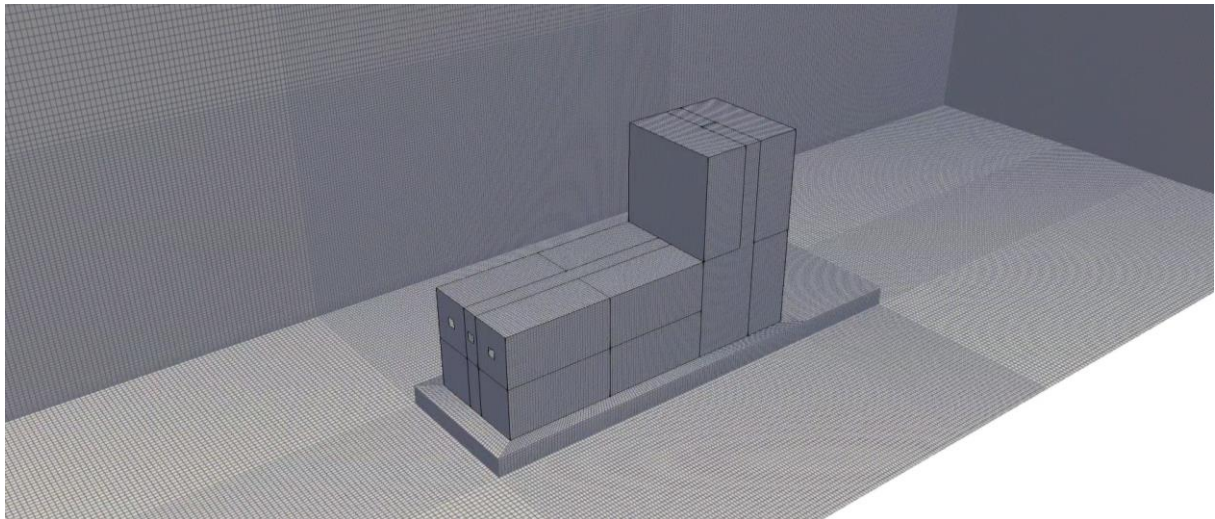
Name of the mesh	Hexa
Type of the cells	Hexahedra
Average size of the cells	3 cm
Total number of cells cellules	252,080

Figure 61 shows the full geometry for the simulations, in which the small building is immersed in the wind tunnel. The latter is represented by a parallelepiped 19.4 m long and 6m x 6m section. The small building is represented on its platform, which is also considered as in the trials. Air flow in the wind tunnel is provided by twenty large fans at the entrance to the wind tunnel.



**Figure 61.** Full geometry of the small building immersed in the wind tunnel in the coupled indoor/outdoor configuration

Figure 62 and Figure 63 present the 3D mesh of the wind tunnel, which was generated with the Ansa software. This is a hexahedral mesh whose cells have a reference size (length of the edges) of 5 cm and 3 cm as close as possible to the building model, in particular at the level of the inlets and outlets. The mesh comprises 7,621,706 cells.



**Figure 62.** Global view of the mesh of the wind tunnel

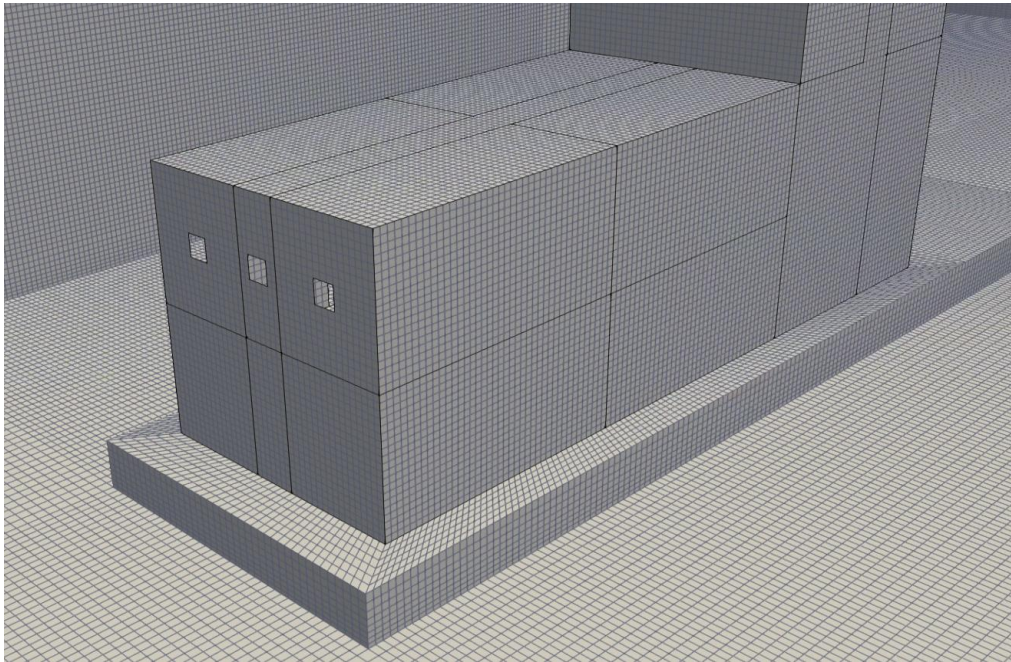


**Figure 63.** Zoom-in view of the mesh of the wind tunnel

### ***Boundary conditions and meshing***

The boundary conditions at the inlet of the wind tunnel are deduced from the data provided by TNO and presented in Figure 64:

- Constant inlet velocity:  $V_{\text{inlet}} = 3.5 \text{ m.s}^{-1}$  ("plug" profile)
- Turbulent intensity deduced from the measurements ( $u'/U$ ):  $I_{\text{turb}} = 15\%$
- Hydraulic diameter:  $D_h = 6 \text{ m}$

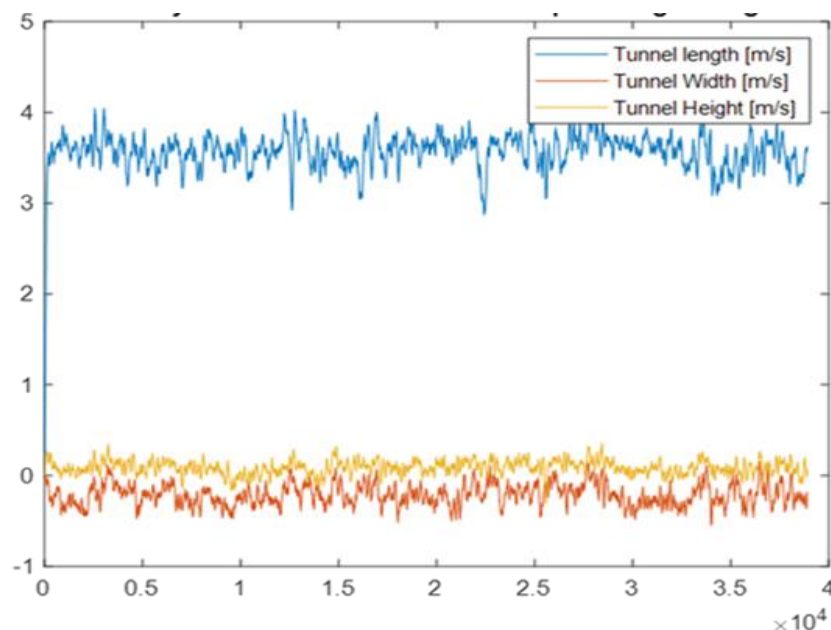


**Figure 64.** Velocity measurements upstream of the small building model in the middle of the wind tunnel

The boundary conditions at the outlet of the wind tunnel are those used typically for this kind of configuration, namely an imposed pressure equal to the atmospheric pressure,

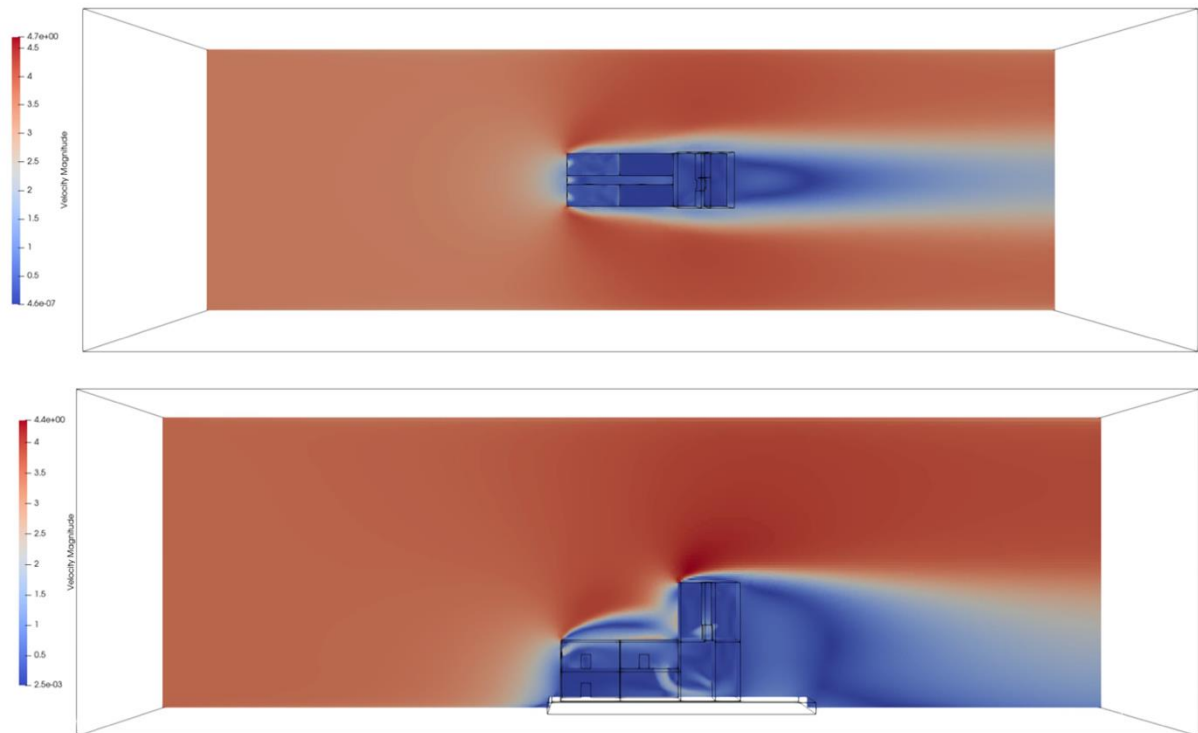
which corresponds to a free outlet in contact with the external atmosphere (called "outlet" in Code\_Saturne).

### Velocity field

The resolution of the stationary velocity field by Code\_Saturne is performed with the "pseudo-steady" solver commented on the previous sub-section, the main parameters of which are presented below:

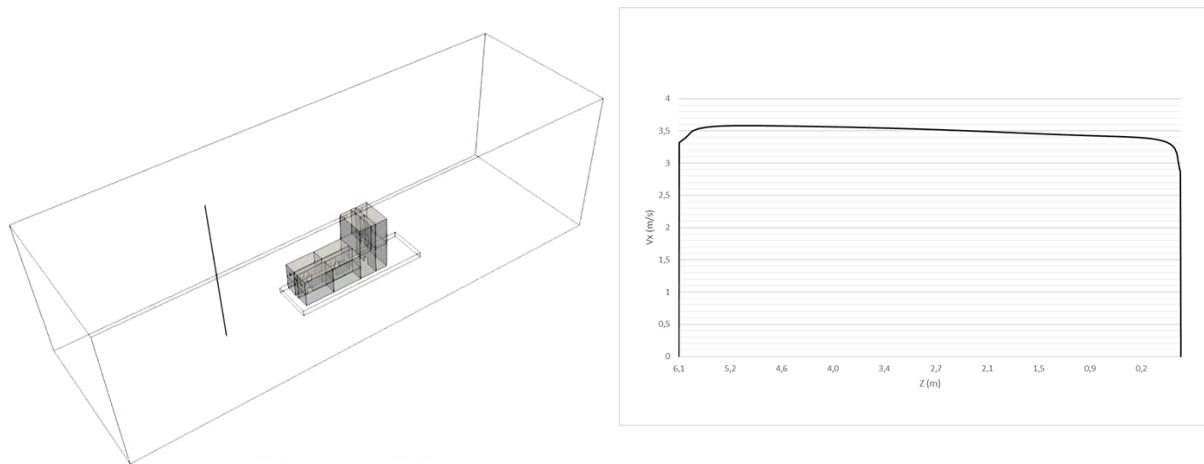
- Code\_Saturne "pseudo-steady" solver;
- Pressure-velocity coupling: SIMPLEC;
- Reference time step: 0.05 s (from 0.005 s to 1.0 s as long as  $CFL < 5$ );
- Outputs / post-processing every 1 second;
- Convergence in 4000 iterations (18 hours on 60 cores of a work station).

Figure 65 shows the velocity field in the horizontal section crossing the air inlets and in the vertical median plane. There is an overall deviation of the air flow due to the presence of the small building in the tunnel. The air is forced to flow between the small building and the walls of the tunnel, which has the effect of accelerating it, whether on the sides or above the small building. At the rear of the small building, one can observe the recirculation of the air flow in a low-pressure zone.



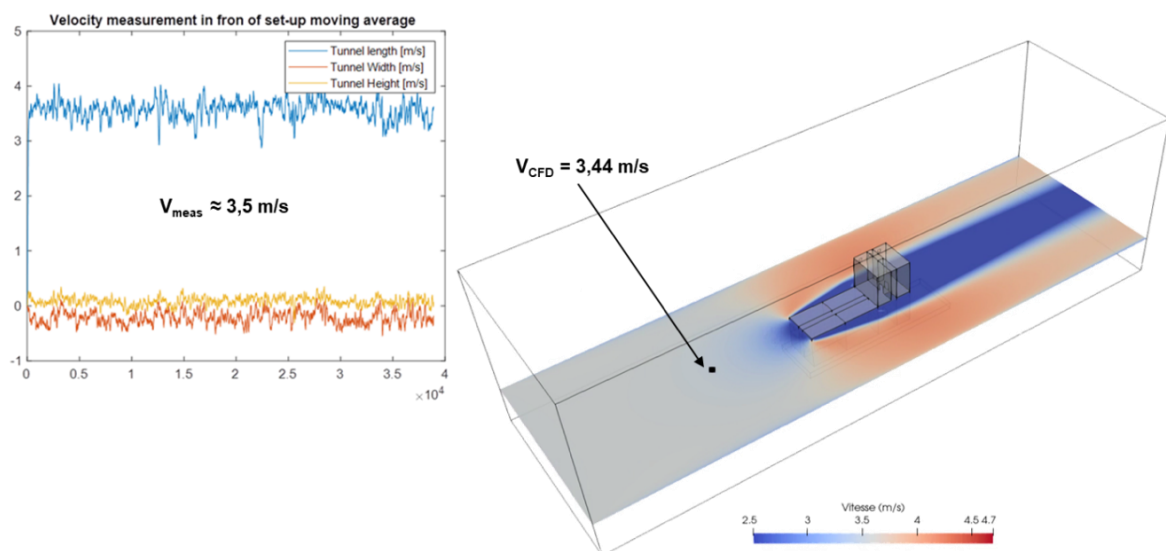
**Figure 65.** Velocity field in the horizontal section crossing the air inlets (top) and in the vertical median plane (bottom)

Figure 66 represents the vertical profile of the air velocity 3 m upstream of the small building. The velocity is almost constant ( $3.5 \text{ m.s}^{-1}$ ). The velocity profile is slightly irregular close to the top of the wind tunnel due to a spatial under-resolution of the upper boundary layer. The lower boundary layer is more finely meshed and the profile is regular.



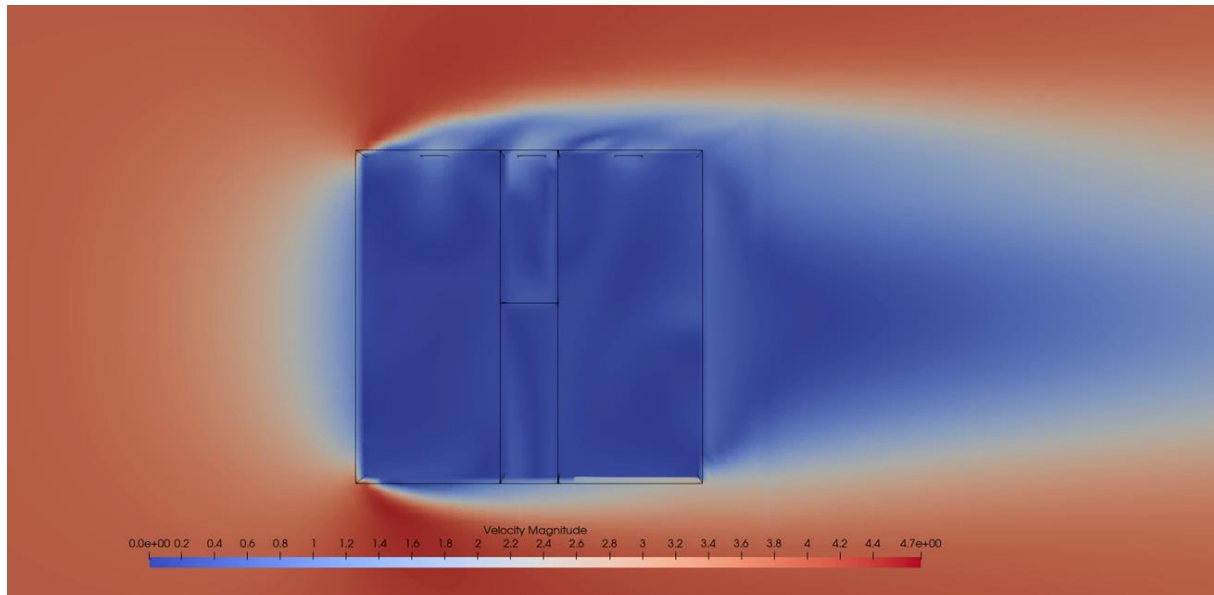
**Figure 66.** Vertical profile of the air velocity upstream the small building

Figure 67 compares the velocity computed by Code\_Saturne with the velocity measured by an anemo-meter at a point located 3 m upstream the small building. Both velocities are close, what demonstrates that the air flow simulated with the CFD model is representative of the air flow in the wind tunnel.

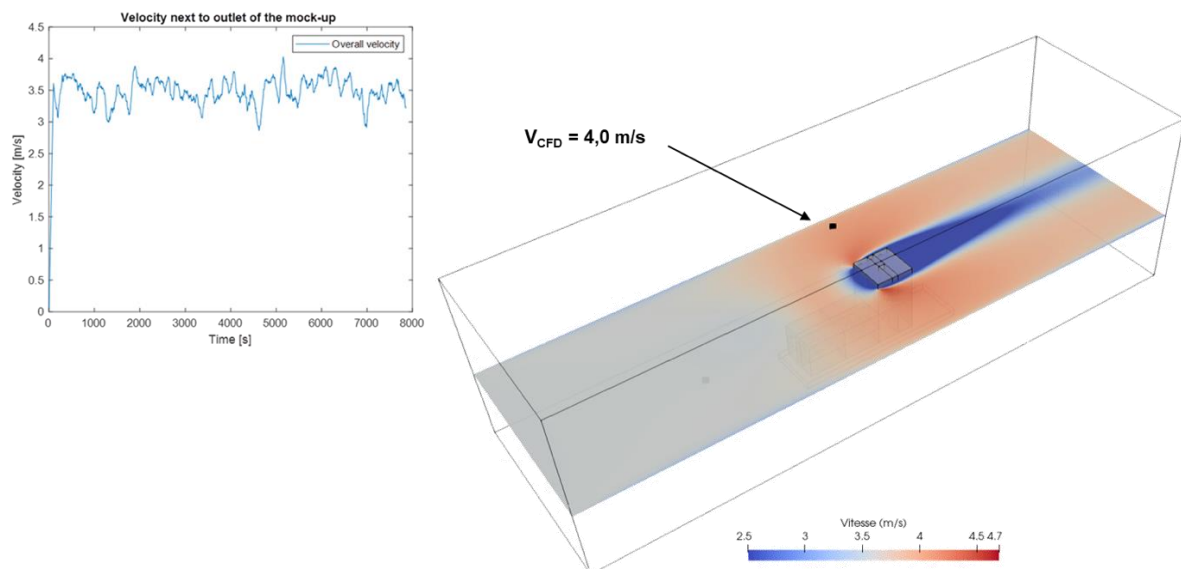


**Figure 67.** Comparison of the measured and computed velocities at a point upstream the small building

Figure 68 and Figure 69 show respectively the velocity field in a horizontal section crossing the small building outlets and the comparison between Code\_Saturne computation and the measurement of the velocity at a point in this cross-section. The simulated velocity is  $4.0 \text{ m.s}^{-1}$ . Due to the acceleration of the flow between the building and the walls of the wind tunnel, this value is higher than upstream in the wind tunnel. One can notice that the computed velocity slightly overestimates (ca.  $0.5 \text{ m.s}^{-1}$ ) the measured velocity. The velocity measured at the point of consideration is identical to that measured upstream of the small building, whereas one should expect a slight over speed as explained before.

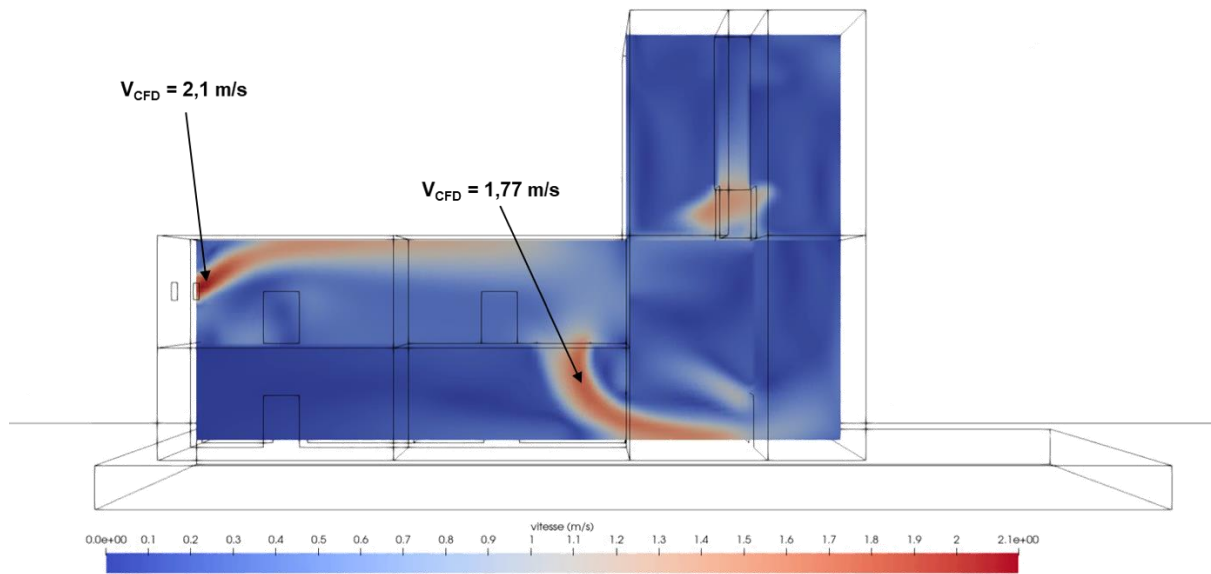


**Figure 68.** Velocity field in a horizontal section crossing the small building outlets

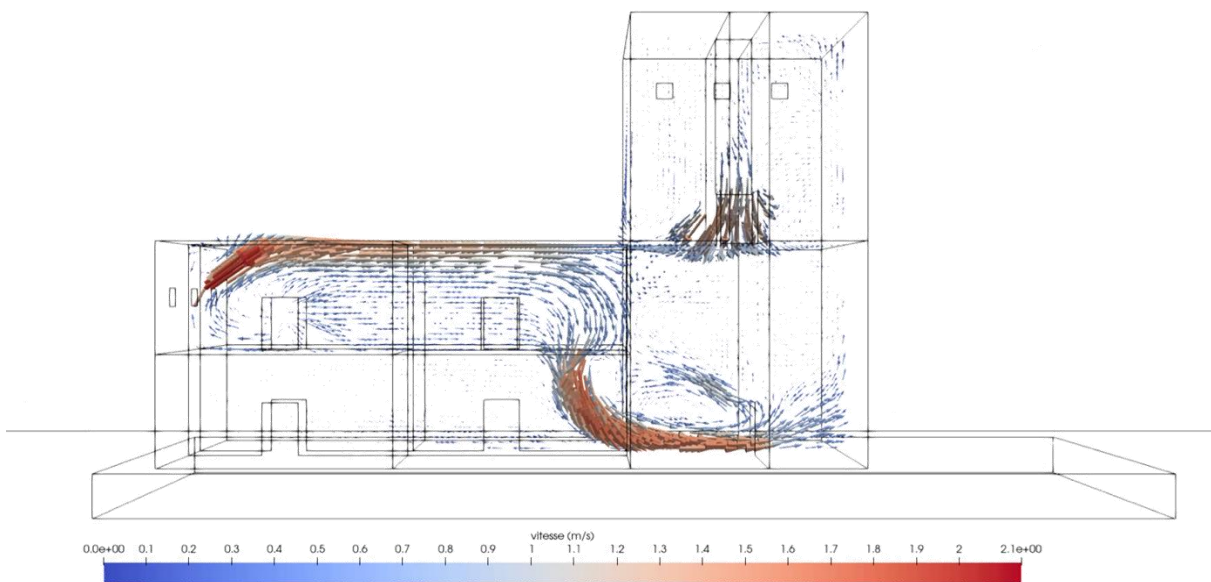


**Figure 69.** Comparison of the measured and computed velocities at a point between the small building and the walls of the wind tunnel

Figure 70 and Figure 71 show respectively the velocity field (in magnitude) and the velocity vectors in the vertical median section plane of the small building. The flow is very similar to that calculated in the building only (indoor calculation) with, however, a higher velocity level in general ( $2.1 \text{ m.s}^{-1}$  in the inlets of the building). The air jets through the inlet openings are deflected upwards. This is an effect of the external air flow which itself is deflected by the platform and building assembly. Inside the building, the configuration of the air flows is similar to the one obtained in the “indoor only” calculation. The velocity of the air flow between the two floors of the low-rise building is  $1.77 \text{ m.s}^{-1}$ . Behind this air jet, there is a very low speed recirculation zone in the downstairs corridor.

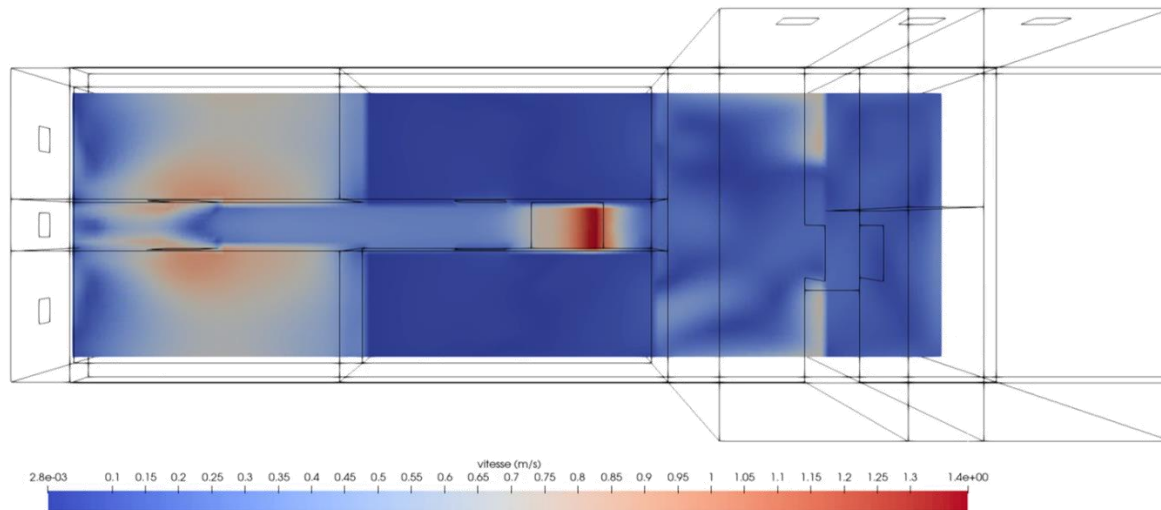


**Figure 70.** Velocity field restricted to the vertical median cross-section through the small building

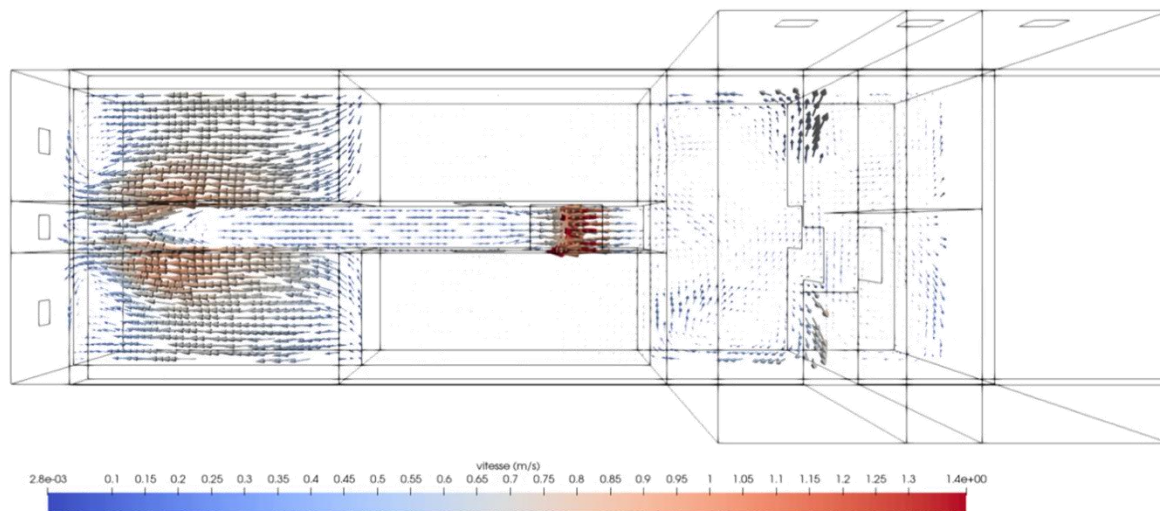


**Figure 71.** Velocity vectors restricted to the vertical median cross-section through the small building

Figure 72 and Figure 73 show respectively the velocity field (in magnitude) and the velocity vectors in the horizontal cross-section located 5 cm above the floor of the second level of the low-rise building, i.e. the approximate height where the sensors were placed during the trials. It is worth noting that some rooms (Room 10, Room 12 and Corridor) present quite high velocities while other rooms (Room 11 and Room 13) present almost zero velocities, a sign of less air renewal.

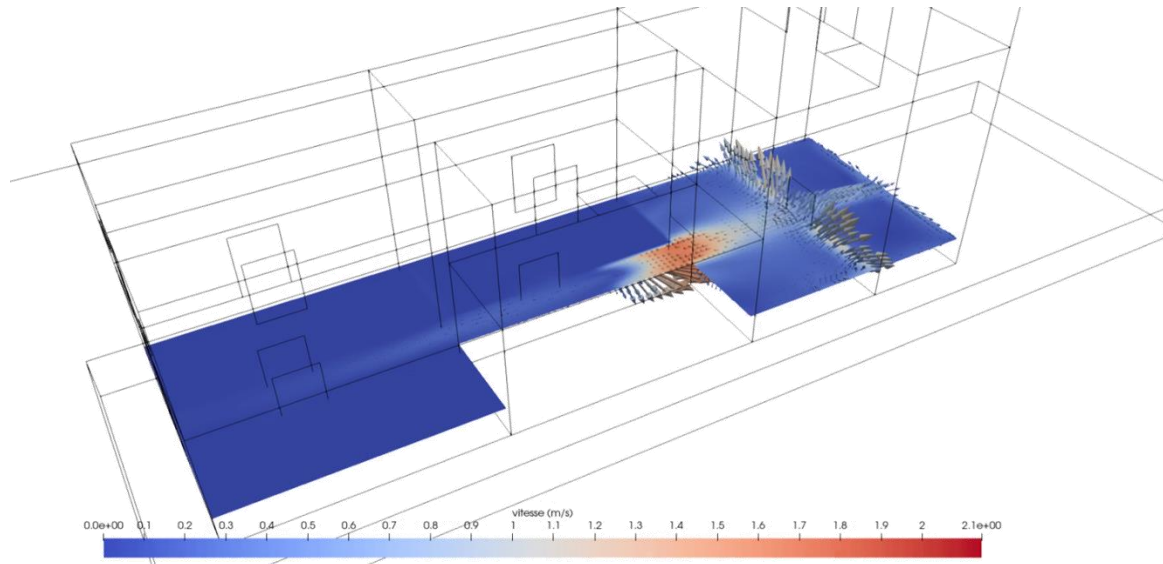


**Figure 72.** Velocity field in the horizontal cross-section located 5 cm above the floor of the second level of the low-rise building



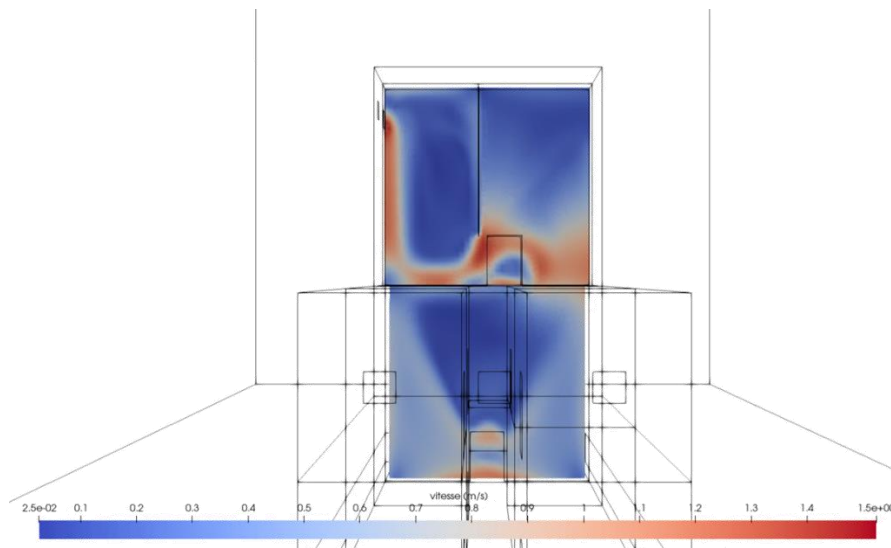
**Figure 73.** Velocity vectors in the horizontal cross-section located 5 cm above the floor of the second level of the low-rise building

Figure 74 shows the velocity field and velocity vectors in the horizontal cross-section located 10 cm above the floor of the first level of the low-rise building, i.e. the approximate height where the sensors were placed during the trials. One can observe that the velocities in the rooms on this ground floor are particularly low (Room 6, Room 8 and Room 9). In these rooms, the air renewal is mainly due to the recirculation created by the shearing with the jet coming from the upper floor (see Figure 71).



**Figure 74.** Velocity field and velocity vectors in the horizontal cross-section located 10 cm above the floor of the first level of the low-rise building

Figure 75 shows the velocity field in a vertical section plane crossing the stairwell (on the right) of the high-rise building. The air outlets are on the top corner left. Upstairs, the flow from the ground floor is distributed among the rooms and follows the floor, and then the back wall of the room (on the left), to the outlets.



**Figure 75.** Velocity field in the vertical cross-section through the stairwell of the high rise

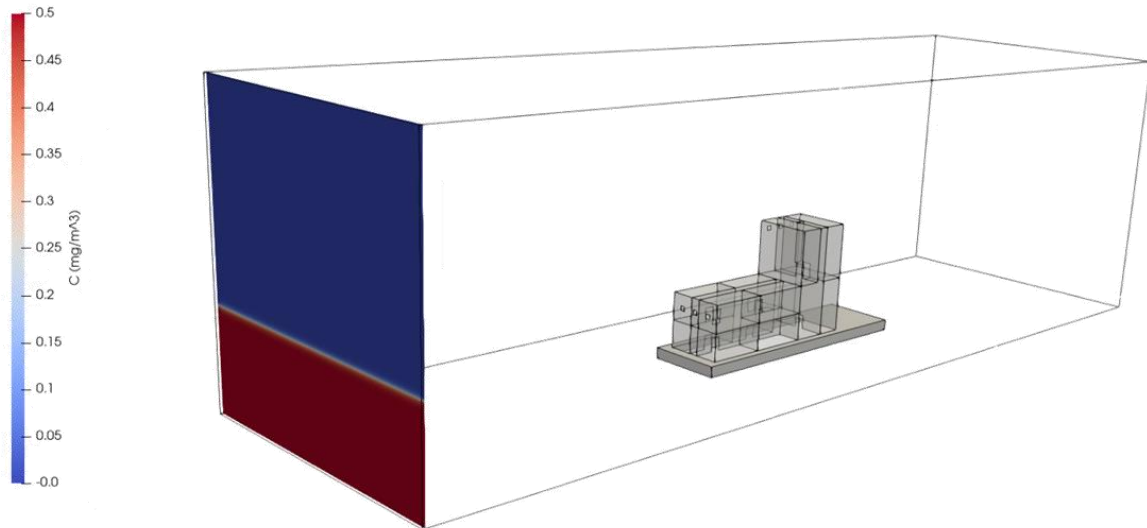
### 3.1.2.2 Simulation of the experimental releases

In the experimental releases under consideration, the chemical agent is the triethylphosphate (TEP). Its density is 1.072 at 25°C. As it is close to 1, it can be assumed that this chemical is neither heavier nor lighter than air and behave as a passive tracer. As for the preliminary calculations carried out before the trials, the dispersion of the chemical is simulated by solving an unsteady transport equation for a passive scalar  $C$  representing the concentration of the chemical. This equation uses the stationary velocity field which is supposed not to change during the experimental releases.

### Scenario 3 - Experiment #1 ("low cloud")

In the so-called "low cloud" experiment, the chemical is released from the wind tunnel entrance on a height of 2 m for 10 minutes. The target concentration downstream of the inlet openings of the small building is  $0.5 \text{ mg.m}^{-3}$ .

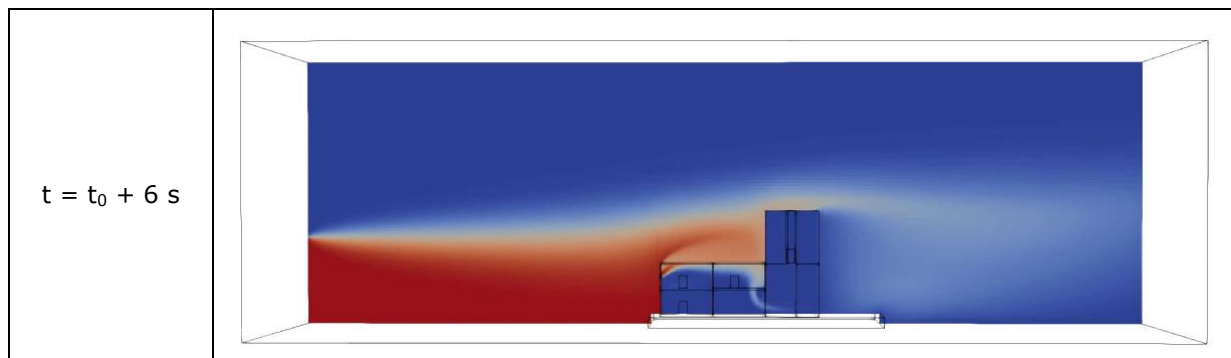
In the CFD simulation, a constant concentration is imposed equal to  $C_0 = 0.5 \text{ mg.m}^{-3}$  at the tunnel entrance on a height of 2 m from  $t = t_0$  and for 10 minutes (Figure 76). The distribution of the chemical in the tunnel and in the small building is calculated from  $t = t_0$ . The total simulated time is 2,400 s.

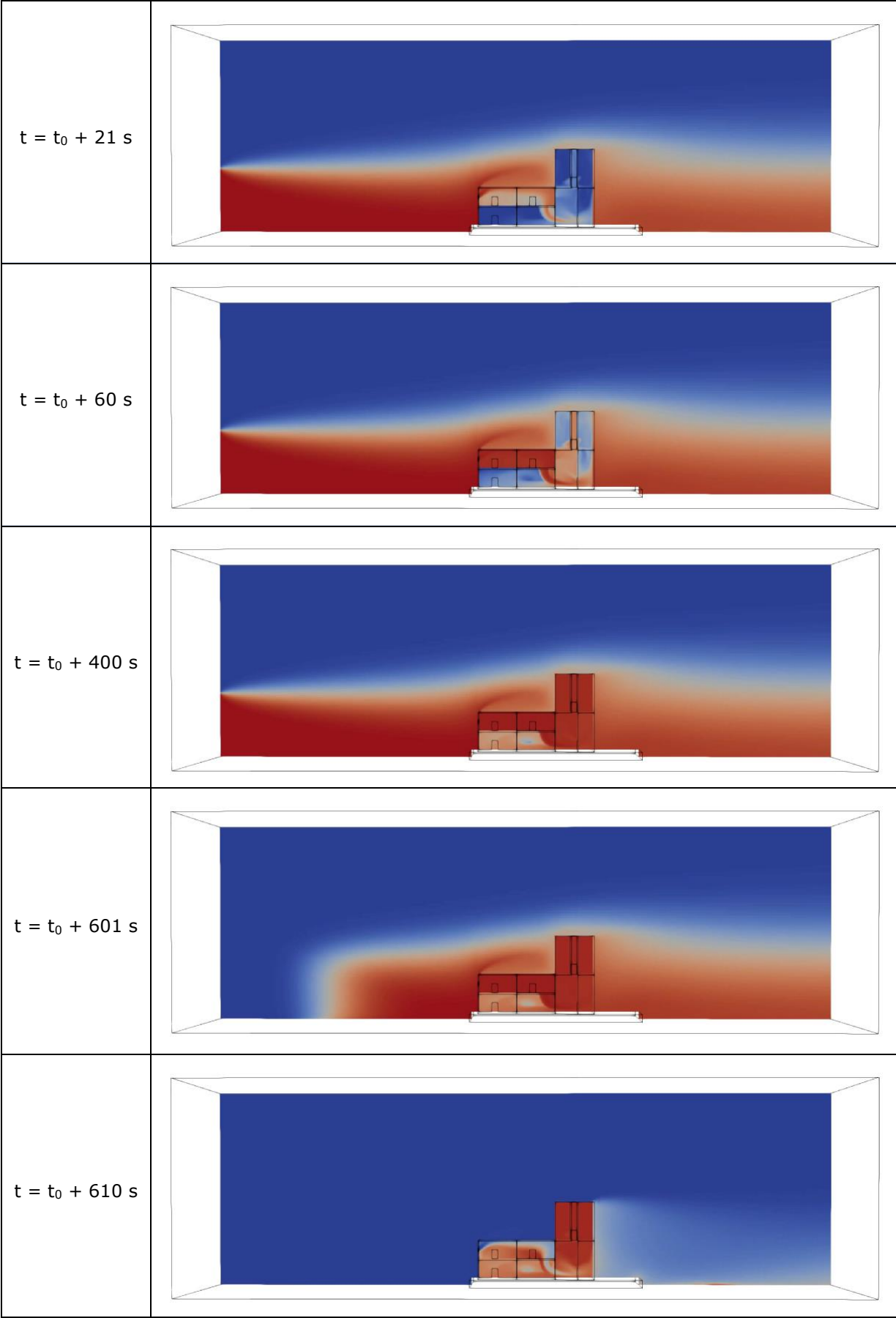


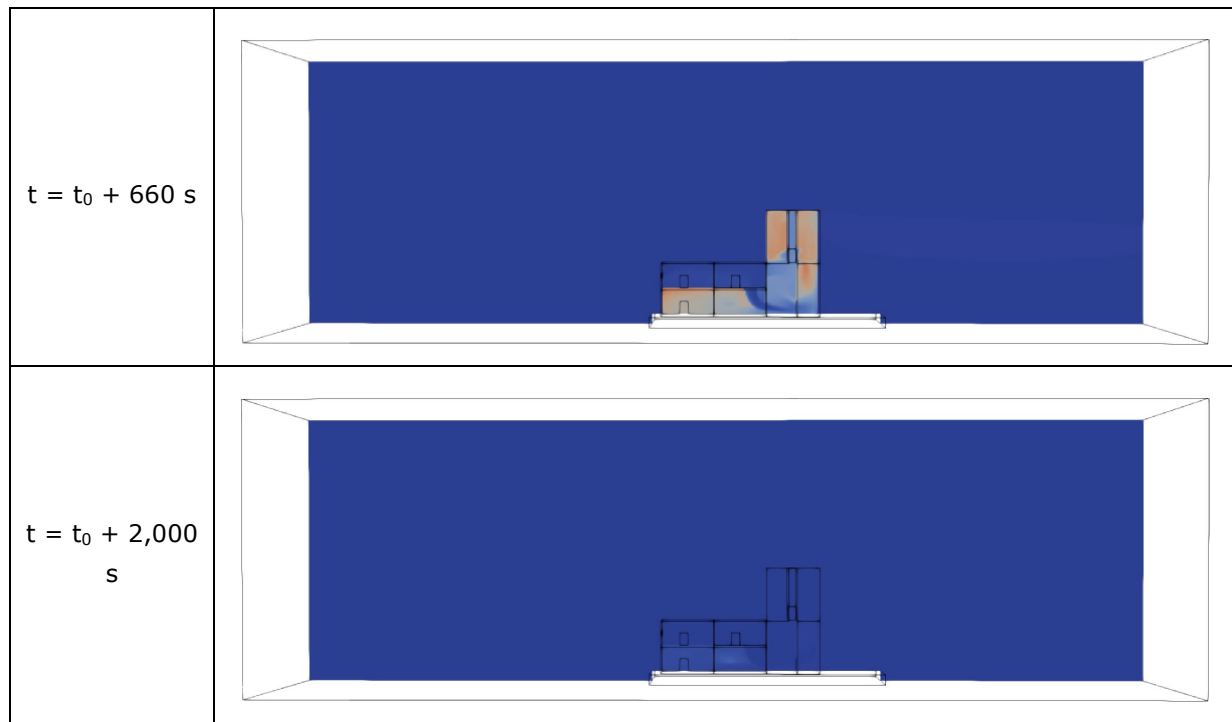
**Figure 76.** Experiment #1 – Initial condition ( $t = t_0$ ) at the entrance to the wind tunnel

Figure 77 presents the concentration field in the median vertical plane of the wind tunnel at different times between  $t = t_0 + 6 \text{ s}$  and  $t = t_0 + 2,000 \text{ s}$ . The scale of the concentration is identical and varies between 0 and  $0.5 \text{ mg.m}^{-3}$ .

From  $t = t_0$ , the boundary condition for the concentration at the entrance to the wind tunnel changes instantly ( $C_0 = 0.5 \text{ mg.m}^{-3}$ ). One can observe the formation of a chemical plume upstream of the small building, which fills the wind tunnel to a height of 2 m. The concentration field outside the building is static from about  $t = t_0 + 20 \text{ s}$ . The building itself quickly fills up with the chemical agent penetrating through the air inlets facing the wind, first the upper floor of the low-rise building (up to  $t = t_0 + 60 \text{ s}$ ), then gradually the high-rise building ( $t = t_0 + 400 \text{ s}$ ). From  $t = t_0 + 600 \text{ s}$ , the boundary condition for the concentration at the entrance to the tunnel changes again ( $C_0 = 0 \text{ mg.m}^{-3}$ ). Consequently, the small building is gradually purged by the supply of fresh air. At  $t = t_0 + 660 \text{ s}$ , the second level of the lower building is almost purged and the plume is progressively diluted in the other parts of the building. At  $t = t_0 + 2,000 \text{ s}$ , the whole building is almost purged. It is worth noticing that the purge is longer in the ground floor of the low-rise building as it is poorly ventilated.

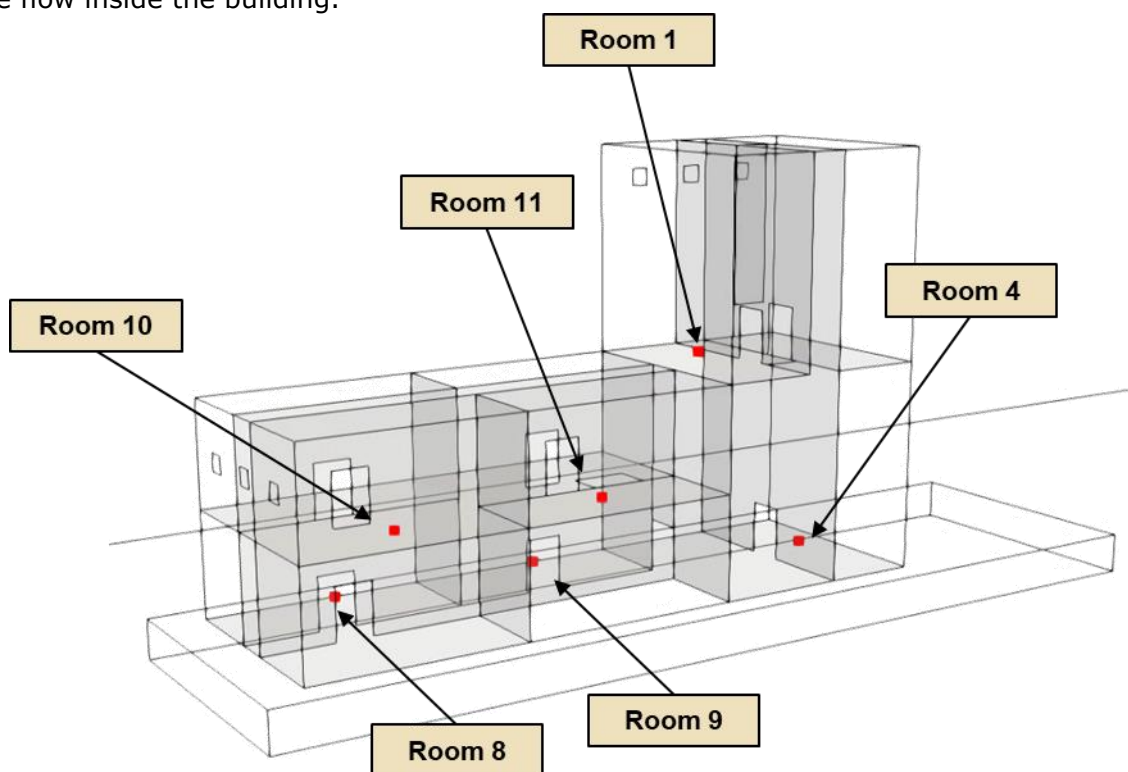




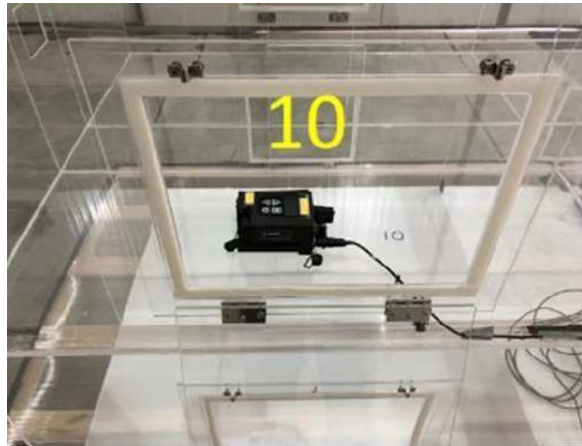


**Figure 77.** Experiment #1 – Concentration field in the median vertical cross-section of the wind tunnel at different instants between  $t = t_0 + 6 \text{ s}$  and  $t = t_0 + 2,000 \text{ s}$

Figure 78 shows the sensors which were set up in the small building for the trials. The six sensors are of the LCD type (Figure 79) and are located in the center of the rooms at a height of 5 cm or 10 cm depending on the rooms. The cabling of the sensors to a laptop outside the small building was done in such a way as to interfere as little as possible with the flow inside the building.



**Figure 78.** Location of the sensors inside the small building

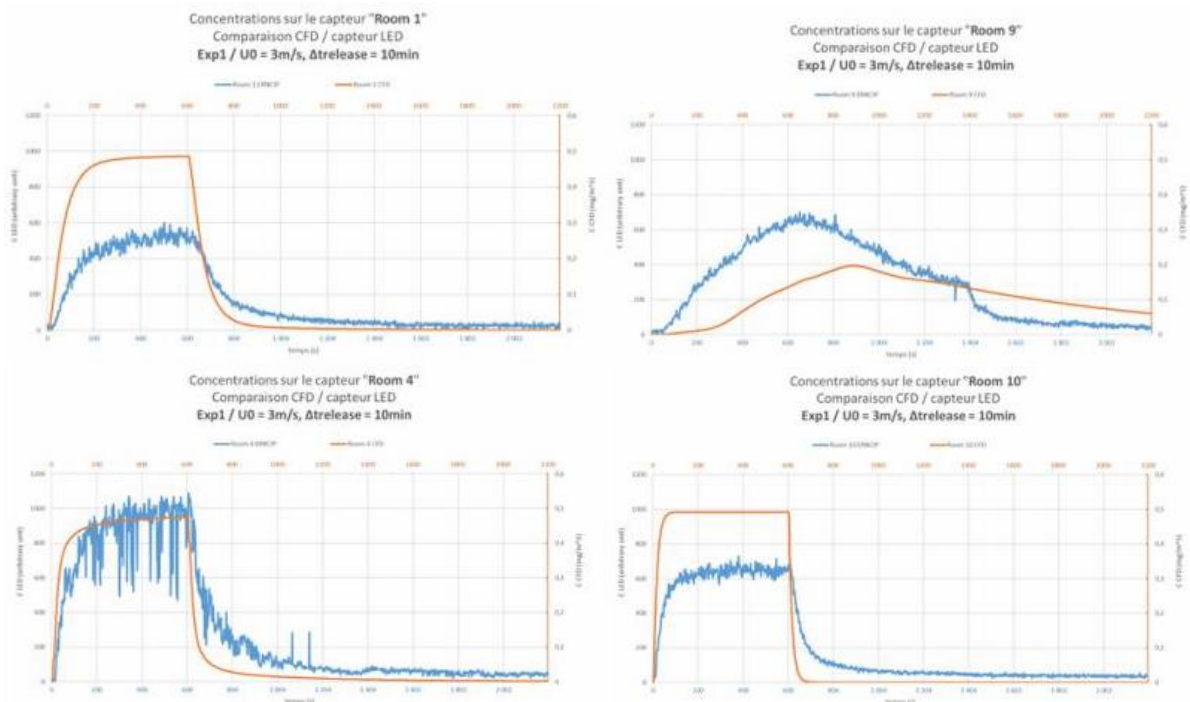


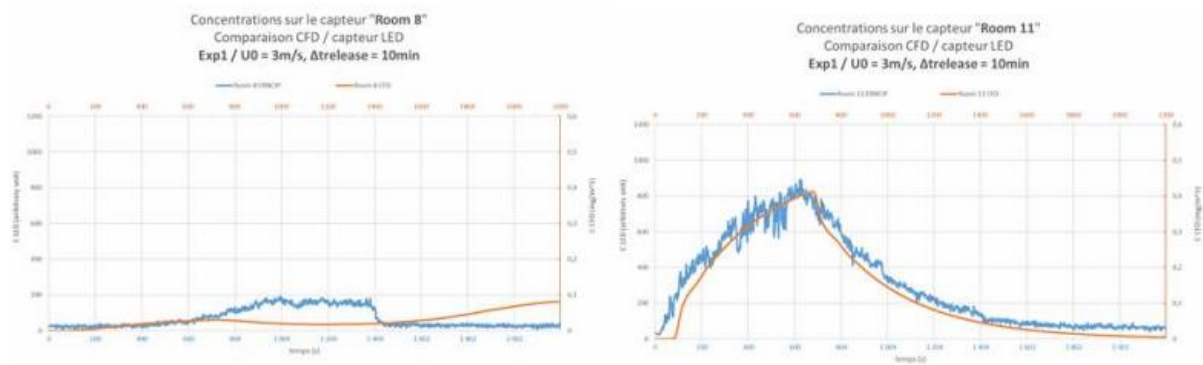
**Figure 79.** LCD sensors

Figure 80 compares the results of the CFD simulation with the measurements provided by TNO. For the results of the calculations, it was considered the evolution of the local chemical concentration on the six points corresponding to the positions of the sensors (virtual sensors).

It must be pointed out that it is very difficult to compare CFD and sensor readings for several reasons:

- First, the exact location of the sampling by the sensors is not clearly identified and the space occupied by the sensors themselves is far from negligible compared to the size of the rooms.
- In addition, the numerical results are computed and presented in  $\text{mg.m}^{-3}$  (scale on the left), while the measurements provided by TNO are in an arbitrary unit (scale on the right) with no useable information to convert these values in  $\text{mg.m}^{-3}$ .



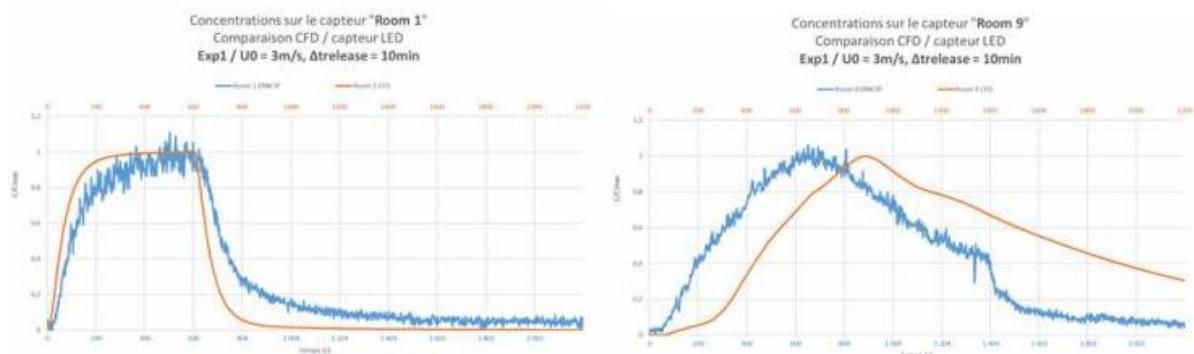


**Figure 80.** Experiment #1 – Comparison of the concentrations obtained by the CFD and by the measurements at the six

In order to compare more efficiently the CFD simulations to the measurements, both numerical and experimental results were made dimensionless by dividing them by the maximum concentration  $C_{max}$ . It was assumed that each sensor was calibrated independently of the others and each sensor was scaled by the maximum recorded concentration. The same approach was used for the virtual sensors in order to be comparable with the measurements.

Figure 81 shows the comparison of the normalized computed and measured concentrations. It can be observed:

- An excellent general reproduction of the dynamics of the dispersion in most rooms;
- A slightly faster filling and purging for the simulations compared to the measurements, which may be the sign of a slight overestimation of the velocity upstream of the small building;
- A delay of the simulation in Room 9 compared to the measurements (about 300 s);
- A different dynamic in Room 8, but this remark has to be qualified as the concentration levels are very low in this room (see Figure 80).



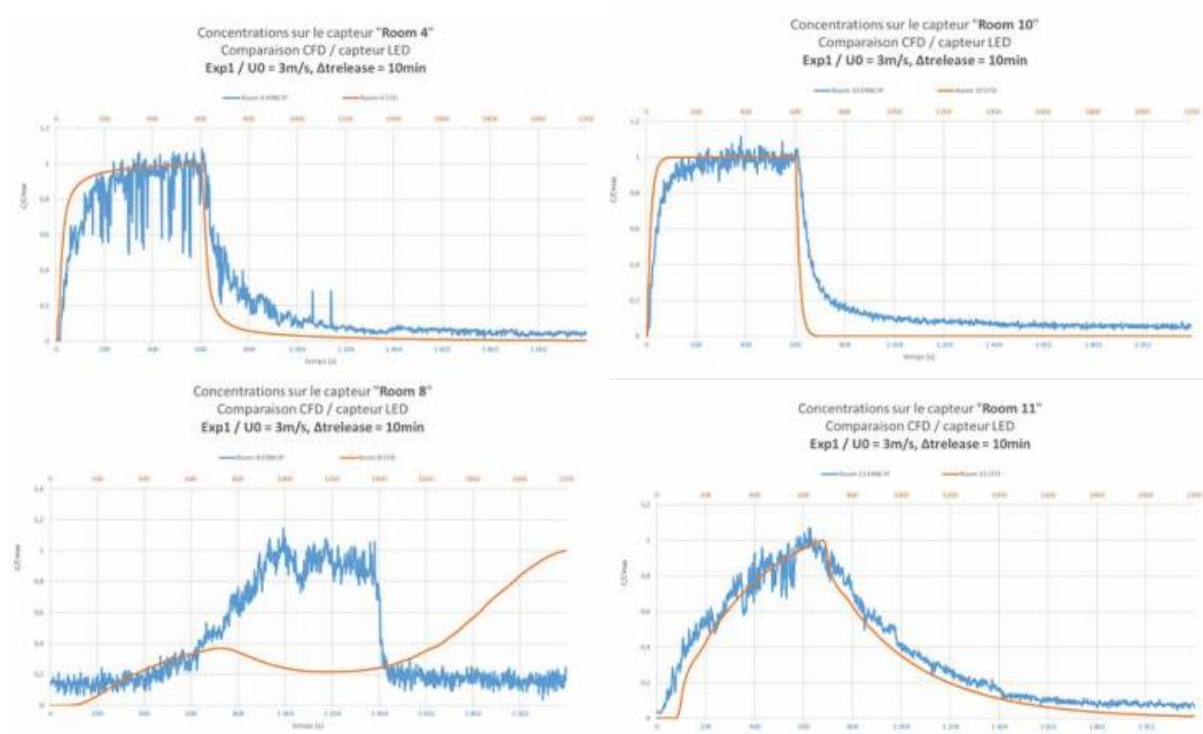
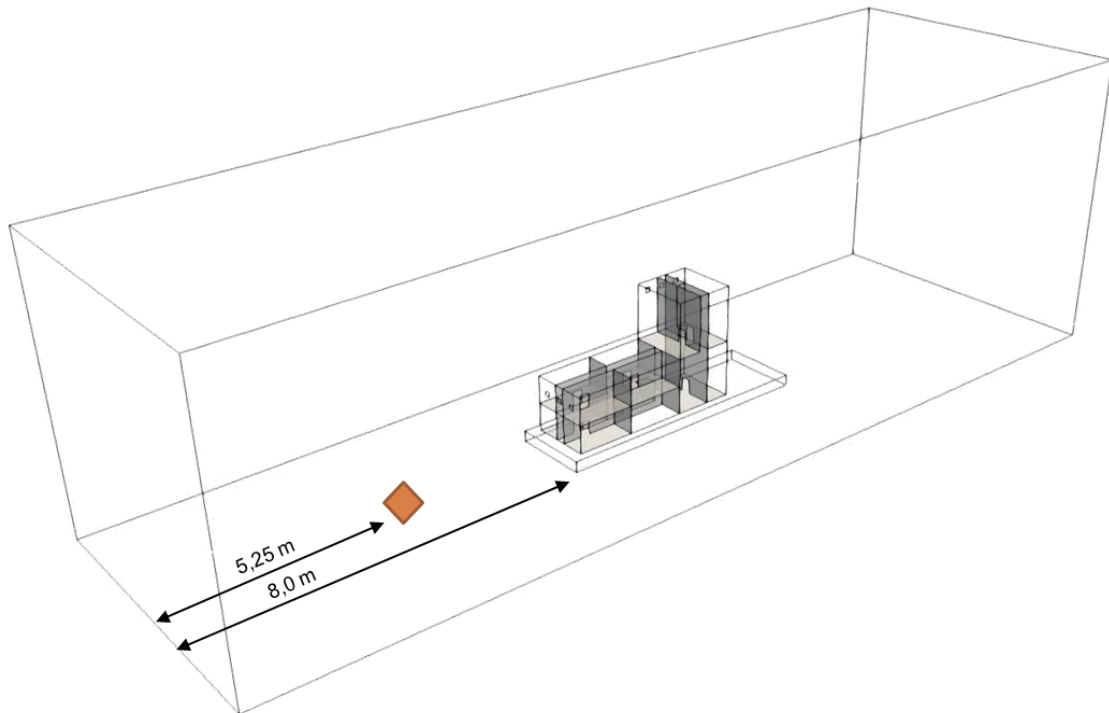


**Figure 81.** Experiment #1 – Comparison of the normalized concentrations obtained by the CFD and by the measurements at the six sensors

### **Scenario 2 - Experiment #6 ("external release")**

In this experiment called "external release", the chemical agent is released from a device (presented in Figure 23) located upstream of the small building at a distance of 3 m and at a height of 50 cm. The total dispersed mass of TEP is 0.93 g over 10 minutes. The mean concentration  $C_{mean}$  of the plume at the entrance to the small building is estimated at approximately  $0.5 \text{ mg} \cdot \text{m}^{-3}$ .

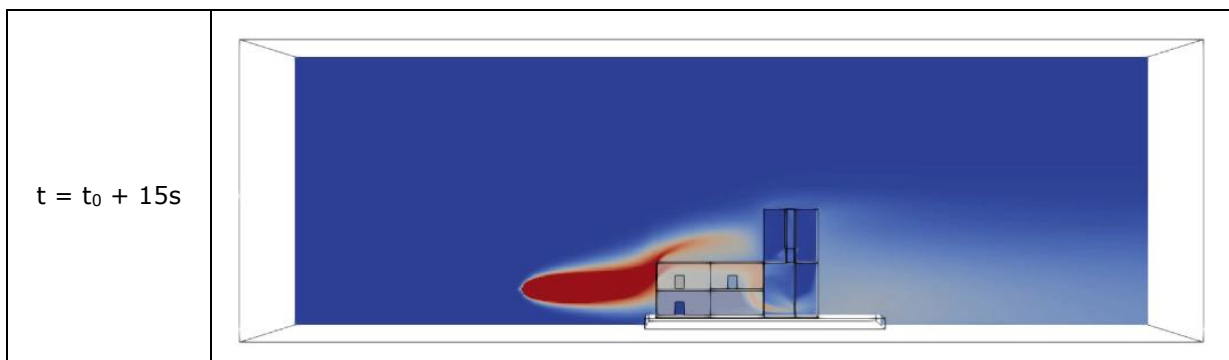
In the CFD simulation, the release is modelled by an intermittent volume source term in the transport equation of the concentration. At  $t = t_0$ , it is assumed that the concentration of the chemical agent, initially zero in the whole domain, becomes non-zero in a cell of the mesh (see Figure 82). The release rate from this source is defined by considering the total dispersed mass and the duration of dispersion, i.e.  $0.93 \text{ g} / 600 \text{ s} = 1.55 \cdot 10^{-3} \text{ g} \cdot \text{s}^{-1}$ . The evolution of the concentration in the tunnel and the small building is simulated for 2,400 seconds.

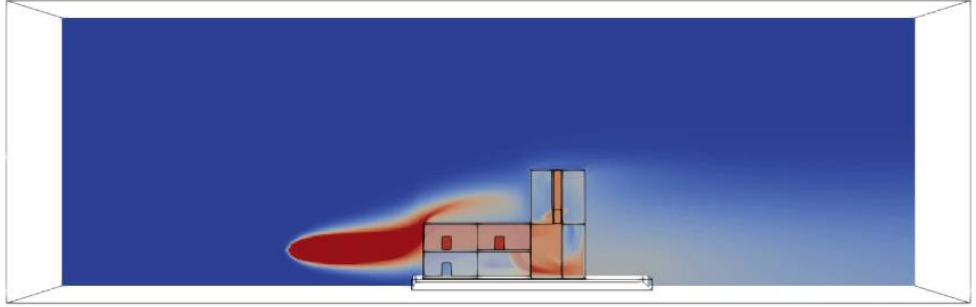
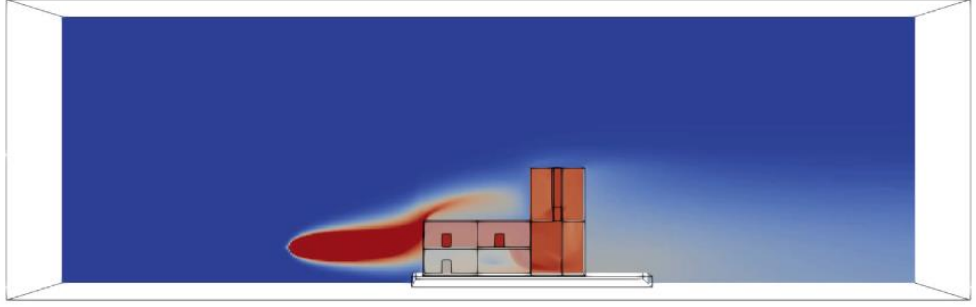
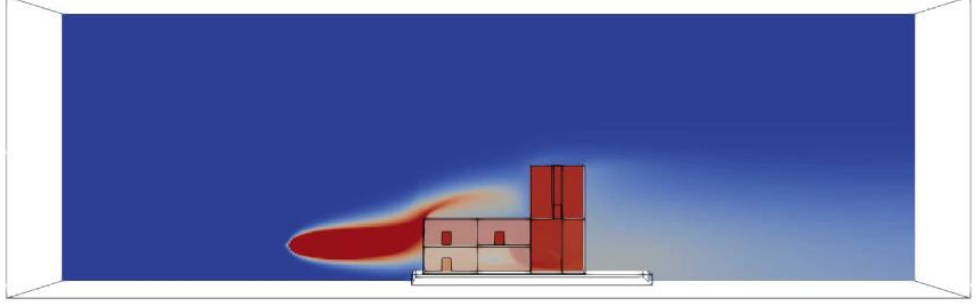
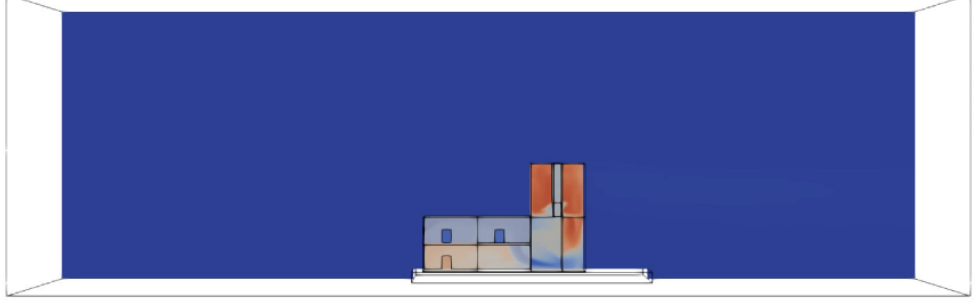
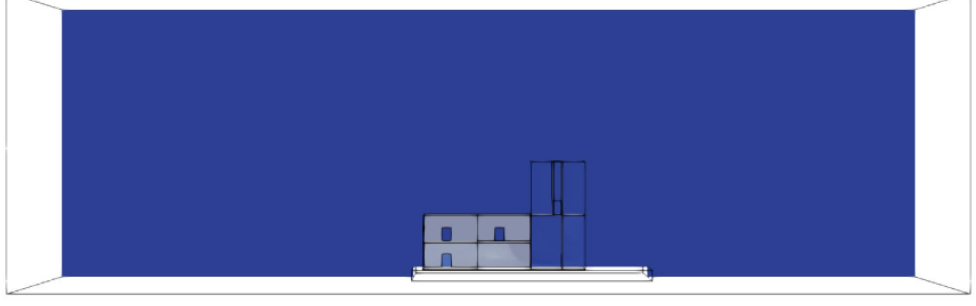


**Figure 82.** Experiment #6 – Location of the source for the external release

Figure 83 presents the concentration field in the median vertical median plane of the tunnel at different times between  $t = t_0 + 15$  s and  $t = t_0 + 1,000$  s. The scale of the concentration is identical and varies between 0 and  $0.5 \text{ mg.m}^{-3}$ .

From  $t = t_0$ , the concentration in the source cell upstream of the building changes instantly ( $C_0 = 0.5 \text{ mg.m}^{-3}$ ) and the generated plume is advected by the air flow in the wind tunnel towards the building. The chemical agent enters the small building through the air inlets on the floor level of the low-rise building. The building fills up quickly, first the upper floor of the low-rise building ( $t = t_0 + 60$  s), then gradually the high-rise building ( $t = t_0 + 400$  s). From  $t = t_0 + 600$  s, the source term becomes zero and the concentration of the chemical agent in the incident air also ( $C_0 = 0 \text{ mg.m}^{-3}$ ). The building is then progressively purged by the supply of fresh air. At  $t = t_0 + 638$  s, the floor level of the lower building is almost purged and the plume is gradually diluted in the other parts of the small building. At  $t = t_0 + 1000$  s, the whole building is almost purged. Similarly, to experiment #1, it is worth noticing that the purge is longer in the ground floor of the low-rise building as it is poorly ventilated.



$t = t_0 + 60 \text{ s}$	
$t = t_0 + 150 \text{ s}$	
$t = t_0 + 400 \text{ s}$	
$t = t_0 + 638 \text{ s}$	
$t = t_0 + 1,000 \text{ s}$	

**Figure 83.** Experiment #6 – Concentration field in the median vertical cross-section of the wind tunnel at different instants between  $t = t_0 + 15$  s and  $t = t_0 + 1,000$  s

Figure 84 compares the results of the CFD simulation with the measurements provided by TNO. For the results of the calculations, it was considered the evolution of the local chemical concentration on the six points corresponding to the positions of the sensors (virtual sensors) shown in Figure 78.

The difficulties described for experiment #1 in comparing the simulations with the experiments are still present. Likewise, the numerical results are computed and presented in  $\text{mg.m}^{-3}$  (scale on the left), while the measurements provided by TNO are in an arbitrary unit (scale on the right) with no useable information to convert these values in  $\text{mg.m}^{-3}$ .

It is important to note that the maximum concentration in the building ( $0.487 \text{ mg.m}^{-3}$ ) is very close to the concentration targeted in the experiment ( $0.5 \text{ mg.m}^{-3}$ ).

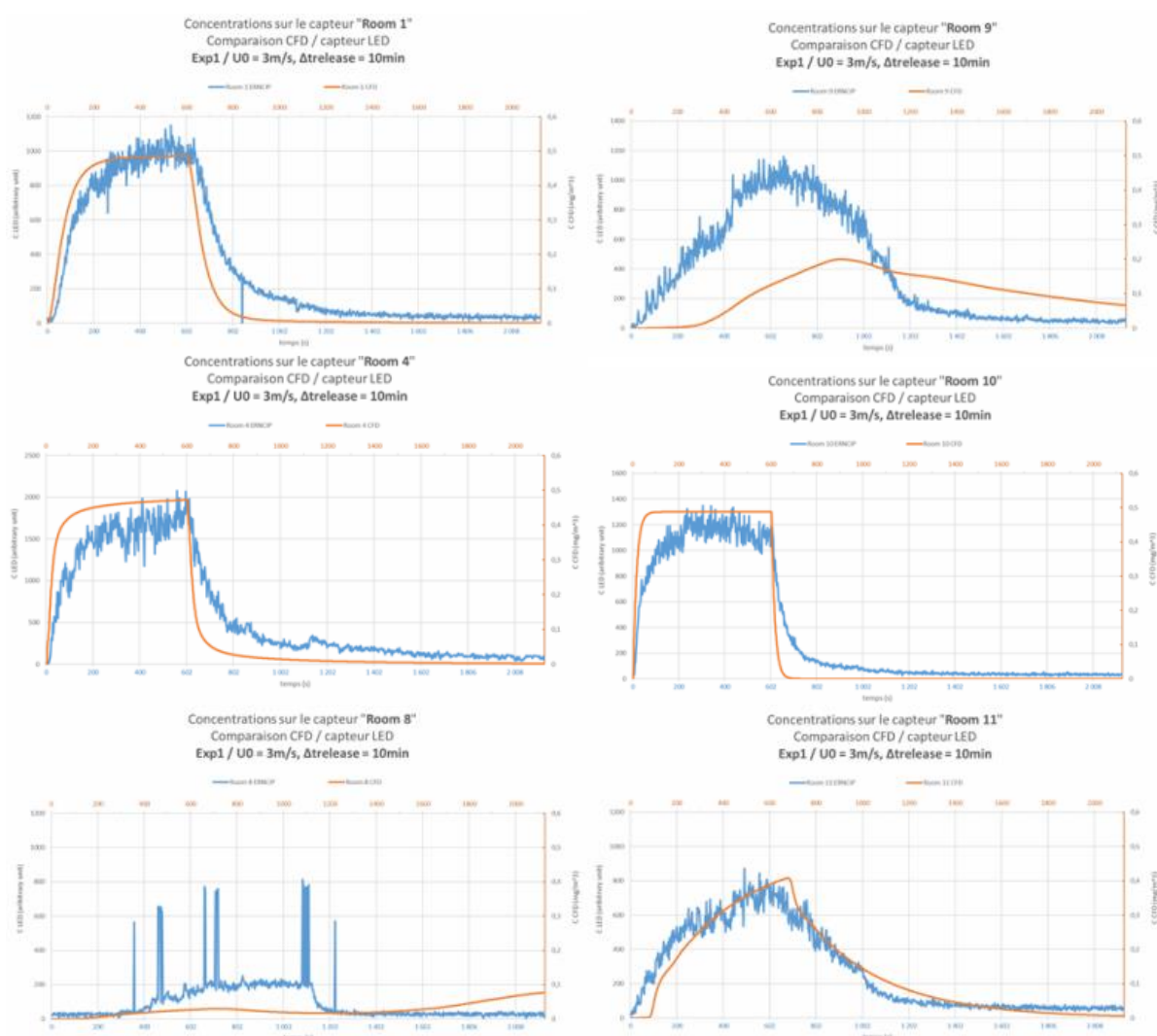


**Figure 84.** Experiment #1 – Comparison of the concentrations obtained by the CFD and by the measurements at the six sensors

Similarly, to experiment #1, both numerical and experimental results were made dimensionless by dividing them by the maximum concentration  $C_{\text{max}}$ . It was assumed that each sensor was calibrated independently of the others and each sensor was scaled

by the maximum recorded concentration. The same approach was used for the virtual sensors in order to be comparable with the measurements.

Figure 85 shows the comparison of the normalized computed and measured concentrations. The observations in experiment #6 are similar to those of experiment #1:

- An excellent general reproduction of the dynamics of the dispersion in most rooms;
- A slightly faster filling and purging for the simulations compared to the measurements, which may be the sign of a slight overestimation of the velocity upstream of the small building;
- A delay of the simulation in Room 9 compared to the measurements (about 300 s),
- A different dynamics in Room 8, but this remark has to be qualified as the concentration levels are very low in this room (see Figure 84).

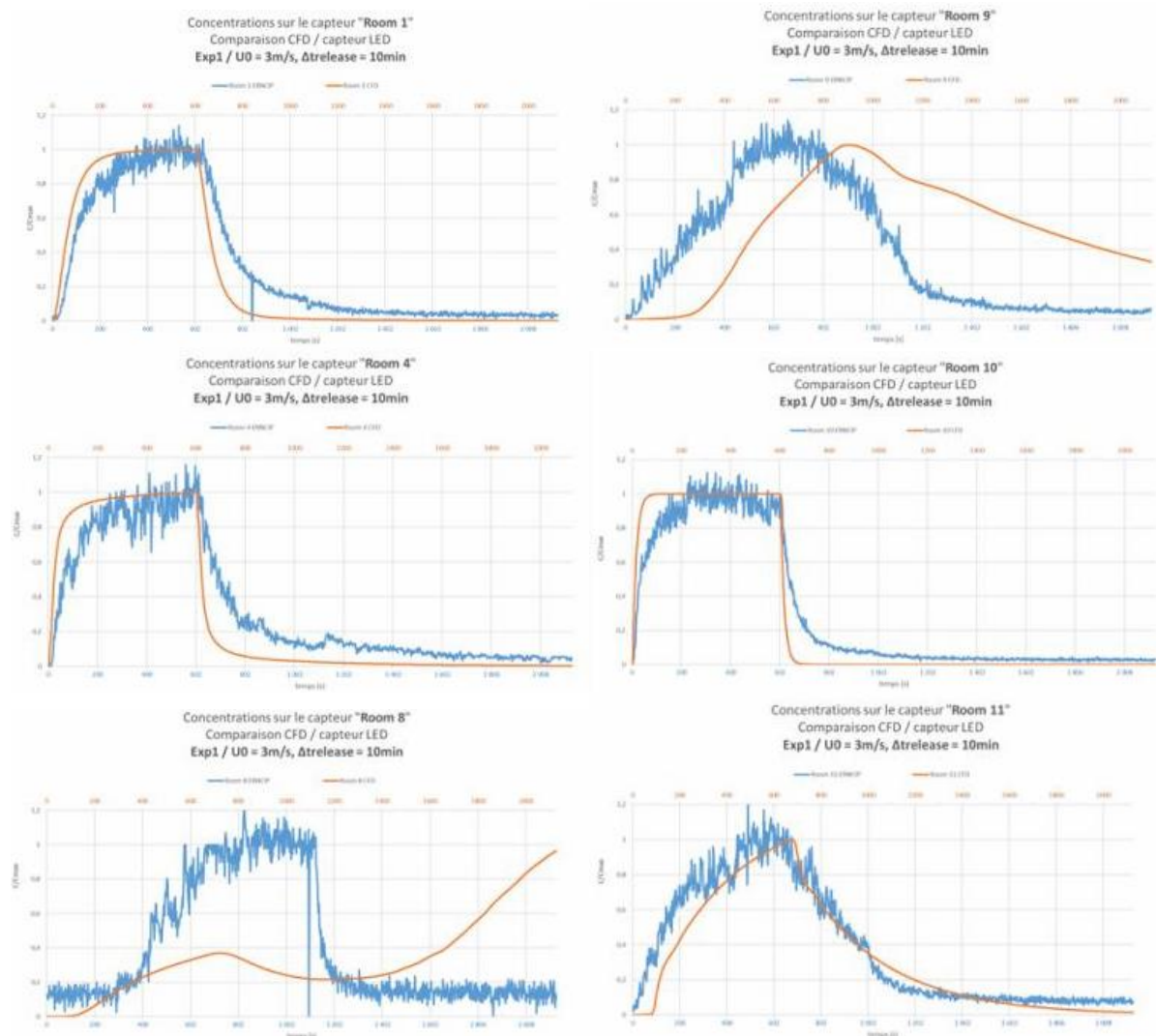


**Figure 85.** Experiment #6 – Comparison of the normalized concentrations obtained by the CFD and by the measurements at the six sensors

Regarding the Room 9, the numerical results exhibit a systematic shift of about 300 s compared to the measurements. One possible explanation is the difference in positioning

between the virtual sensors (in the CFD) and the real sensors (in the experiments). In order to investigate the variability of the numerical results depending on the location of the sensor, four alternative positions of the virtual sensor close to its initial position (plus or minus 5 cm) in Room 9 were studied (see Figure 86).

Figure 87 shows the results with the orange curve representing the concentration on the virtual sensor at its initial position and the other curves concentrations obtained by varying the position of the virtual sensor. One can notice that the results vary significantly when the position of the sensor is modified. For example, for a position closer to the door of Room 9, the concentration increases much earlier (pink curve) and is more synchronous with the values measured by the sensor during the experiment. Still, it seems that the maximum concentration is always reached at about the same time, that is to say 300 s later than in the experiment.



**Figure 86.** Experiment #6 – Alternative positions of the virtual sensor in Room 9

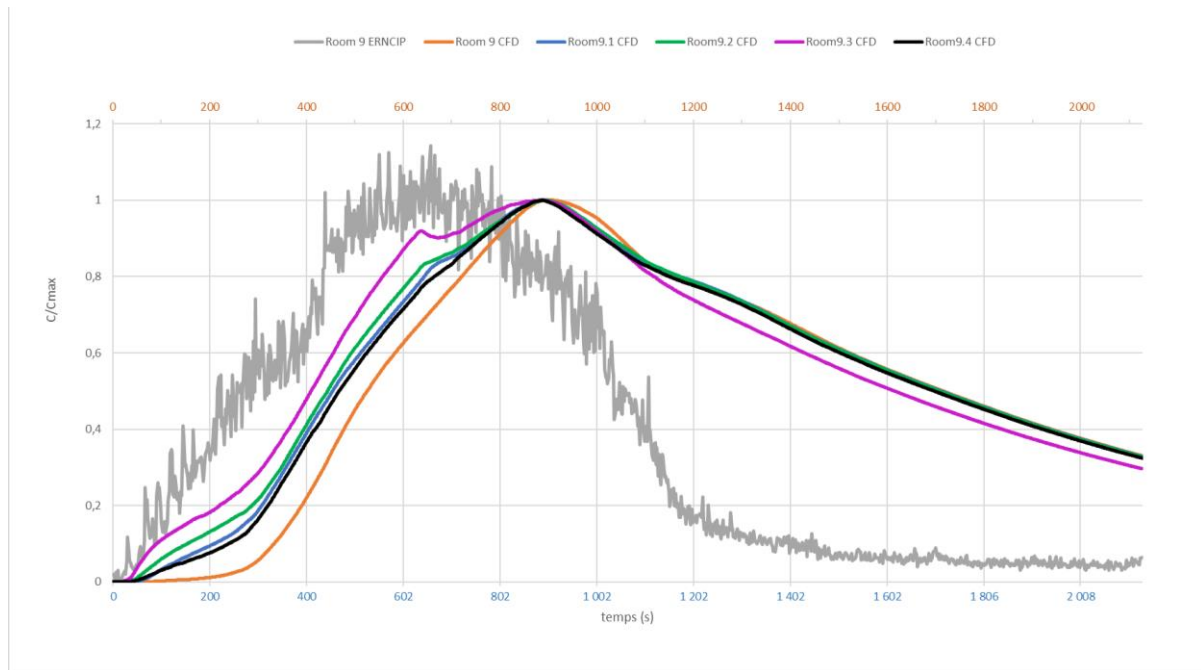


**Figure 87.** Experiment #6 – Comparison between the simulated concentrations on close virtual sensors in Room 9 and the measured concentrations in Room 9

There are several potential explanations for this difference:

- The shift can come from the real sensor. Indeed, it is quite astonishing that the concentration increases instantaneously at  $t = t_0$ , whereas a certain time is necessary for the plume to fill in progressively the different rooms, especially Room 8 and Room 9.
- There may be leakages in the small building mock-up or they may be differences between the geometry of the building in the experiment and the geometry and mesh created for performing the simulations, resulting in differences in the evaluation of the transfers within the building.
- The flow simulation may be a bit less accurate in Room 9 (and also in Room 8) than in the rest of the small building. As a matter of fact, these two rooms are located in a “dead zone” of the flow. The ventilation is weak and only ensured by the recirculation which is generated by the shear of the air jet coming from the floor of the low-rise building. This is certainly difficult for our “k-epsilon” turbulent model to deal with this configuration. Moreover, the flow in this part of the building is probably unstable and intermittent, contrarily to the simplifying stationarity assumption made in the numerical study. Thus, the fluid dynamics in this part of the small building would probably need more sophisticated flow solver and turbulence modelling.

### **Scenario 1 - Experiment #12 (“internal release”)**

In the experiment called “internal release”, the chemical agent is released from a device (presented in Figures 28-29) located in the middle of Room 8 at a height of 7 cm. During the trial, the dispersal device is connected to an evaporation system located at the rear of the small building model so as not to disturb the incident air flow upstream of the building.

According to TNO which conducted the trials, the internal dispersion experiment resulted in several successive trials which were unsuccessful due to various problems with condensation in the system, adjustment of the dispersed amount or malfunction of the LCD sensors. In the end, none of the trials carried out were fully satisfactory because

even in the trial that was chosen for the simulation work, the LCD sensor placed in the same room as the source (Room 8) quickly saturated giving no usable measurements, while for the other sensors placed in the building, the signal remained almost zero.

In the trial selected for this report, the total dispersed quantity of TEP is 2  $\mu\text{L}$  (microliter), i.e. a mass of approximately  $2.35724 \cdot 10^{-3}$  mg for 2 minutes. The concentration targeted in Room 8 is evaluated at approximately  $6 \text{ mg} \cdot \text{m}^{-3}$ .

In the CFD simulation, the release is modelled using the same approach as in experiment #6 by an intermittent volume source term in the transport equation of the concentration. At  $t = t_0$ , it is assumed that the concentration of the chemical agent, initially zero in the whole domain, becomes non-zero in a cell of the mesh (see Figure 88). The release rate is defined by considering the total dispersed mass and the duration of dispersion, i.e.  $2.35724 \cdot 10^{-3} \text{ mg} / 120 \text{ s} = 1.964 \cdot 10^{-5} \text{ mg} / \text{s}$ . The plume is advected from the source into the small building by the air flow without any other mechanism to disperse the chemical being modelled. The evolution of the concentration in the small building is simulated for 1,300 seconds.

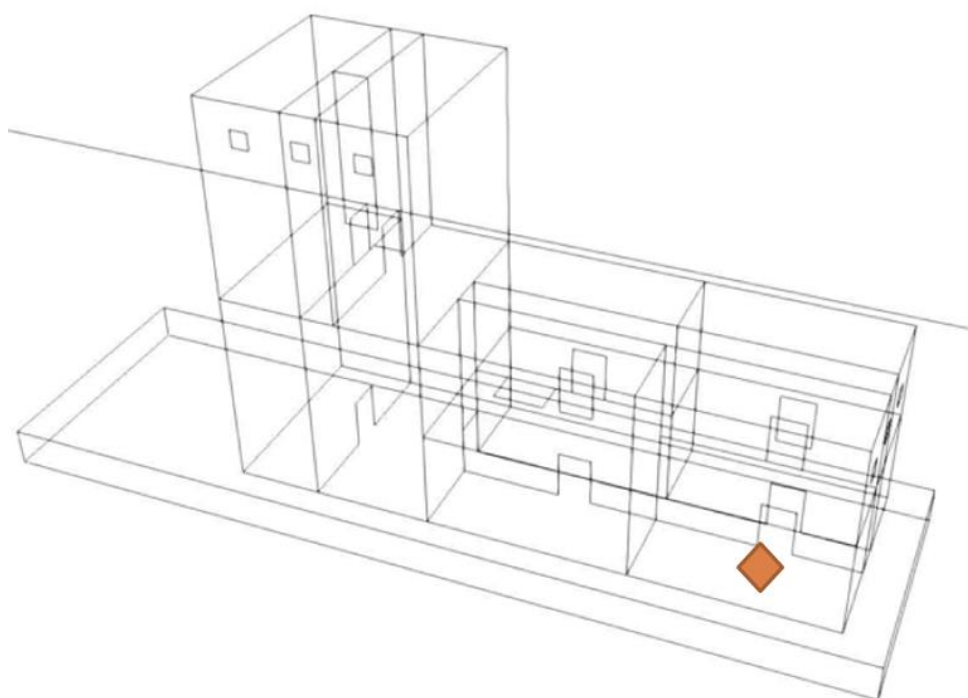


**Figure 88.** Experiment #12 – Location of the source for the internal release (Room 8)

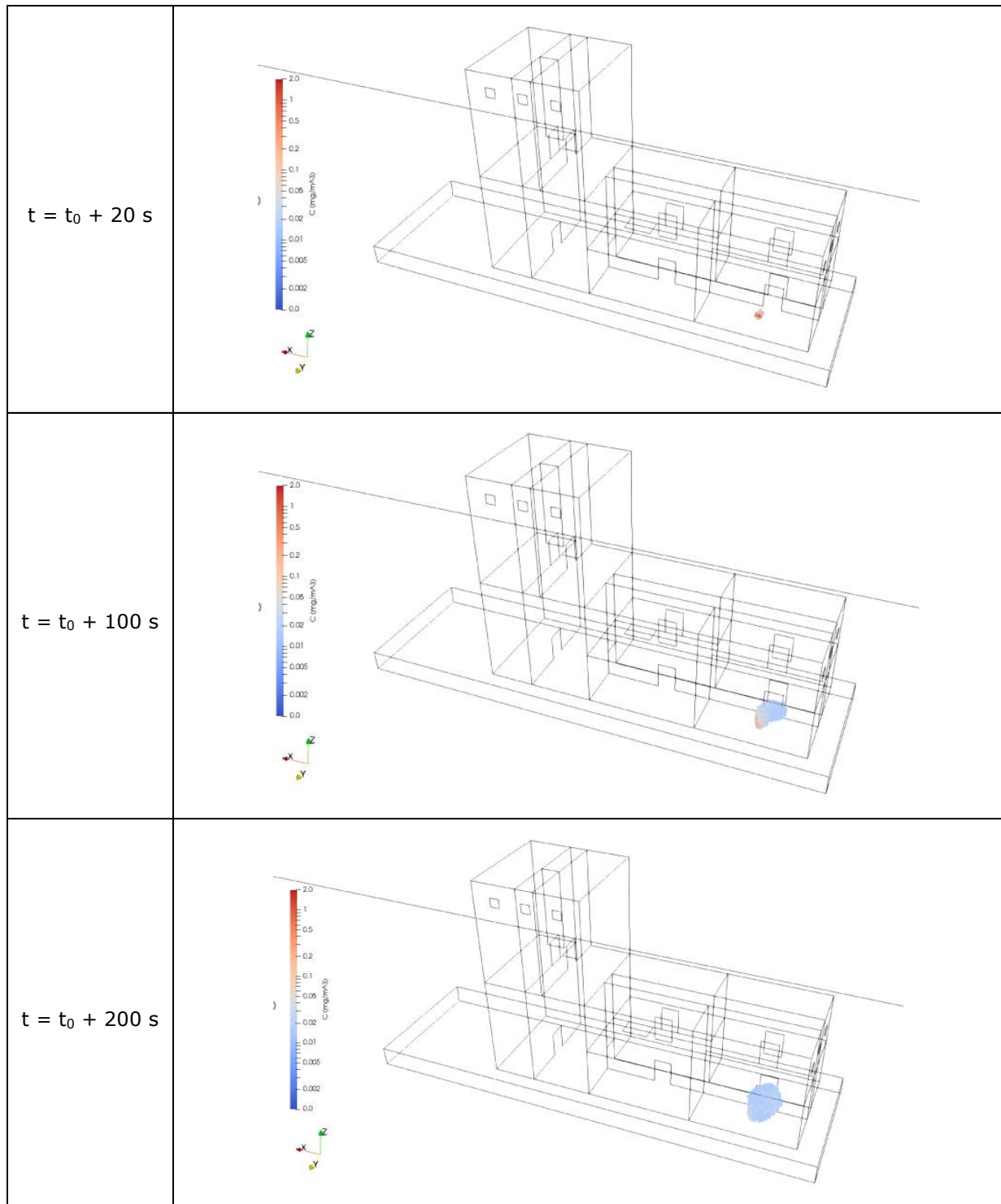
Table 11 presents the maximum concentrations on the virtual sensors obtained in the simulation. One can notice a ratio of at least 10,000 between the sensor in Room 8 where the source is located, and the other sensors. Obviously, there is an accumulation of the dispersed chemical only in Room 8.

**Table 11.** Experiment #12 – Maximum concentration on the six virtual sensors

	Room 1	Room 4	Room 8	Room 9	Room 10	Room 11
<b>Maximum concentration (<math>\text{mg} \cdot \text{m}^{-3}</math>)</b>	$6.44 \cdot 10^{-5}$	$2.05 \cdot 10^{-4}$	1.94	$2.53 \cdot 10^{-4}$	$6.29 \cdot 10^{-27}$	$1.31 \cdot 10^{-21}$

Figure 89 shows the chemical plume defined by the volume whose concentration  $C$  is less than or equal to the  $C_{\max}$  maximum concentration at different times between  $t = t_0 + 20$  s and  $t = t_0 + 1,045$  s. The scale of the concentration is logarithmic because the plume keeps very local in space and the gradients are very large in this configuration.

It can be seen that after the initial phase of dispersion up to  $t = t_0 + 120$  s, the plume remains mainly contained in Room 8 throughout the simulation without spreading into the rest of the small building. It gradually dilutes in the room and ends up being evacuated slowly. Note that the visualization adopted does not allow to apprehending the extremely low concentrations during the purge of the building.



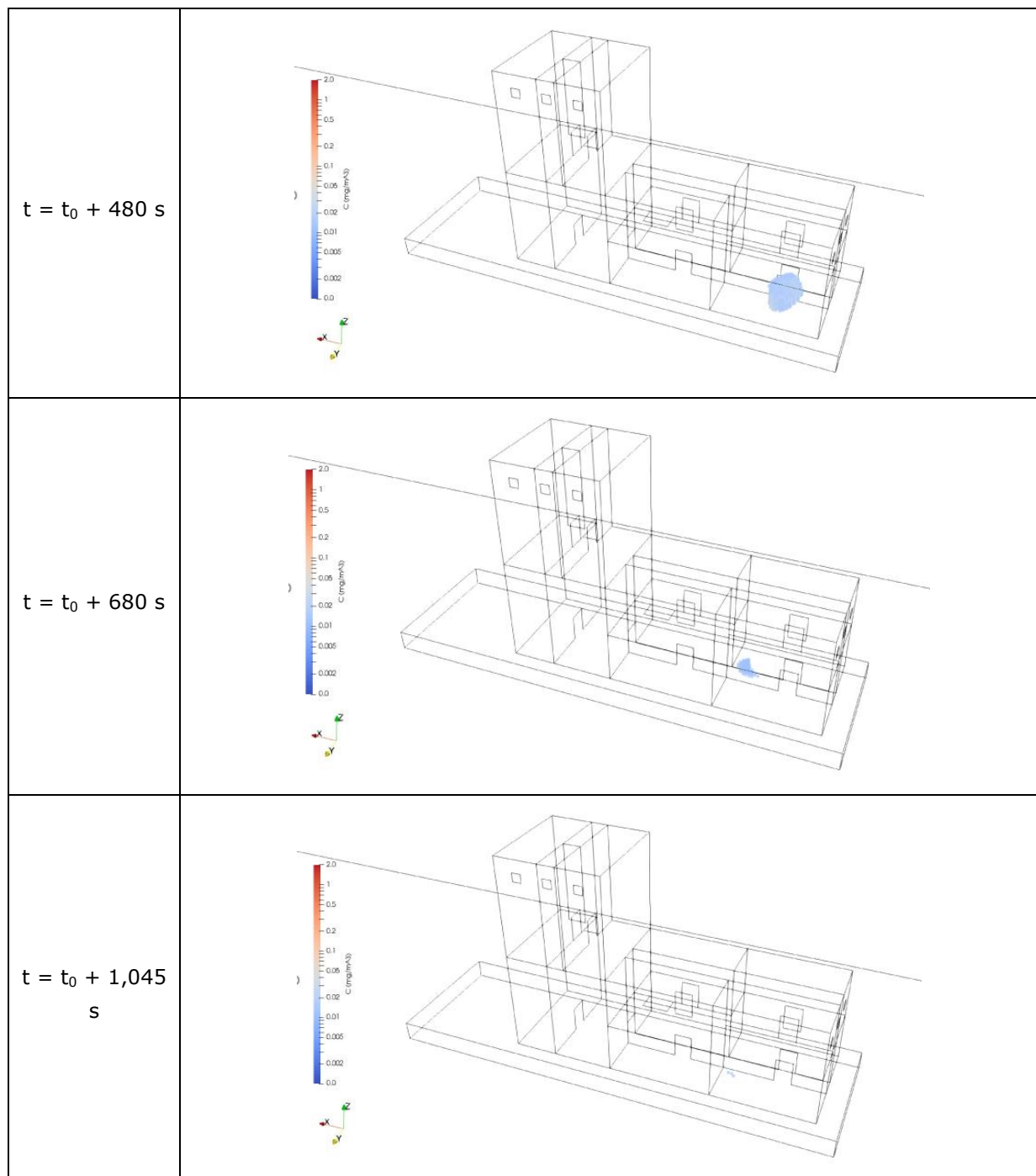


**Figure 89.** Experiment #12 – Visualization of the chemical plume defined by the volume  $C \leq C_{\max}$  inside the small building at different instants between  $t = t_0 + 20 \text{ s}$  and  $t = t_0 + 1,045 \text{ s}$

Figure 90 presents the concentrations on the virtual sensors in the CFD simulation. One can observe that the concentration on the sensor in Room 8 is much greater than the concentrations on the sensors in the other rooms. During the experiment conducted by TNO, the response of the actual sensor in Room 8 was saturated making the comparison between the numerical results and the measurements impossible for this trial.

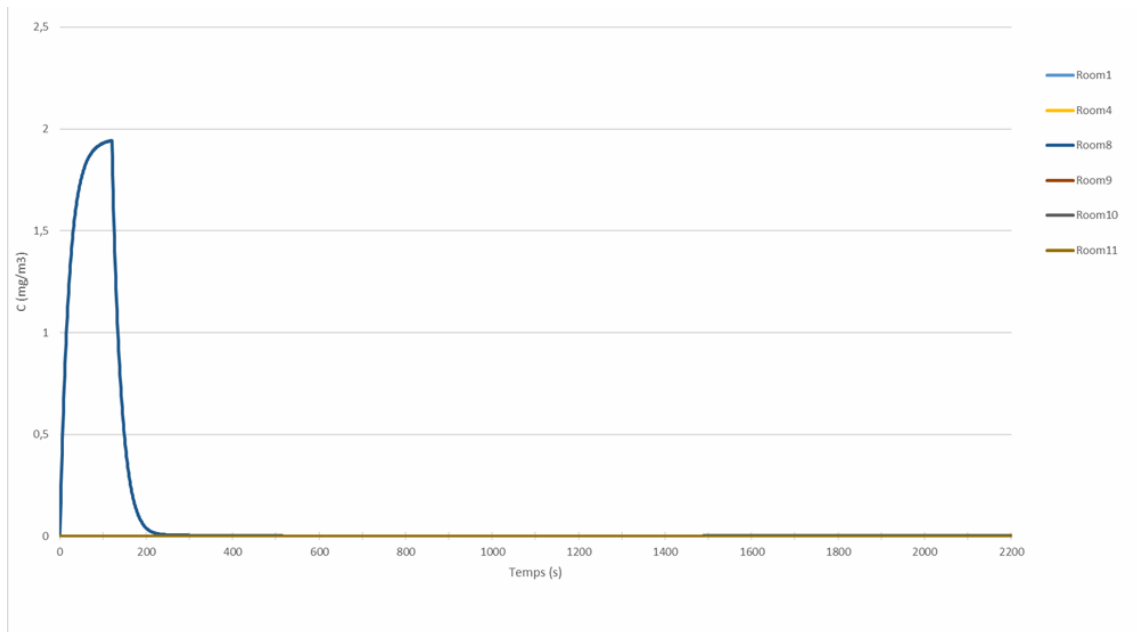


**Figure 90.** Experiment #12 – Concentrations on the virtual sensors in the CFD simulation

### 3.1.3 Conclusions of Code\_Saturne simulations

#### *Pre-experimental modelling*

The first set of simulations was done before the experimental trials as a preparatory work. A 3D digital mock-up was generated which faithfully represents the small building. The digital mock-up was utilized for performing aerodynamic CFD simulations with Code\_Saturne. The simulations were carried out inside the building disregarding the wind tunnel ("indoor" simulations). A mesh sensitivity study was also performed to identify the best compromise in terms of stability and robustness of the air flow solution.

It should be noted that the studied fluid dynamics problem has intrinsic unstable low velocity flow zones with intermittency and unsteady turbulent perturbations. The location planned for the internal release trials is one of those unstable flow zones. It was immediately identified and reported during the first set of simulations that the measurements and the comparison with the numerical results in this critical zone would therefore prove to be tricky.

Two types of dispersion simulations were run with Code\_Saturne depending on whether the source is outside or inside the small building. These computations relate only to the mock-up disregarding the wind tunnel. They have been compared with the simulations carried out by using ADREA-HF code (see section 3.2.4).

#### *Comparison of modelling and experimental trials (Post-experimental modelling)*

The second set of simulations was done after the experimental trials with the view to replicating them. A 3D global digital model was generated including the building mock-up immersed in the wind tunnel. The digital model was used for coupled "indoor/outdoor" simulations of the air flow in the tunnel and the small building, then for three dispersion simulations, the sources of which were positioned differently according to the trials which one sought to reproduce.

The 3D aerodynamic simulations show velocity fields consistent with the air flow in the wind tunnel. The velocity measurements taken in the tunnel during the trials are close to the CFD results with, however, a slight overestimation of the calculated speed

(approximately  $0.5 \text{ m.s}^{-1}$ ) near the building outlets. This deviation may be due to an error in the positioning of the sensor or in the provided experimental data of the velocity profile generated by the fans at the entrance to the wind tunnel.

The flow in the building mock-up is consistent and similar to the results of the indoor simulation, with the exception that the velocity level is higher in the case of the coupled indoor/outdoor simulation. In fact, the air jets at the building inlets are deflected upwards. This is an effect of the external air flow which is itself deflected by the platform and building assembly. Inside the small building, the general configuration of the air flow is similar to that obtained in the indoor calculation. On the ground floor of the low-rise part of the building, one can notice a low velocity recirculation zone in the corridor at the rear of the air jet between the two floors, and the poor ventilation of the side rooms in this zone, notably in Room 8, the targeted place for internal dispersion. This observation had already been made during the preparatory simulations.

Dispersion simulations were carried out to reproduce the three types of release trials in the wind tunnel (Scenarios 3, 2, 1). TEP was the chemical agent release in all experiments. In particular:

- In **Scenario 3** a “**low cloud**” of chemical with an almost uniform concentration of  $0.5 \text{ mg.m}^{-3}$  is generated at the entrance to the wind tunnel and heads to the small building. The numerical results show a general excellent agreement with the trial in terms of dispersion dynamics in most of the rooms where sensors were set up. The filling and purging of the rooms seem a bit faster in the simulations compared to the measurements. This could be due to a slight overestimation of the flow velocity upstream of the mock-up building. Furthermore, there is a time shift of around 300 s (delay) in the rise of the numerical concentration in Room 9 compared to the experimental concentration. There is also a different dynamics in Room 8 between the computation and the trial, but this has to be considered in the light of the very low concentrations in this room.
- In **Scenario 2**, an **external release** is arranged from a dispersal device installed at a distance of 3 m from the mock-up building. As shown by the simulations, this distance is such that the chemical concentration at the small building inlets is almost equal to the target concentration of  $0.5 \text{ mg.m}^{-3}$ . Very logically, the conclusions are thus identical to Scenario 3.
- In **Scenario 1**, an **internal release** is performed from a dispersal device installed in Room 8 of the mock-up building. A ratio of at least 10,000 is observed between the numerical concentration on the virtual sensor in Room 8, where the source is located, and the other sensors. This clearly signs an accumulation of the chemical agent only in Room 8. Moreover, the response of the sensor in Room 8 reaches its saturation level, which makes any comparison with the CFD irrelevant.

In the first two scenarios, a lag of the CFD results in comparison to the measurements in Room 9 has been noticed. In order to study the variability of the results depending on the position of the virtual sensor in Room 9, we have considered alternative locations for this sensor. The numerical results vary significantly when the position of the sensor is changed. It shows that there are sharp concentration gradients in the room. However, the maximum concentration is reached at about the same time, that is to say 300 s later in the computations than in the experiment. The explanations can be as follows:

- The shift can originate from the real sensor. Indeed, it is surprising that the concentration increases instantaneously in Room 9, while a certain time is necessary for the plume to reach gradually the different rooms of the mock-up building, especially Room 8 and Room 9.
- There may be leakages in the building mock-up or differences between the actual geometry of the small building and the geometry and mesh created for performing the CFD simulations, resulting in differences in the transfers within the

building.

- The simulations may not accurately replicate the flow in Room 9 (and in Room 8) which are located in a “dead flow” zone of the small building, which is poorly ventilated. This zone is characterized by a recirculation generated by the shear of the air jet coming from the floor of the low-rise part of the building. The fluid dynamics in this zone is extremely complex. First, the flow is intermittent and unstable, contrarily to the stationarity assumption made to simplify the computations. Then, the turbulence is difficult to model and would perhaps deserve a more detailed approach than the one exploited in these simulations.

### 3.2. Computation Approach (ADREA-HF)

A series of passive releases with a specific time duration  $\Delta T$  have been simulated using CFD RANS/LES ADREA-HF. Both external and internal sources were considered. The positions of the sources are the experimental ones.

For the pre-experimental modelling the release rate is unity whereas for post experimental modelling the real experimental releases have been considered.

In order to study the dispersion problem, a number of imaginary and real sensors are considered, one per each room and corridor to reveal the behaviour of the agents as it is spreading through the various compartments of the building. The position of the imaginary sensors has been put in the middle of the room at a height of 0.26 m corresponding roughly to the human height in real scale. Additional positions of sensors have been added that correspond to the experimental ones. In particular:

1. The first effort concerns **pre-trials computations**. Two main cases were considered:
  - Case I: The building is immersed into the tunnel, so that the setup is close to experimental conditions;
  - Case II: The building is surrounded by free atmosphere, so that the setup is closer to reality.

It is noticed that intercomparison between the two cases will enable us to get a feeling to what degree the experimental setup represents reality. To this purpose, this pre-experimental modelling study has considered:

- Internal and external source releases at the experimental positions;
  - In all cases the agent was considered passive;
  - In each source there has been considered two release conditions:
    - a) the release lasts 1 min;
    - b) the release is continuous.
  - These conditions:
    - a) reveal the behaviour of the agent dispersion under relatively short release;
    - b) enable to estimate dosages under any release time (Bartzis et al, 2021).
2. The second effort concerns **post-trials computations** where internal and external source releases are at the experimental positions.

For reason of simplicity and given the preliminary character of the experimental simulations it is assumed that the agent behaves as passive gas. It is noticed that the experimental agent was TEP with a Molecular Weight (MW= 182.15g/mol) significantly higher than ambient air (MW=28.97g/mol). This assumption could be considered valid for low TEP concentrations in air. The reason is that, in this case, the density of the air mixture could be comparable with the density of normal air. It is noticed that the modelling of the agent dense gas behaviour would require more detailed relevant measurements at the release exhaust cross section that goes beyond the scope of this

study.

The experimental modelling considers both external and internal sources. The emphasis was given to the shortest time releases (External Experiment #8 ( $\Delta T=200s$ ) and Internal Experiment #12 ( $\Delta T=120s$ )). Those cases are expected to be the most challenging due to relatively strong concentrations temporal gradients in combination with the spatial gradients due to geometry complexity. The other experiments have also been considered.

### **ADREA-HF Methodology**

ADREA-HF code is a 3D finite volume compressible flow model treating passive as well as buoyant/multiphase releases. It uses the Eulerian approach but, in the passive mode, can use the Lagrangian approach as well. It can handle concentration statistics. It has been widely used indoors and outdoors for air quality assessment as well as safety applications. (Venetsanos et al, 2010). ADREA-HF code is used in Cartesian grid. Geometry is reproduced with high accuracy (no stair-case effect) with the use of porosities, with the help of EDes pre-processor<sup>6</sup>.

In the present study the RANS mode with  $k-\varepsilon$  turbulence model has been used. In particular:

- **Domain and Grid:** The computation domain includes both indoor and outdoor micro-environments.
  - In Case I, the domain was extended up to the wind tunnel entrance and side and top walls. In the downstream direction it extends up to  $10H$  where  $H$  is the building height (i.e  $H=2,05\text{ m}$ ).
  - In Case II the domain was extended up  $4H$  upstream,  $15H$  downstream  $6H$  vertically and  $6H$  laterally. Concerning the grid size the minimum  $dx$ ,  $dy$ ,  $dz$  were confined by the building wall thickness i.e.  $0.005\text{m}$ .  $211 \times 134 \times 114$  for Case I and  $186 \times 143 \times 115$  is the number of cells.
- **Concentrations and Exposure:** The agent spread into the air environment was quantified at specific predetermined locations considering a real or fictitious sensor. The agent burden at the above locations was expressed with two exposure parameters: (a) the ensemble average concentration as a function of time and (b) the ensemble average dosage. The dosage  $D$  ( $\text{kg s/m}^3$ ) as a function of the concentration time series  $C(t)$  ( $\text{kg/m}^3$ ) at a specific sensor was defined as follows:

$$D = \int_0^{\infty} C(t) \cdot dt \quad (1)$$

The modelled ensemble average  $C(t)$  was provided by the RANS CFD simulations. The prediction of ensemble average  $D$  was obtained by running RANS CFD at steady state mode as suggested by (Bartzis et al, 2021). In this case the source release rate was equal to the source release rate of the finite release. It was noticed that such an approximation is as valid as RANS approximation itself. In this case:

$$\bar{D} = \bar{CS} \cdot \Delta TS \quad (2)$$

Where:

$\bar{CS}$  is the ensemble average (mean) steady state concentration

<sup>6</sup> [https://www.researchgate.net/profile/George-Efthimiou-3/publication/320181386\\_CFD\\_SIMULATIONS\\_OF\\_POLLUTANT\\_SPATIAL\\_DISTRIBUTION\\_IN\\_A\\_LARGE\\_OFFICE/links/59d32e584585150177f92788/CFD-SIMULATIONS-OF-POLLUTANT-SPATIAL-DISTRIBUTION-IN-A-LARGE-OFFICE.pdf?origin=publication\\_detail](https://www.researchgate.net/profile/George-Efthimiou-3/publication/320181386_CFD_SIMULATIONS_OF_POLLUTANT_SPATIAL_DISTRIBUTION_IN_A_LARGE_OFFICE/links/59d32e584585150177f92788/CFD-SIMULATIONS-OF-POLLUTANT-SPATIAL-DISTRIBUTION-IN-A-LARGE-OFFICE.pdf?origin=publication_detail)

$\Delta TS$  is the release time duration

The above-mentioned modelled parameters have been presented in a normalized form as follows:

$$\text{Normalized Concentrations: } \frac{C(t) \cdot U_{REF}}{Q} \quad (3)$$

$$\text{Normalized Dosages: } \frac{D \cdot U_{REF}}{QTS} \quad (4)$$

Where:

$U_{REF}$  is the specified inlet velocity (m/s)

$Q$  is the source release rate (kg/s)

$QTS$  is the total mass released (kg) i.e.

$$QTS = Q \cdot \Delta TS \quad (5)$$

The convenience of the above-mentioned normalizations is justified from the fact that the relevant numbers produced are good approximations for different source releases and different inlet velocities.

### 3.2.1 The Pre-Experimental Phase

Pre-experimental modelling exercises have been performed mainly focusing on short time (i.e., 1 min) releases internally and externally. The ADREA-HF code has been used to perform the simulations utilizing the CFD RANS approximation and the standard k- $\epsilon$  turbulence model.

#### 3.2.1.1 The external source

The source was located at the experimental position, i.e., at the central vertical plane, 50 cm above the ground and 5.25 m upward the mock-up.

#### ***Steady state and dosage***

Steady state simulations have been performed for Case I and Case II as explained above. The dosage at a sensor location was given by the relationship (Bartzis et al, 2021):

$$(D \cdot U_{REF}) / QTS = (CS \cdot U_{REF}) / Q \quad (6)$$

In Figure 91, the normalized dosages at the building inlets are compared for Case I and Case II.

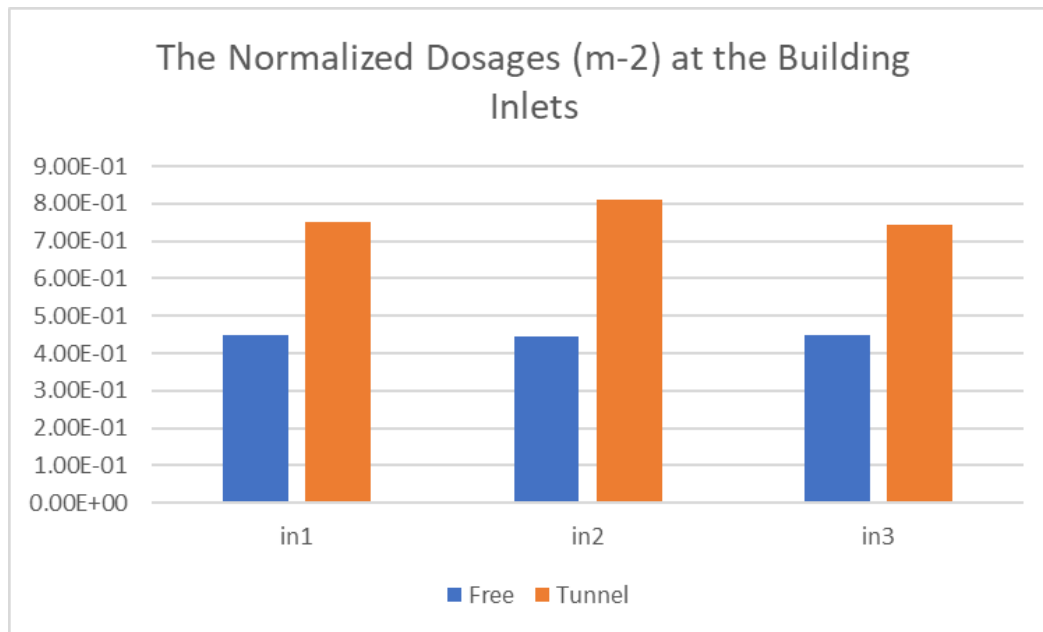


**Figure 91.** Building inlet dosages under in free and wind tunnel environment

The dosages under the free atmosphere were almost half compared with the wind tunnel case. This was expected since the free atmosphere provided more space for the agent to escape from the building. In other words, the presence of the tunnel gives a more conservative picture compared with reality for the upwind external source.

### ***The 1- min short release***

In this section only the wind tunnel case was considered since the experiments took place under this set up. It was noticed that the dosages here can be approximated by the relationship (Eq. 6) as this has been derived from the steady state simulations. Thus, the normalized dosage approximations as derived by the corresponding steady state simulations, are given in Figure 92.

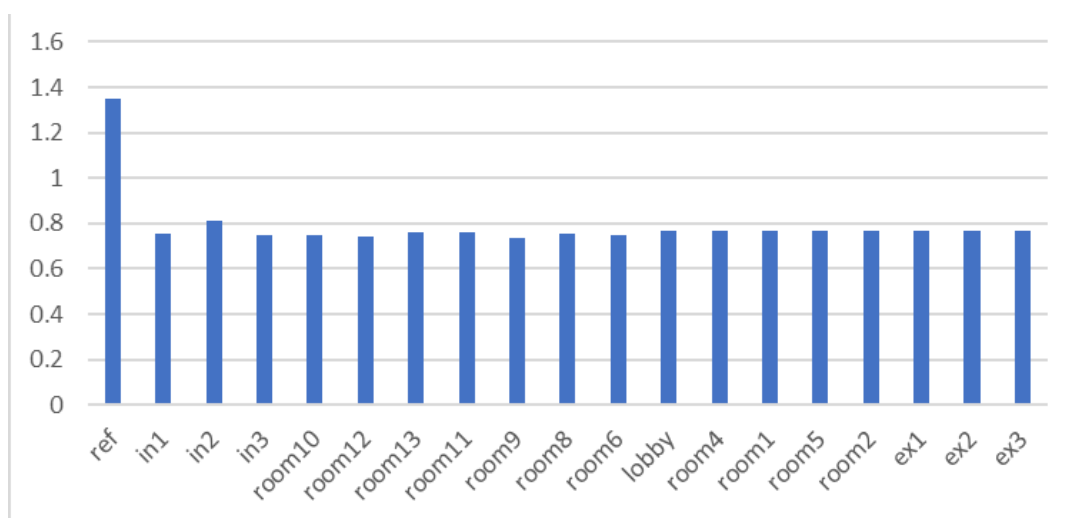


**Figure 92.** External source, 1-min release: estimation of the normalized dosages (m<sup>-2</sup>)

The normalized dosages at the outdoor upstream reference point, the inlet and outlet centers in the rooms are given. As expected, the steady state concentrations and

consequently dosages become uniform indoors as a result of the long-lasting incoming pollutant spreading everywhere. What makes the difference is the temporal behaviour as we will see below. It was noticed that the dosage indoors was substantially lower than the dosage upstream outdoors due to the fact that a significant mass of the agent escapes the building.

The agent concentration as a function of time, in each sensor considered, is given in Figures 93-94.

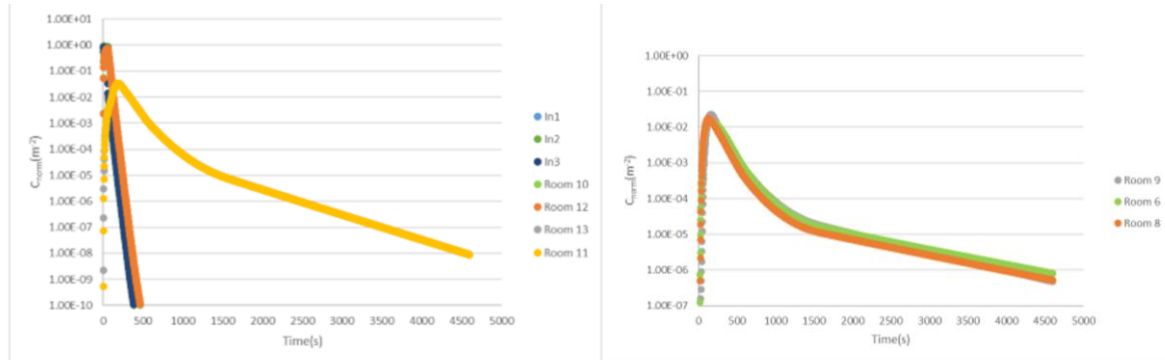


**Figure 93.** Low building normalized concentrations: top floor (left) and ground floor (right)

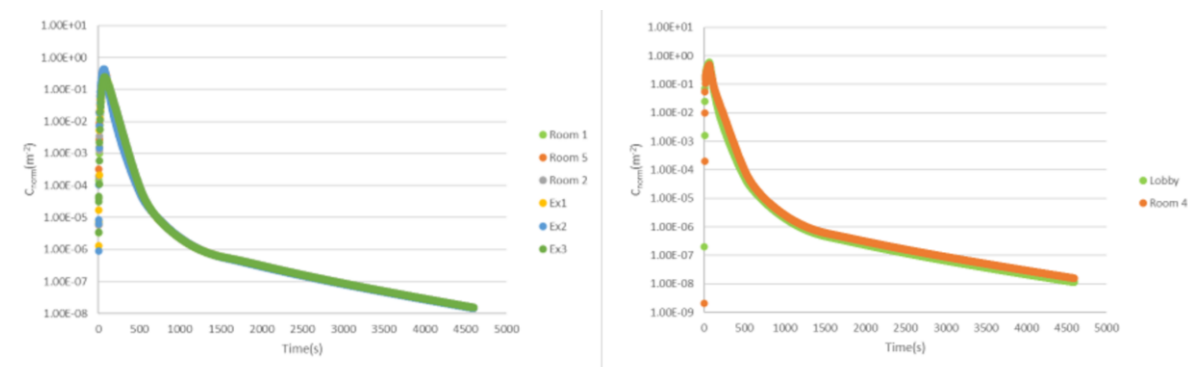


**Figure 94.** High building normalized concentrations: top floor (left) and ground floor (right)

It is clear that the rooms concentrations time profiles can be quite different. This can be explained from the fact that rooms did not have the same ventilation capabilities and inflow pattern.

The normalized peak concentrations in the various rooms and building inlets/outlets are shown in Figure 95.

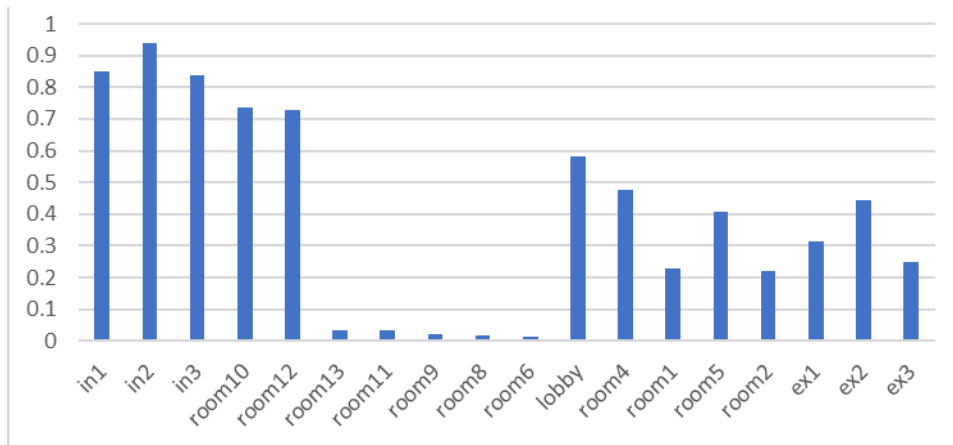


**Figure 95.** External source, 1-min release: The normalized peak concentrations (m<sup>-2</sup>)

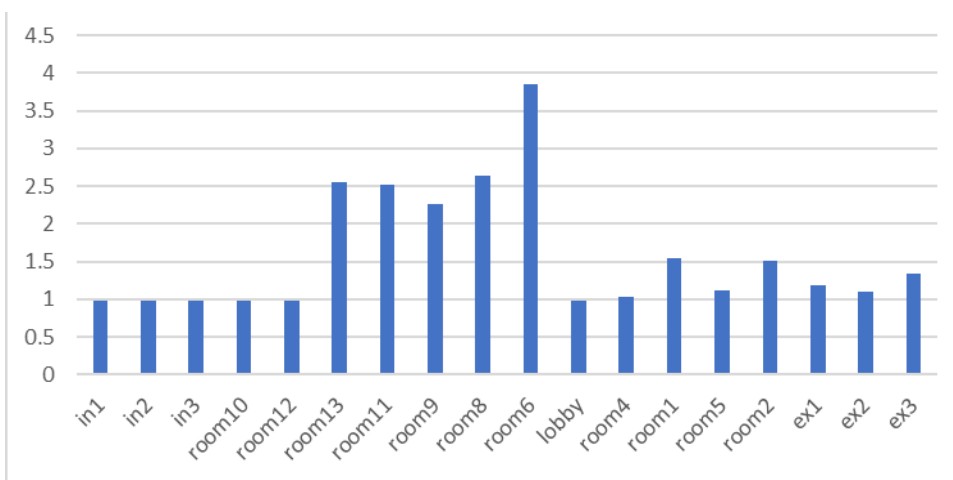


**Figure 96.** External source, 1-min release: The residence times

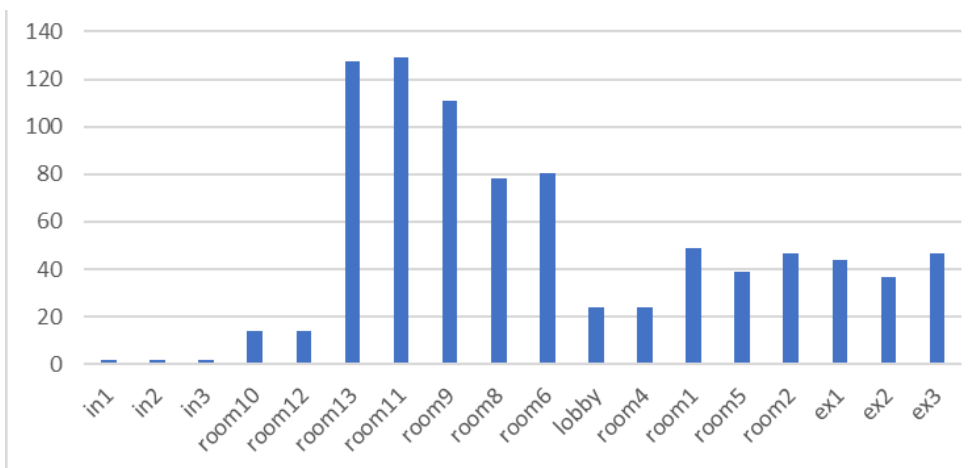


**Figure 97.** External source, 1-min release: The arrival times

Figure 96 and Figure 97 concern arrival and residential times respectively. They refer to the time that the concentration reached half of its peak value ( $t_{1/2}$  arrival) and the time that the concentration remained above half of its peak value ( $\Delta t_{1/2}$  residence).

The rooms 6,8,9,11 and 13 were characterized by a relatively poor ventilation where the agent arrived relatively late, it kept low concentrations but its presence lasted for a long time.

Higher peak concentrations appear in the low building top floor compared with peak concentrations in the high building which seems reasonable.

### 3.2.1.2 The internal source

The source was located at the experimental position, i.e., at the center of room 8 at a distance 7 cm above the floor.

#### ***Steady state and dosage***

Steady state simulations have been performed also here, for Case I and Case II as explained above. In Figure 98 the normalized dosages indoors are compared.

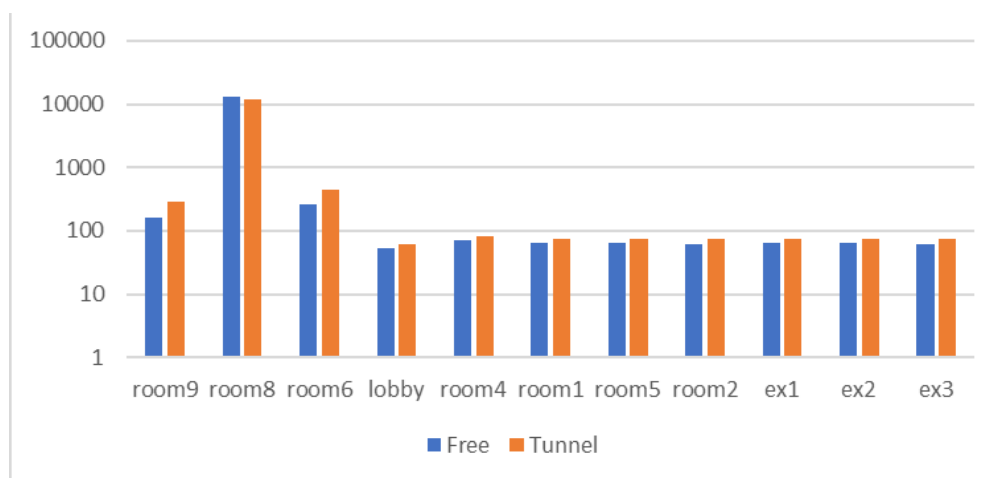


**Figure 98.** Indoor Normalized Dosages under in free and wind tunnel environment

For the indoor release, the dosages for the free and wind tunnel environment were rather close indicating that the wind tunnel results are more comparable with a real case.

#### ***The 1-min short release***

In this section only the wind tunnel case was considered. It was noticed that the dosages here can be approximated by the relationship (Eq. 6) as this has been derived from the steady state simulations. Thus, no extra estimations were needed for the dosage.

The agent concentration as a function of time, in each sensor considered, is given in Figures 99-100.

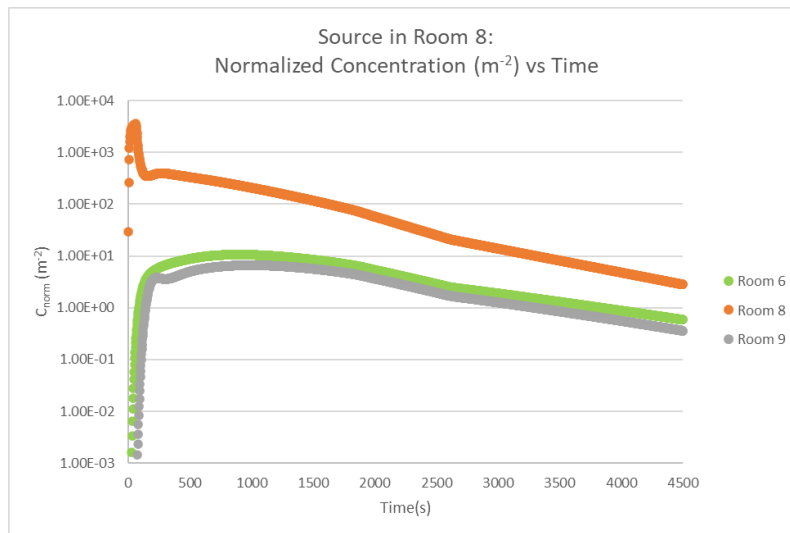


**Figure 99.** Low building ground floor normalized concentrations

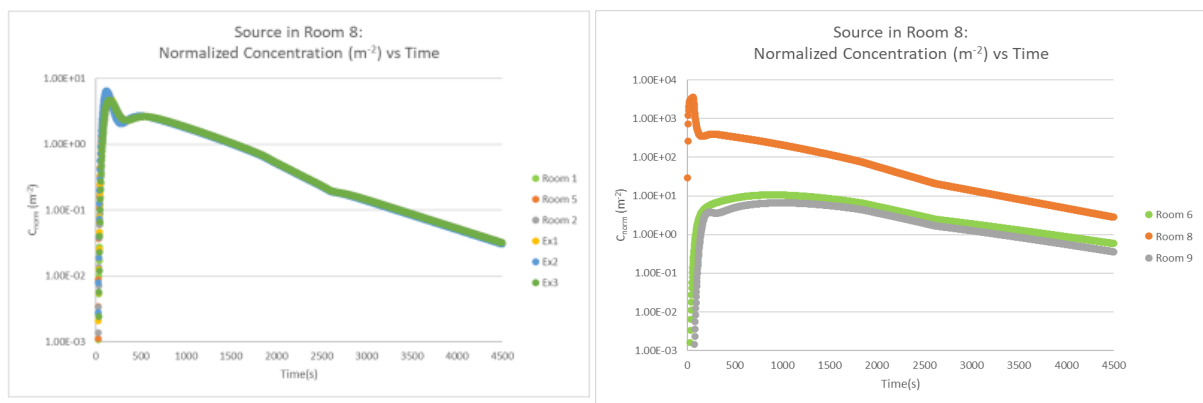


**Figure 100.** High building normalized concentrations: top floor (left) and ground floor (right)

As explained before the rooms concentrations time profiles are quite different due to the fact that rooms do not have the same ventilation capabilities and inflow pattern. The normalized peak concentrations in the various rooms are shown in Figure 101.

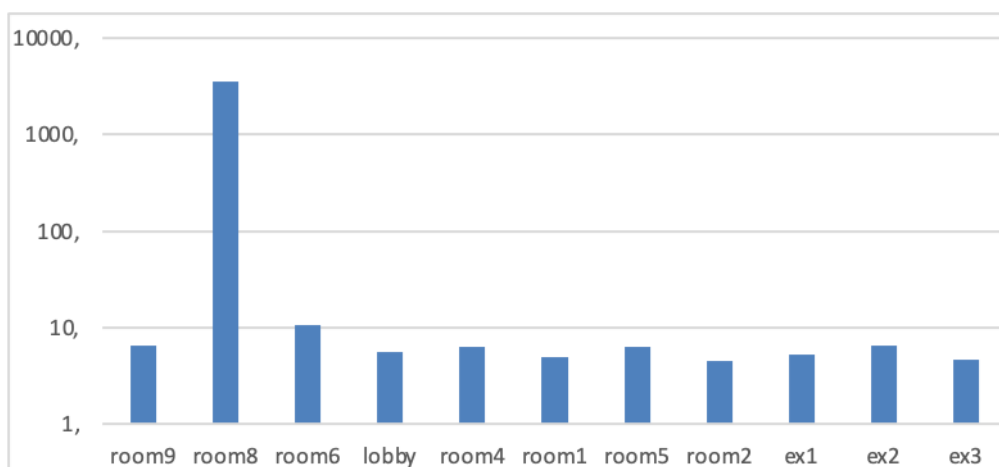


**Figure 101.** Internal source, 1-min release: The normalized peak concentrations (m<sup>-2</sup>)

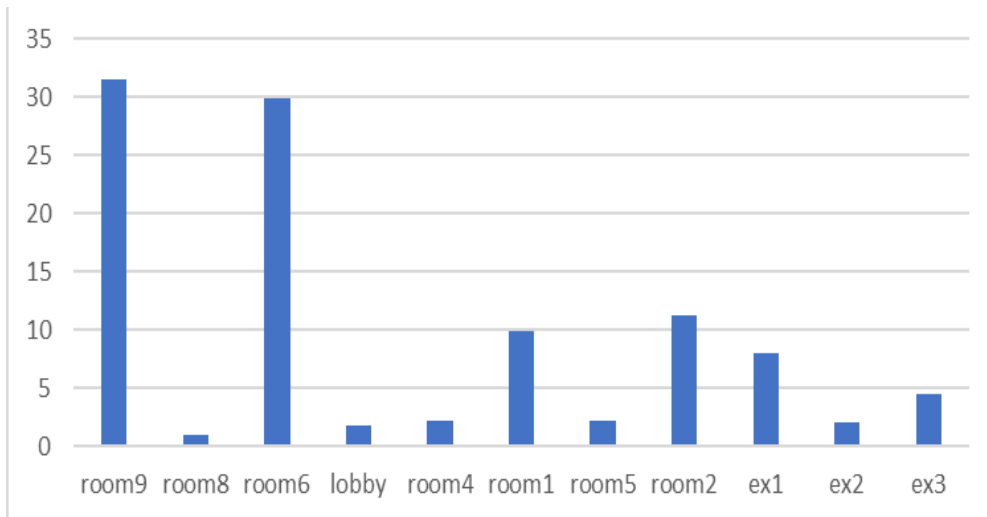


**Figure 102.** Internal source, 1-min release: The residence times (seconds)

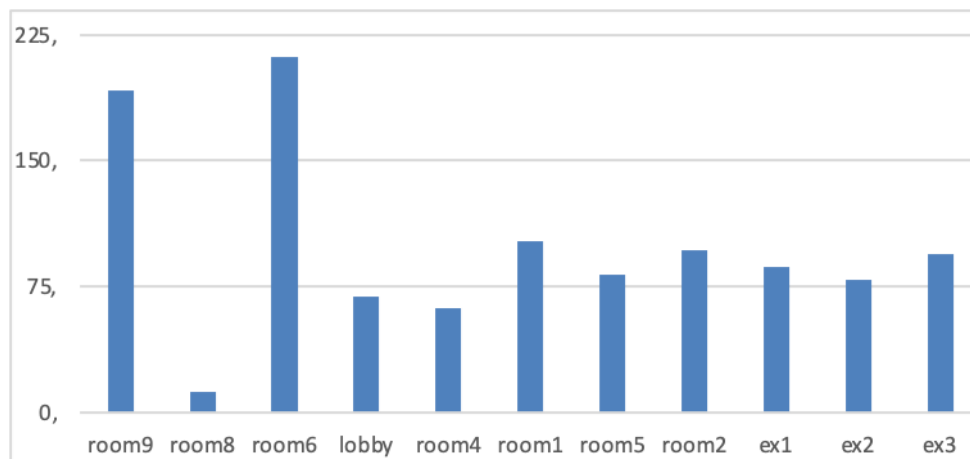


**Figure 103.** Internal source, 1-min release: The arrival times (seconds)

Figures 102 and 103 concern residential and arrival times respectively.

The rooms 6 and 9 are characterized by a relatively high residence and arrival times mainly due to poor ventilation. In those rooms although are near the source are experiencing modest peak concentrations.

Due to the specific flow patterns, the exposure on the low building top floor is almost non-existent.

### 3.2.2 The Post-Experimental Phase

#### ***The Inflow conditions***

After setting up the problem geometry and the sensors position, the next task was to define the inflow conditions. As shown in Figure 22, there are two wind flow sensors: a Gill flow meter upstream and a Young flow meter close to one side of the building. An initial remark is that the Gill flow meter is relatively far from the entrance i.e. 7.25 m.

Looking at the time series of the wind data, the following additional remarks can be made:

- a) In all experiments the Young wind velocities were lower than Gill wind velocities of the order of 4%. One would expect the opposite: the presence of the building

- would accelerate the flow at the sides of the building and decelerate the flow upstream, near the building;
- b) There was a small but not negligible drift lateral velocity (i.e. from -0.2m/s to -0.4 m/s). This is in consistency with the observed lower wind speed at the side where Young flow meter was installed.

With respect to model inflow conditions, the best we could do was to assume uniform inflow conditions with the inlet velocity 3.6 m/s representing the measured wind velocities upstream. It was noticed that the precise model inlet velocity was not critical due to the fact that the passive agent concentrations were well scaled with the inflow velocity.

Another point that needs to be noticed, is that the above-mentioned remarks on the experimental flow behaviour were not consistent with the uniform inflow conditions which means that an inherent modelling uncertainty was expected due to ignorance of the precise inflow conditions.

Concerning the inflow turbulent kinetic energy in both wind flow sensors, it measured:

$$k^{1/2}/VEL \approx 0.13 \quad (7)$$

Where k is the turbulent kinetic energy and VEL is the wind speed at the specific location. Adopting the same relationship for inflow conditions we specify  $k=0.22\text{m}^2/\text{s}^2$  at the inlet.

### 3.2.2.1 The external source

There have been performed four successful experiments with  $\Delta T$  time releases. The following refer to Scenario 2:

- Experiment #6 ( $\Delta T=600\text{s}$ ),
- Experiment #7 ( $\Delta T=610\text{s}$ ),
- Experiment #8 ( $\Delta T=200\text{s}$ ),
- Experiment #9 ( $\Delta T=1800\text{s}$ ).

For all four experiments the same total TEP mass was released: 930mg. Experiment #7 ( $\Delta T=600\text{s}$ ) is almost a repetition of Experiment #6 ( $\Delta T=610\text{s}$ ). Concentration measurements have been performed at specific locations by sampling and in the rooms 1,4,8,9,10 and 11 (Figure 13) by LCD Instrumentation.

It was noticed that the comparisons with LCD measurements was not straightforward. More specifically, the time series, with time resolution 2 s show:

- a) significant 'background' mean values of the order of  $0.08 \text{ mg}/\text{m}^3$ ;
- b) significant fluctuations with comparable intensity for the actual measurements and the 'background' measurements.

For better interpretation, the time series have been smoothed by applying a 20 s moving average. For all sensors the same calibration relationship suggested by TNO has been used although this needs to be double checked. As explained above, the emphasis here was given on Experiment 8 as the most challenging due to the shortest time release:  $\Delta T= 200\text{s}$ .

### **Scenario 2 - Experiment #8 ("external release")**

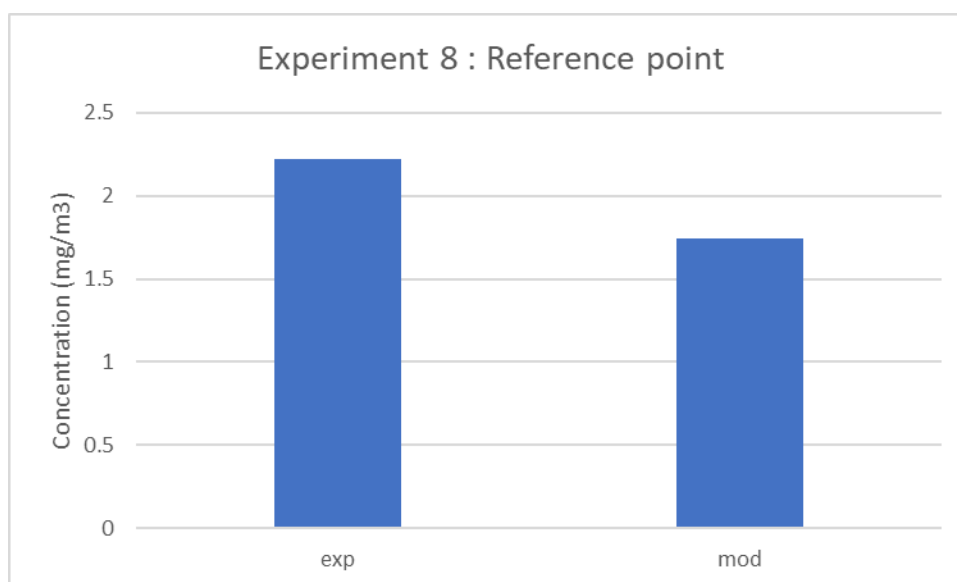
The experiment layout outside the building is shown in Figure 22.

Concentration measurements have been performed at the reference point (Figure 22) by sampling and in the rooms 1,4, 8,9,10 and 11 (Figure 13) by LCD Instrumentation.

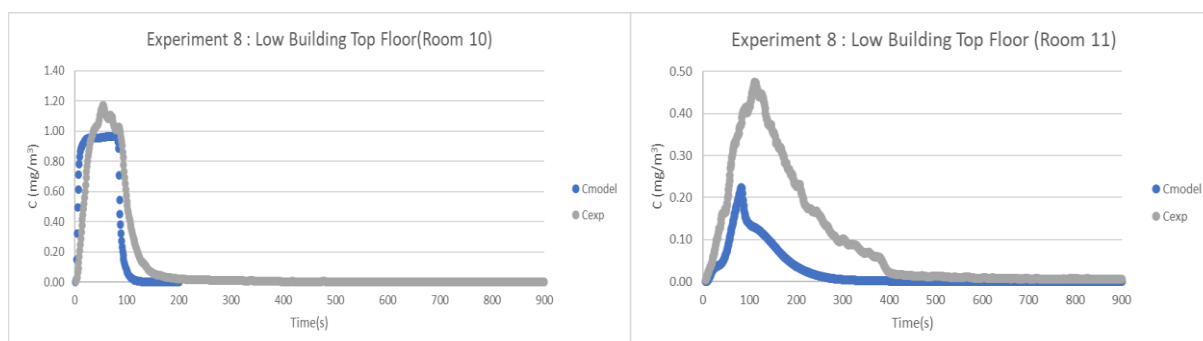
Figure 104 shows the concentration comparison at the reference point. There is a 10% model underestimation. Given the above-mentioned inflow uncertainties those results can be considered quite satisfactory. It was noticed that since the reference point was located upstream the building, some model underprediction on the building contamination was expected.

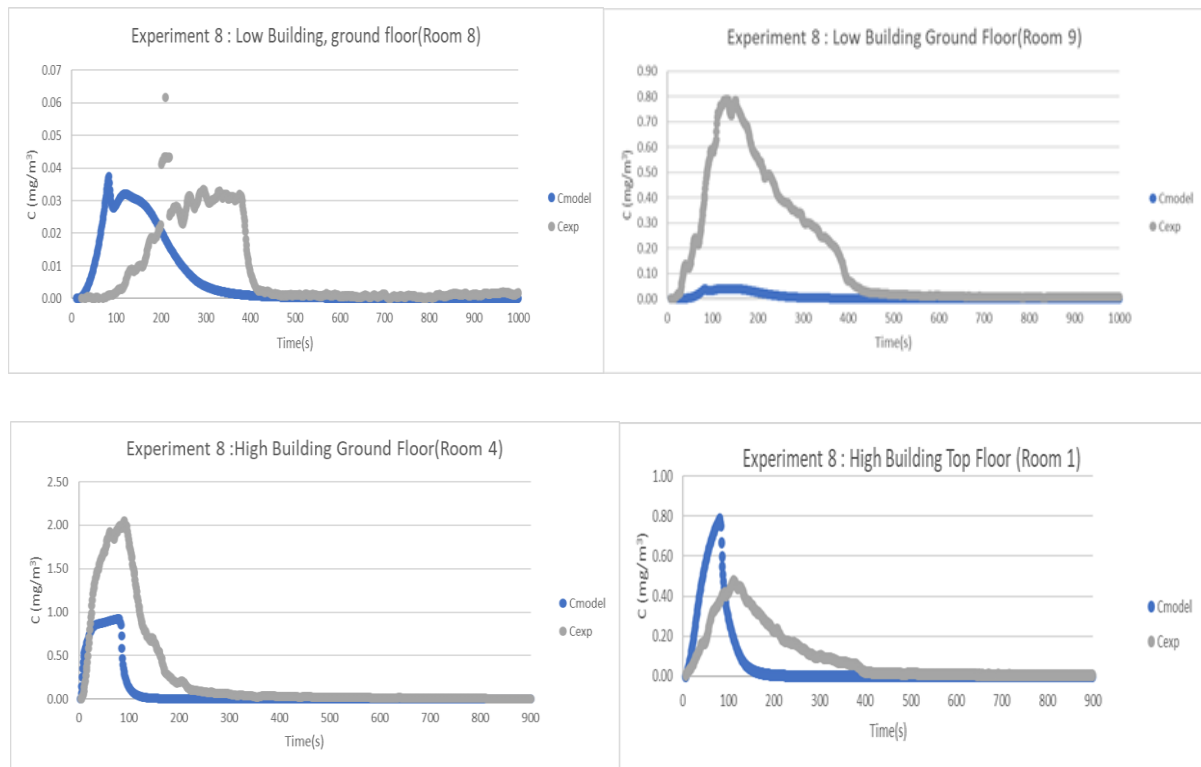
Figure 105 shows the concentrations comparison in the rooms. In general, there is a model underestimation with exception of rooms 1 and 8. 50% of peak concentration predictions are well within a factor of 2 which despite of the above-mentioned inherent uncertainties, well within the state-of-the-art modelling.

Figure 106 indicates the cloud temporal behaviour indoors. The arrival times are comparable except for the room 8 showing that the model predicted too fast cloud arrival. This is something that needs to be looked further. The model in general predicted lower residence times although both model and experiment follow the same trend except for room 11.



**Figure 104.** Experiment #8 - reference point: Concentrations comparisons





**Figure 105.** Experiment #8 - Room concentrations comparisons

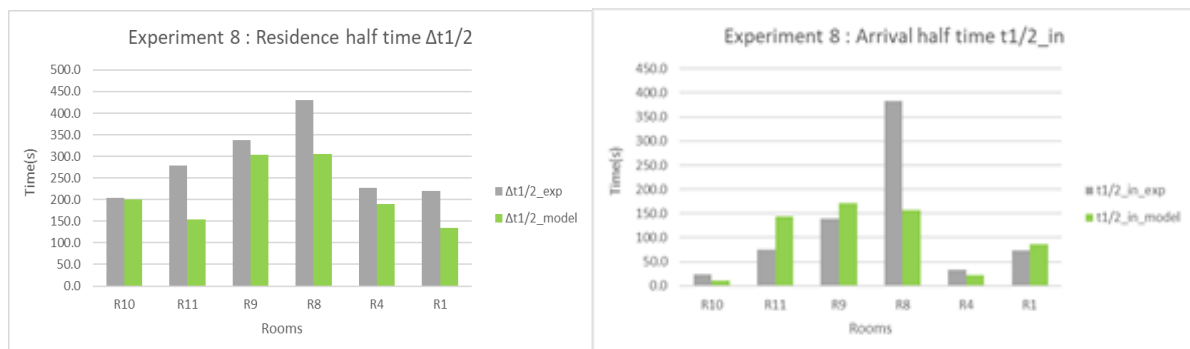


**Figure 106.** Experiment #8 - Room residence and arrival times

### **Scenario 2 - Experiments #6,7,9 ("external release")**

Modelling of the other external source experiments (i. e. 6,7, and 9) have been successfully performed. A summary of the obtained results is shown in Figure 107 in terms of room peak concentrations. Concerning the peak experimental concentrations estimation:

- The time series have been smoothed by applying a 20 s moving average;
- The artificial spikes have been ignored;
- A further smoothing is assumed based on visual inspection;
- In the rooms where LCD measurements and sampling exist, the highest value has been taken.

The results model vs experiment shows a fairly good agreement with a trend towards underprediction. The estimated uncertainty within a factor of two is  $FAC2 = 65\%$ . It is noticed that, based on the state of the art of such models, the  $FAC2$  needs to be greater

than 30% (COST ES1006, 2015). The obtained results show that the uncertainties in terms of model vs observation discrepancies are well within the above-mentioned margin.

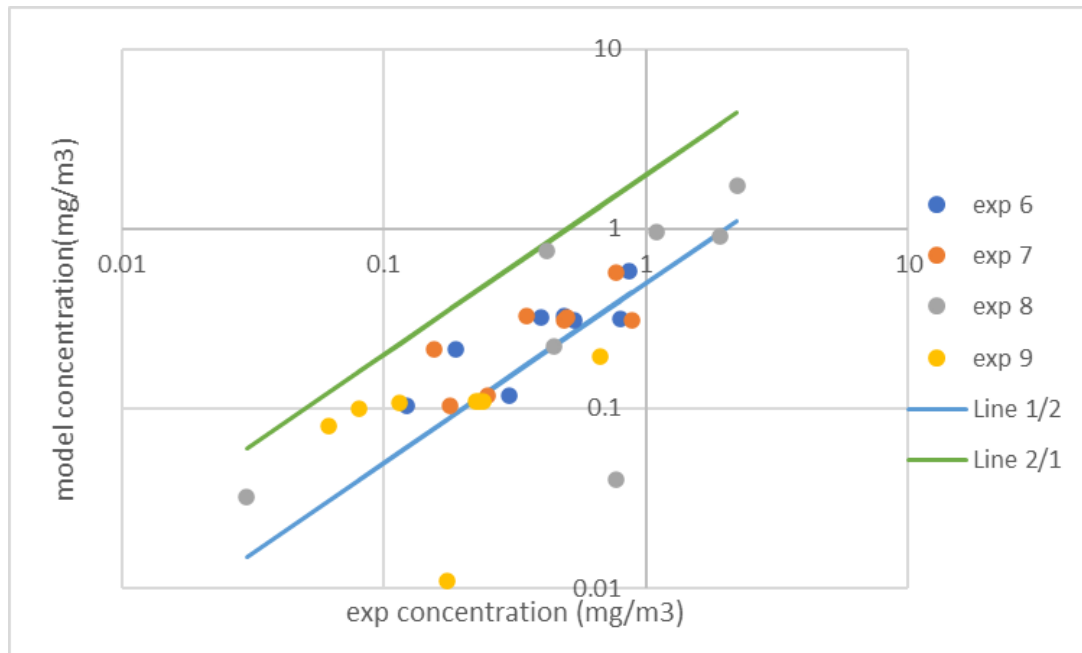


**Figure 107.** External source experiments: peak concentrations intercomparison

### 3.2.2.2 The internal source

There have been performed three successful experiments with  $\Delta T$  time releases. Here the total TEP mass released per experiment was different. The following refer to Scenario 1:

- Experiment #11 ( $\Delta T=120s$ ) and ( $QTS=0.5mg$ ),
- Experiment #12 ( $\Delta T=120s$ ) and ( $QTS=2.14mg$ ),
- Experiment #13 ( $\Delta T=240s$ ) and ( $QTS=4.28mg$ ).

There were no concentration measurements by active sampling and there was the need to rely only to LCD time signals. The LCD signal analysis has shown that the measurements, except for room 8, were relatively too low and therefore the measurement part could not be easily distinguished from the 'background' part. The only exception was room 8 but the signal was experiencing saturation when the concentrations became too high.

In Figure 108 the experimental concentration in the room 8 is shown. Its temporal behaviour is puzzling.

In experiment #11 where the mass release was the smallest, the signal did not show significant disturbance but in the same time the concentration level before starting the release was already elevated of the order of  $0.3 \text{ mg/m}^3$  well above the bias value:  $0.075 \text{ mg/m}^3$ . A probable explanation might be agent prior existence unless there was problem with the instrument calibration.

In experiments #12 and #13 there was no significant bias problem but the concentration started building up after a significant delay of the order of 150 s. It was noticed that the release time was of this order of magnitude. The peaks came much later (i.e., after 300s).

It is important to understand the release conditions in sufficient detail. This behaviour might indicate 'heavy gas' behaviour. The rather stagnant flow conditions within room 8 might complicate things further. Such phenomena cannot be modelled reliably without additional measurements at the release cross section and its neighbourhood. The release structure might also play a role and it needs to be described in more detail.

Despite the above difficulties, the experiments modelling with the passive gas approximation has been performed as it has been planned for this study. The emphasis was given to experiment #12 where the mass release rate was the highest, expecting more readable experimental concentrations.

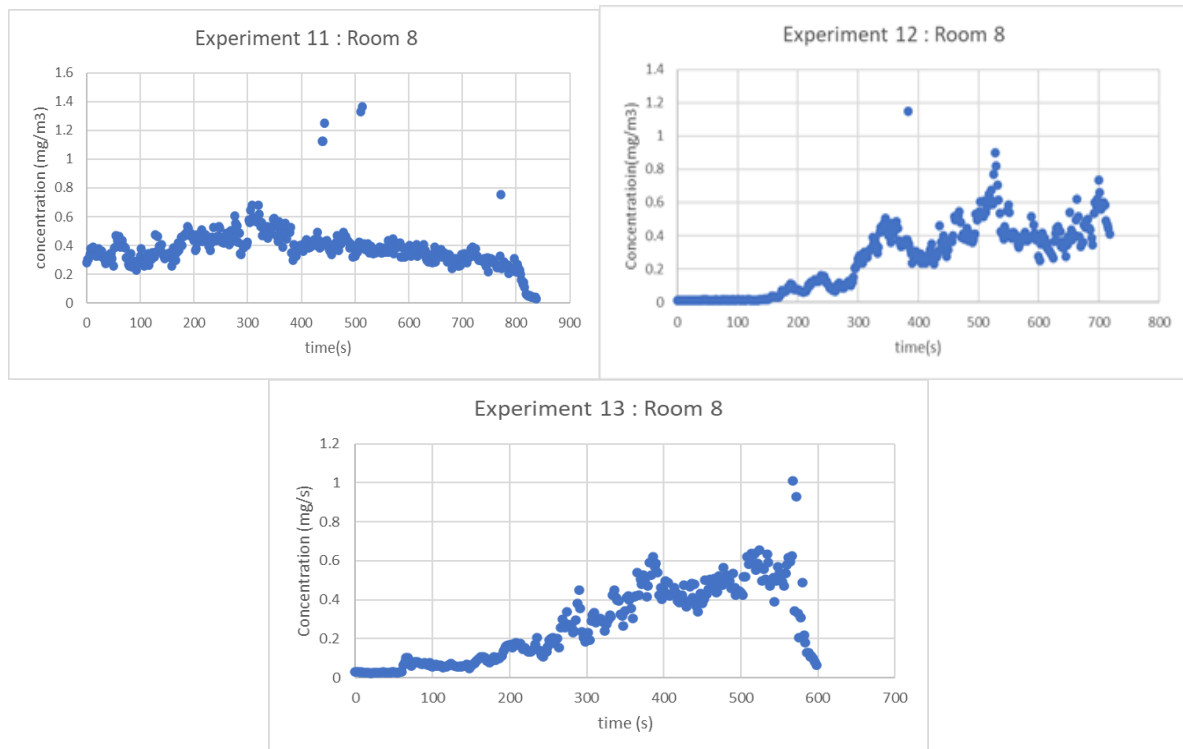


**Figure 108.** Internal source: Room 8 concentration measurements

### ***Scenario 1 - Experiment #12 ("internal release")***

The experiment layout outside the building is shown in Figure 28.

Concentration measurements have been performed in the rooms 1,4,8,9,10 and 11 (Figure 13) by LCD Instrumentation.

Figure 109 shows the concentration comparisons. The relatively slow concentration built up was visible in all rooms in consistence with the room 8 behaviour discussed above. In the rooms 10 and 11 both predicted and modelled concentrations were negligible as expected.

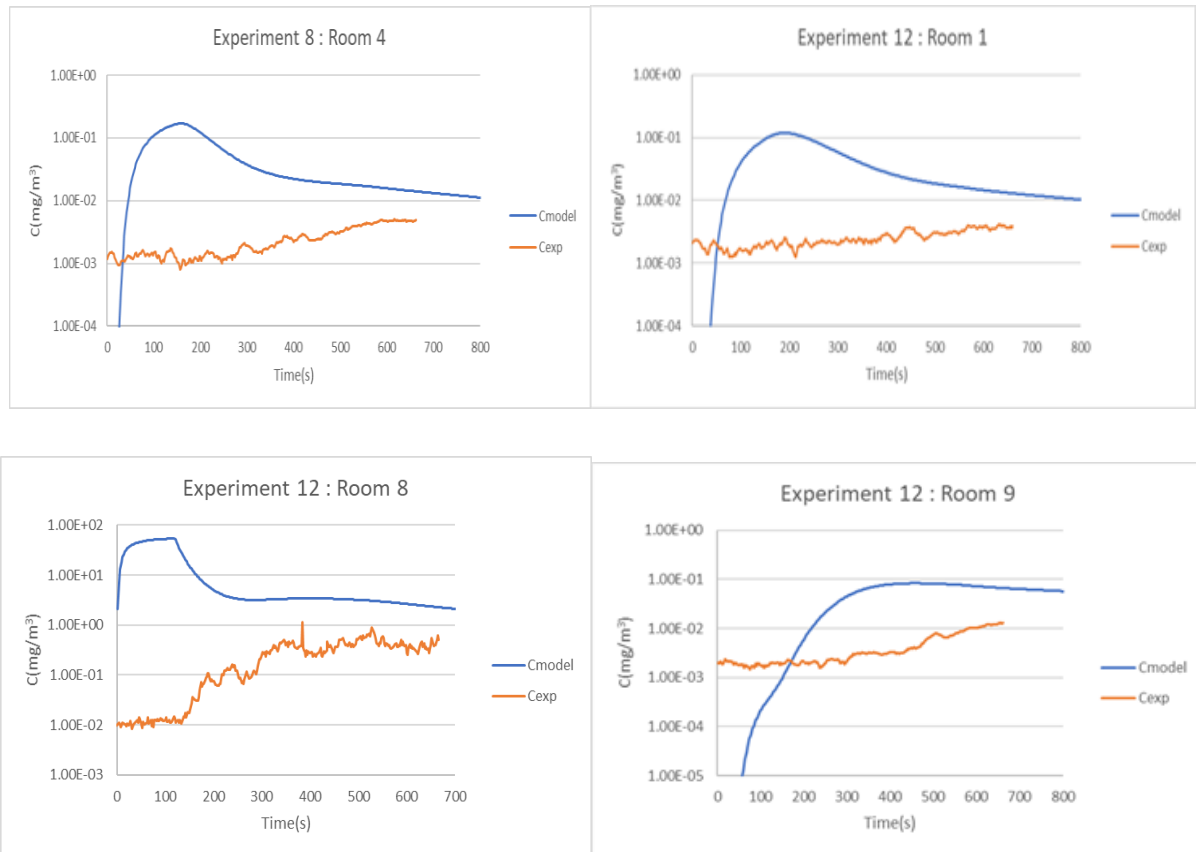


**Figure 109.** Experiments #8 and #12 - Room concentrations comparisons

### 3.2.3 Conclusions of ADREA-HF simulations

#### *Pre-experimental modelling*

Pre-experimental modelling exercises have been performed mainly focusing on short time (i.e., 1 min) releases internally and externally. The ADREA-HF code has been used to perform the simulations utilizing the CFD RANS approximation and the standard  $k-\epsilon$  turbulence model.

The following concluding remarks of general interest, can be made at this stage.

The wind tunnel set up is more likely to give a rather conservative picture compared with reality for the upwind external source. For the internal source the results were expected to be more realistic.

For the external source, the steady state concentrations (and consequently finite time dosages) became uniform indoors as a result of the long-lasting incoming agent spreading everywhere indoors.

For the internal source, dosages could become non-uniform with higher values near the source as expected.

In all cases, the rooms concentrations time profiles can be quite different. The room specific location with respect to the source and the associated ambient air pattern played an important role to this differentiation.

The poorly ventilated rooms were associated with relatively long residence and arrival times, and tended to lower the peak concentrations.

### ***Comparison of modelling and experimental trials (Post-experimental modelling)***

The first attempt of experiments vs model comparison was not straightforward due to inherent uncertainties mainly to the inflow air conditions, the release conditions at the exhaust duct cross section, the LCD signals calibration and possible pre-existing agent material in some experiments.

For the external source, the concentration comparisons can be characterized satisfactory. The FAC2 parameter for peak concentrations is relatively high: 65%. The model as it has been applied, shows that for most sensors the concentration and the cloud residence time was underpredicted especially in the rooms of low building ground floor.

For the internal source the problem looks more problematic. The concentration temporal behaviour especially in the source room 8, a room with the lowest ventilation capacity, is puzzling. In addition, the specific experiments duration seemed to be not long enough. The experiment vs model discrepancy may be due to various reasons such as the lack of knowledge of the precise exit duct conditions, the validity of the passive gas approximation, pre-existing agent material, LCD signal measurement interpretation, etc. The limited number of measurements is also an additional element of model uncertainty.

### **3.2.4 Conclusions of CFD simulations**

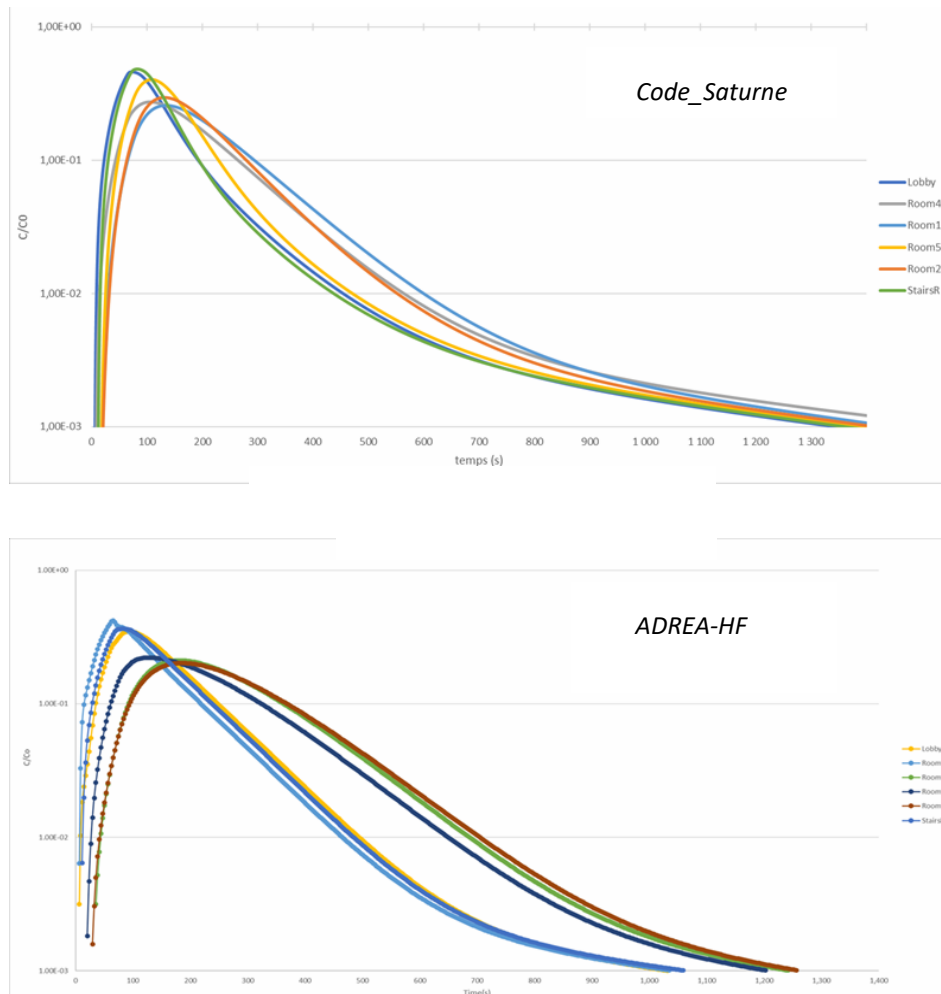
#### ***Comparison of modelling approaches (Code\_Saturne & ADREA-HF code)***

It is important to notice that the general results obtained by the modelling performed with Code\_Saturne and ADREA-HF are remarkably comparable although some disparities remain, perhaps due to differences in the geometric representation of the mock-up, in particular the height of the doors.

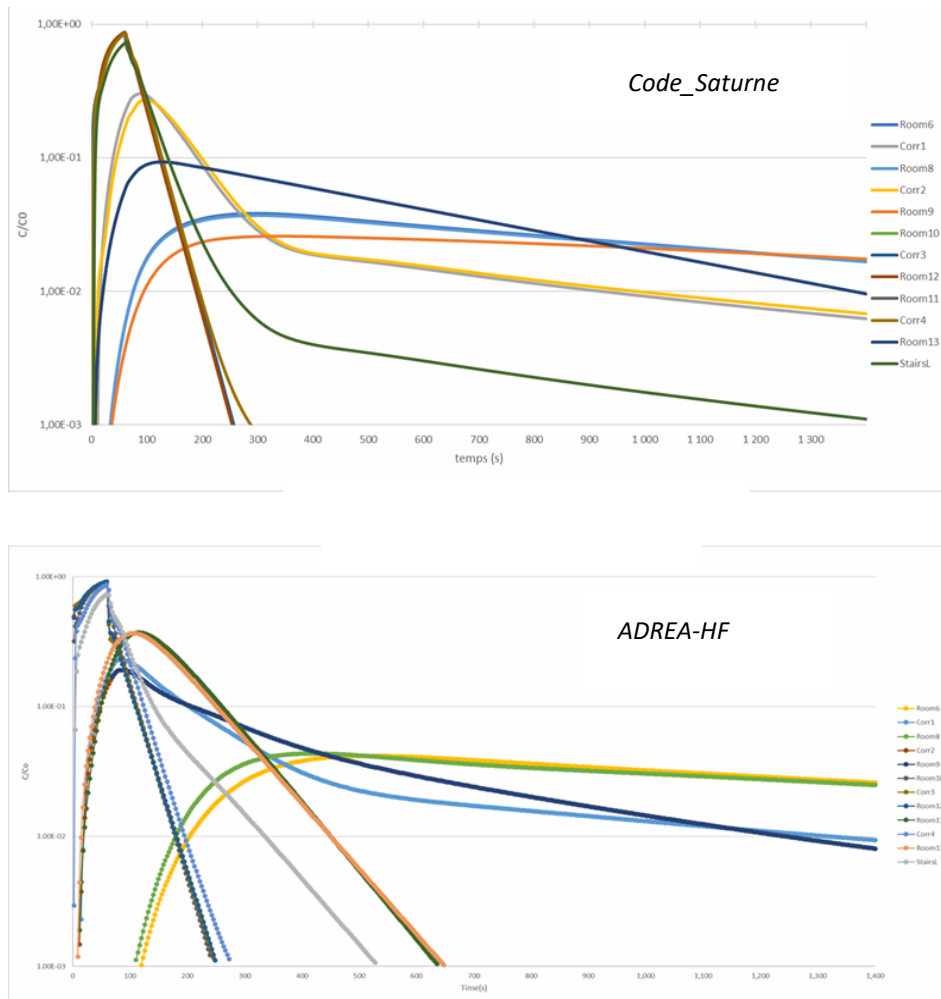
The numerical results of ADREA-HF and Code\_Saturne CFD models lead to the same comments on the dispersion patterns in the test-cases with either an external or an internal release.

Figure 110 and Figure 111 show the average concentrations over time in the different parts of the mock-up as they are identified in Figure 13.

In more details, concerning the high-rise building (Figure 110), the behaviours are similar for the rooms marked Lobby, Room 1, Room 2, Room 5 and Stairs R while a slightly different behaviour is observed for the room marked Room 4. Regarding the low-rise building (Figure 111), similar behaviours are noticed for almost all of the rooms except the rooms marked Room 9, Room 11, Room 13 and Stairs L. It is also visible that the purge of the rooms is longer with Code\_Saturne compared to ADREA-HF.



**Figure 110.** Average concentrations in the different rooms of the upper part of the mock-up with release located outside the mock-up upstream of the flow. Top: Code\_Saturne results. Bottom: ADREA-HF results



**Figure 111.** Average concentrations in the different rooms of the lower part of the mock-up with release located outside the mock-up upstream of the flow. Top: Code\_Saturne results. Bottom: ADREA-HF results

The maximum concentrations reached in each of the rooms of the mock-up during the simulation are shown in Figure 112. As before, the results obtained by Code\_Saturne are broadly in agreement with those obtained by ADREA-HF. As already mentioned, the differences could be explained by different transfers due to more or less large openings between the rooms.

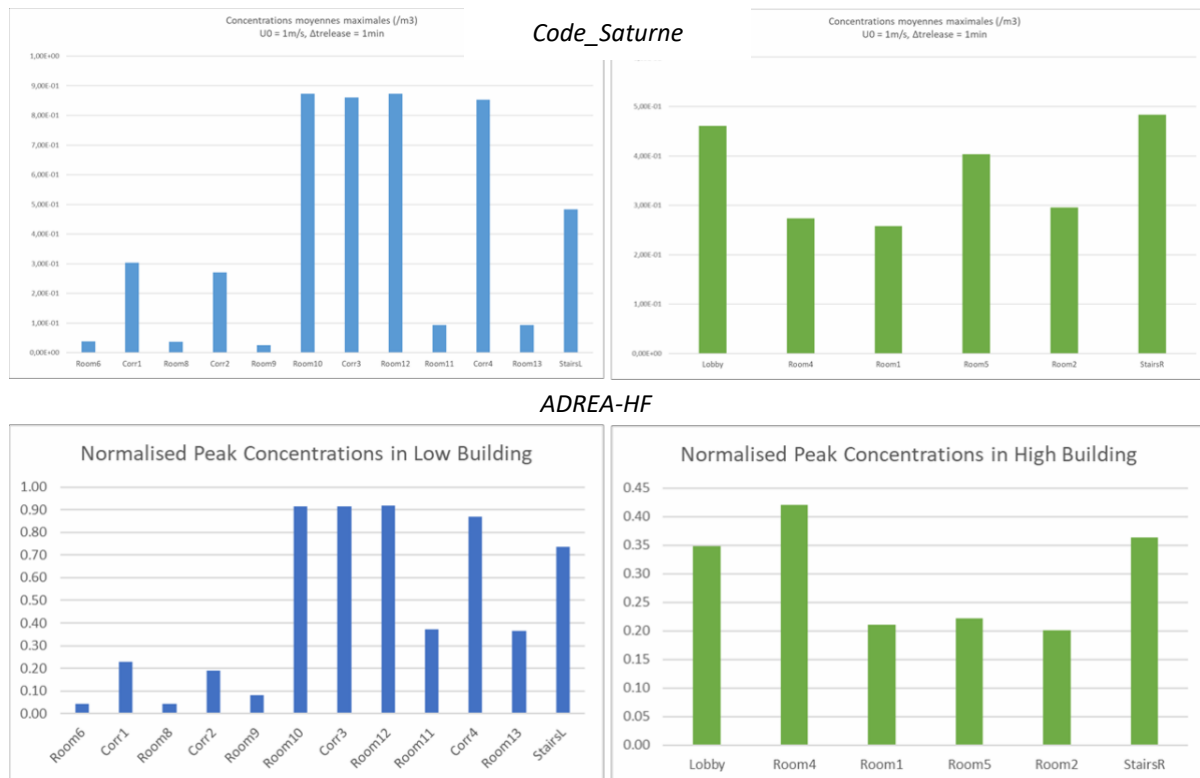


**Figure 112.** Maximum concentrations in the different rooms of the mock-up with release located outside the mock-up upstream of the flow. Top: Code\_Saturne results. Bottom: ADREA-HF results

## 4. Conclusions

The subsidiary aim of the research described in this technical report was to develop knowledge on the behaviour of chemical releases, given some likely attack scenarios, and to propose ways to optimally detect those inside buildings.

From the early stages of the Indoor Airborne TG, it has been highlighted that a key component of the efficient detection of the relevant threats is the optimization of the sensors location, and this can only be obtained by making use of a combined approach consisting of experiments and dispersion modelling, which is considered a strong endeavour towards this aim. This is clearly highlighted by the multi-disciplinarity and the expertise of the respective group members, that resulted in the comprehensive study that has been carried out and described above.

In this case, a high-end facility (ambient breeze tunnel (AMB)) has been used under controlled release of simulant chemicals in a mock-up of a simple building, of a scale 1:5. For all the release scenarios of the TEP that has been selected as simulant (for nerve gases), the aim was (a) the successful detection (with an ion mobility spectrometry (IMS)) and (b) to simulate the dispersion process and (c) to evaluate the dispersion modelling against the measured concentration gradients in time and space.

The experiments involved three mimicked attack scenarios: i) focal release from within the mimicked building and external release of agent approaching the mock-up from the outside from a ii) short and iii) a larger distance. TEP was selected as simulant (for nerve gases). The detector used was an ion mobility spectrometry (IMS) instrument. Subsequent 2 different dispersion modelling approaches were undertaken to understand and describe those differences, namely (a) the ADREA-HF code, used to perform the simulations utilizing the CFD RANS approximation and the standard k- $\epsilon$  turbulence model and (b) the Code\_Saturne, used to perform the simulations both before and after the experiments.

Methodologically speaking, it was shown that medium-scale experiments with representative simulant chemicals, can simulate potential threat events in a very sufficient way, while computational models are able to simulate the dispersion of a chemical agent very sufficiently. Release of TEP was successful in all three exposure scenarios, it resulted in reproducible detection signals from 6 IMS instrument placed in 6 rooms of the building mock-up. The speed and magnitude in which TEP levels were recorded in the respective rooms showed a clear and reproducible picture in the sense that some of the rooms appeared to be better reachable for the externally released TEP than others.

From the modelling results, it has been illustrated that the rooms concentrations time profiles can be quite different. The room specific location with respect to the source and the associated ambient air pattern plays an important role to this differentiation. The poorly ventilated rooms are associated with relatively long residence and arrival times, and tend to lower the peak concentrations. Pre-trials computations illustrate the differences in the dispersion pattern when an internal versus an external released is considered. Post-trials computations are fully consistent with the pre-trials computations and the physical phenomena enlightened in the different trials. At the same time, it is worth to mention that the two independent modelling efforts have resulted in similar outcomes, while both modelling efforts corroborate excellent with the measurements results.

Overall, this successful combined experimental and modelling exercise, illustrates that refined computational modelling can identify the significant differences in concentration-time gradients after various release conditions. This has three major implications:

- Optimal design of sensor locations in a critical infrastructure, where sensors should be located where the highest elevation of contamination levels is expected to occur, ensuring the early identification;
- Integrate modelling results in a chemical reconnaissance system that relies on machine learning, modelling algorithms, as well as the contaminant dispersion model to combine signals from different sensors, thus ensure early identification and reduce false alarm rates;
- Optimisation of evacuation plan in the case of an event.

This extraordinary experimental effort with highly complex structures with rooms of significant ventilation capability variability, apart from the highly important results produced, has set up a solid ground for the design and execution of new targeted experiments advancing the knowledge in understanding the behaviour of dispersed malicious airborne agents inside buildings and into the interaction of detection equipment.

## References

- Busker, R. (2016). Technology Review for Detection of Airborne Chemical Agents in Critical Infrastructures. Ispra: JRC [106323]
- Bartzis, J.G.; Efthimiou, G.C.; Andronopoulos, S. "Modelling Exposure from Airborne Hazardous Short-Duration Releases in Urban Environments." *Atmosphere*, Vol 12 No 2, 2021, pp130. <https://doi.org/10.3390/atmos12020130>
- COST ES1006 - Model Evaluation Protocol, COST Action ES1006, April 2015
- COST Action ES1006 - Evaluation, improvement and guidance for the use of local-scale emergency prediction and response tools for airborne hazards in built environments, April 2012
- Karakitsios, S. e. (2016). Definition of relevant scenarios of indoor airborne threats (chemical and biological) in critical infrastructure. Ispra: JRC [102091]
- Karakitsios, S. (2019). Report on gaps for research and standardization. Ispra: JRC [117096]
- Karakitsios, S. et al. (2020). Challenges on detection, identification and monitoring of indoor airborne. *Safety Sciences* 129(5):104789
- Venetsanos A. G., Papanikolaou E. and Bartzis J. G., 2010: "The ADREA-HF CFD code for consequence assessment of hydrogen applications. *Int. J. Hydrogen Energy*, 35, 3908].

## List of abbreviations

2/3D	2/3 Dimensional
ADREA HF	code
AMB	Ambient Breeze Tunnel
Ansa	software
C	Concentration
CB	Chemical and Biological
CEA	Atomic and alternative Energies Commission
CEM	Controlled Evaporator Mixer
CEREA	Atmospheric Environment Center
CFD	Computational Fluid Dynamics
CFL	Courant–Friedrichs–Lewy
Code_Saturne	code
D	Dosage
EC	European Commission
EDF	the French electricity board
ERNICIP	European Reference Network for Critical Infrastructure Protection
FAC2	fraction of predictions within a factor of 2 observations
FOI	Swedish Defence Research Agency
Gill	anemometer
H	building height
IMS	Ion Mobility Spectrometry
JRC	Joint Research Centre
LCD	Lightweight Chemical Detector
LES	Large Eddy Simulation
MQ	square metre
MW	Molecular Weight
N	North
NCSRD	National Center for Scientific Research Demokritos
Paraview	software
PID	Photo Ionization Detector
QTS	Total Mass Released
R&D	Research and Development
RANS	Reynolds-Averaged Navier–Stokes
SIMPLEC	Semi-Implicit Method for Pressure Linked Equations-Consistent algorithm
TEP	Tri-EthylPhosphate
TG	Thematic Group
TIC	Tentatively Identified Compounds
TNO	Netherlands Organisation for Applied Scientific Research
UK	United Kingdom
UREF	specified inlet velocity
UTP	Unshielded Twisted Pair
Young	anemometer
$\Delta$ TS	release time duration

## List of figures

<b>Figure 1.</b> Internal details and subdivision of the mock-up .....	5
<b>Figure 2.</b> External details and openings of the mock-up .....	6
<b>Figure 3.</b> External view and levels of the mock-up.....	6
<b>Figure 4.</b> Details of the mock-up shipment in NCSR Demokritos, Greece .....	7
<b>Figure 5.</b> The mock-up at TNO, The Netherlands .....	7
<b>Figure 6.</b> AMB front side view .....	9
<b>Figure 7.</b> AMB back side view .....	9
<b>Figure 8.</b> View from inside the ABM showing the 6 tubes that distribute vapor .....	10
<b>Figure 9.</b> LCD 3.3 detector (left) and Young Anemometer (right) .....	10
<b>Figure 10.</b> Tri-ethylphosphate (TEP) .....	11
<b>Figure 11.</b> Schematic position of mock-up in AMB .....	13
<b>Figure 12.</b> Actual mock-up positioned in AMB .....	13
<b>Figure 13.</b> Arrangement of the rooms in the mock-up.....	14
<b>Figure 14.</b> Six LCD 3.3 detectors installed in the mock-up rooms indicated with numbers .....	14
<b>Figure 15.</b> Ground Floor level detector/sampling positions.....	15
<b>Figure 16.</b> Middle Floor level detector/sampling positions.....	16
<b>Figure 17.</b> Top Floor level detector /sampling positions.....	16
<b>Figure 18.</b> Scenario 3 - schematic overview of position of windspeed sensors and reference sample location around mock-up .....	18
<b>Figure 19.</b> Experiment #1 - LCD 3.3 signals plotted against time .....	19
<b>Figure 20.</b> Experiment #2 - LCD 3.3 signals plotted against time .....	20
<b>Figure 21.</b> Experiment #3 - LCD 3.3 signals plotted against time .....	22
<b>Figure 22.</b> Scenario 2 - schematic overview of position of windspeed sensors, reference sample and source location around mock-up.....	22
<b>Figure 23.</b> Scenario 2 - Release apparatus used as point source (right) in front of mock-up (left).....	23
<b>Figure 24.</b> Experiment #6 - LCD 3.3 signals plotted against time .....	24
<b>Figure 25.</b> Experiment #7 - LCD 3.3 signals plotted against time .....	25
<b>Figure 26.</b> Experiment #8 - LCD 3.3 signals plotted against time .....	27
<b>Figure 27.</b> Experiment #9 - LCD 3.3 signals plotted against time .....	28
<b>Figure 28.</b> Scenario 1 - Schematic overview of position of windspeed sensors and source location around mock-up.....	29
<b>Figure 29.</b> Scenario 1 - Evaporator positioned behind the mock-up .....	29
<b>Figure 30.</b> Experiment #11 - LCD signals plotted against time.....	30
<b>Figure 31.</b> Experiment #12 - LCD signals plotted against time.....	31
<b>Figure 32.</b> Experiment #13 - LCD signals plotted against time.....	32
<b>Figure 33.</b> Principle of the experiment .....	35
<b>Figure 34.</b> Positioning of the mock-up in the wind tunnel .....	35
<b>Figure 35.</b> Positioning of the external release in the wind tunnel .....	36
<b>Figure 36.</b> Positioning of the internal release .....	36
<b>Figure 37.</b> Geometry of the mock-up consisting in a low-rise building and a high-rise building... ..	37
<b>Figure 38.</b> View of the four tested meshes .....	38
<b>Figure 39.</b> View of the vertical section plane across the mock-up .....	39
<b>Figure 40.</b> 2D velocity fields in a vertical section plane. Results for the four meshes.....	39
<b>Figure 41.</b> Influence of the four meshes on the convergence of the velocity field .....	40
<b>Figure 42.</b> Velocity field in two section planes across the mock-up .....	41
<b>Figure 43.</b> Velocity field and velocity vectors in two section planes of the lower building .....	41
<b>Figure 44.</b> Velocity field and velocity vectors in a section plane of the higher building.....	42
<b>Figure 45.</b> Streamlines in the mock-up .....	42
<b>Figure 46.</b> First test-case – Boundary condition for the concentration at the mock-up inlets $C_0 = 1$ for one minute ( $t = 0$ to $60$ s).....	43
<b>Figure 47.</b> First test-case – Chemical cloud delimited by the concentration $C = 0.1$ at $t = 8$ s....	44
<b>Figure 48.</b> First test-case – Chemical volume concentration in a vertical section plane at $t = 53.2$ s .....	45
<b>Figure 49.</b> First test-case – Chemical volume concentration in a vertical section plane at $t = 74.2$ s .....	45
<b>Figure 50.</b> First test-case – Quantity of the chemical in the mock-up (in blue) and average concentration of chemical in the mock-up (in orange, logarithmic scale) over time .....	46
<b>Figure 51.</b> Second test-case – Location of the source inside the mock-up in the corridor of the ground floor.....	47
<b>Figure 52.</b> Second test-case – Chemical cloud delimited by the concentration $C = 0.01$ at $t = 43.0$ s .....	48

<b>Figure 53.</b> Second test-case – Chemical volume concentration in a vertical section plane at $t = 51,0$ s .....	48
<b>Figure 54.</b> Second test-case – Quantity of the chemical remaining in the mock-up (in blue) and average concentration of the chemical in the mock-up (in orange, logarithmic scale) over time ..	49
<b>Figure 55.</b> Second test-case – Average concentrations in the different rooms of the upper part of the mock-up .....	50
<b>Figure 56.</b> Second test-case – Average concentrations in the different rooms of the lower part of the mock-up .....	50
<b>Figure 57.</b> Second test-case – Maximum concentrations in the different rooms of the mock-up .	51
<b>Figure 58.</b> Second test-case – Maximum concentrations in the different rooms of the mock-up (on the left: upper part; on the right: lower part) .....	51
<b>Figure 59.</b> Installation of the small building mock-up in the wind tunnel .....	52
<b>Figure 60.</b> Geometry of the small building in the coupled indoor/outdoor configuration .....	53
<b>Figure 61.</b> Full geometry of the small building immersed in the wind tunnel in the coupled indoor/outdoor configuration.....	54
<b>Figure 62.</b> Global view of the mesh of the wind tunnel .....	54
<b>Figure 63.</b> Zoom-in view of the mesh of the wind tunnel.....	55
<b>Figure 64.</b> Velocity measurements upstream of the small building model in the middle of the wind tunnel .....	55
<b>Figure 65.</b> Velocity field in the horizontal section crossing the air inlets (top) and in the vertical median plane (bottom) .....	56
<b>Figure 66.</b> Vertical profile of the air velocity upstream the small building .....	57
<b>Figure 67.</b> Comparison of the measured and computed velocities at a point upstream the small building.....	57
<b>Figure 68.</b> Velocity field in a horizontal section crossing the small building outlets.....	58
<b>Figure 69.</b> Comparison of the measured and computed velocities at a point between the small building and the walls of the wind tunnel .....	58
<b>Figure 70.</b> Velocity field restricted to the vertical median cross-section through the small building .....	59
<b>Figure 71.</b> Velocity vectors restricted to the vertical median cross-section through the small building.....	59
<b>Figure 72.</b> Velocity field in the horizontal cross-section located 5 cm above the floor of the second level of the low-rise building .....	60
<b>Figure 73.</b> Velocity vectors in the horizontal cross-section located 5 cm above the floor of the second level of the low-rise building .....	60
<b>Figure 74.</b> Velocity field and velocity vectors in the horizontal cross-section located 10 cm above the floor of the first level of the low-rise building .....	61
<b>Figure 75.</b> Velocity field in the vertical cross-section through the stairwell of the high rise .....	61
<b>Figure 76.</b> Experiment #1 – Initial condition ( $t = t_0$ ) at the entrance to the wind tunnel.....	62
<b>Figure 77.</b> Experiment #1 – Concentration field in the median vertical cross-section of the wind tunnel at different instants between $t = t_0 + 6$ s and $t = t_0 + 2,000$ s .....	64
<b>Figure 78.</b> Location of the sensors inside the small building.....	64
<b>Figure 79.</b> LCD sensors.....	65
<b>Figure 80.</b> Experiment #1 – Comparison of the concentrations obtained by the CFD and by the measurements at the six .....	66
<b>Figure 81.</b> Experiment #1 – Comparison of the normalized concentrations obtained by the CFD and by the measurements at the six sensors .....	67
<b>Figure 82.</b> Experiment #6 – Location of the source for the external release.....	68
<b>Figure 83.</b> Experiment #6 – Concentration field in the median vertical cross-section of the wind tunnel at different instants between $t = t_0 + 15$ s and $t = t_0 + 1,000$ s .....	70
<b>Figure 84.</b> Experiment #1 – Comparison of the concentrations obtained by the CFD and by the measurements at the six sensors .....	70
<b>Figure 85.</b> Experiment #6 – Comparison of the normalized concentrations obtained by the CFD and by the measurements at the six sensors .....	71
<b>Figure 86.</b> Experiment #6 – Alternative positions of the virtual sensor in Room 9 .....	72
<b>Figure 87.</b> Experiment #6 – Comparison between the simulated concentrations on close virtual sensors in Room 9 and the measured concentrations in Room 9.....	73
<b>Figure 88.</b> Experiment #12 – Location of the source for the internal release (Room 8) .....	74
<b>Figure 89.</b> Experiment #12 – Visualization of the chemical plume defined by the volume $C \leq C_{max}$ inside the small building at different instants between $t = t_0 + 20$ s and $t = t_0 + 1,045$ s ..	76
<b>Figure 90.</b> Experiment #12 – Concentrations on the virtual sensors in the CFD simulation .....	77
<b>Figure 91.</b> Building inlet dosages under in free and wind tunnel environment .....	82
<b>Figure 92.</b> External source, 1-min release: estimation of the normalized dosages ( $m^{-2}$ ) .....	82
<b>Figure 93.</b> Low building normalized concentrations: top floor (left) and ground floor (right) .....	83

<b>Figure 94.</b> High building normalized concentrations: top floor (left) and ground floor (right).....	83
<b>Figure 95.</b> External source, 1-min release: The normalized peak concentrations (m-2) .....	84
<b>Figure 96.</b> External source, 1-min release: The residence times.....	84
<b>Figure 97.</b> External source, 1-min release: The arrival times .....	84
<b>Figure 98.</b> Indoor Normalized Dosages under in free and wind tunnel environment .....	85
<b>Figure 99.</b> Low building ground floor normalized concentrations.....	86
<b>Figure 100.</b> High building normalized concentrations: top floor (left) and ground floor (right)....	86
<b>Figure 101.</b> Internal source, 1-min release: The normalized peak concentrations (m-2) .....	86
<b>Figure 102.</b> Internal source, 1-min release: The residence times (sec) .....	87
<b>Figure 103.</b> Internal source, 1-min release: The arrival times (sec).....	87
<b>Figure 104.</b> Experiment #8 - reference point: Concentrations comparisons .....	89
<b>Figure 105.</b> Experiment #8 - Room concentrations comparisons.....	90
<b>Figure 106.</b> Experiment #8 - Room residence and arrival times.....	90
<b>Figure 107.</b> External source experiments: peak concentrations intercomparison .....	91
<b>Figure 108.</b> Internal source: Room 8 concentration measurements .....	92
<b>Figure 109.</b> Experiments #8 and #12 - Room concentrations comparisons .....	93
<b>Figure 110.</b> Average concentrations in the different rooms of the upper part of the mock-up with release located outside the mock-up upstream of the flow. Top: Code_Saturne results. Bottom: ADREA-HF results.....	95
<b>Figure 111.</b> Average concentrations in the different rooms of the lower part of the mock-up with release located outside the mock-up upstream of the flow. Top: Code_Saturne results. Bottom: ADREA-HF results.....	96
<b>Figure 112.</b> Maximum concentrations in the different rooms of the mock-up with release located outside the mock-up upstream of the flow. Top: Code_Saturne results. Bottom: ADREA-HF results. ....	97

## List of tables

<b>Table 1.</b> General overview of experiments performed.....	16
<b>Table 2.</b> Detailed overview of experiments performed (agents and releases).....	17
<b>Table 3.</b> Experiment #2 - Sampling start time .....	20
<b>Table 4.</b> Experiment #3 - Sampling start time .....	21
<b>Table 5.</b> Experiment #6 - Sampling start time .....	24
<b>Table 6.</b> Experiment #7 - Sampling start time .....	25
<b>Table 7.</b> Experiment #8 - Sampling start time .....	26
<b>Table 8.</b> Experiment #9 - Sampling start time .....	28
<b>Table 9.</b> Characteristics of the four tested meshes.....	38
<b>Table 10.</b> Characteristics of the small building in the coupled indoor/outdoor configuration .....	53
<b>Table 11.</b> Experiment #12 – Maximum concentration on the six virtual sensors .....	74

## **GETTING IN TOUCH WITH THE EU**

### **In person**

All over the European Union there are hundreds of Europe Direct information centres. You can find the address of the centre nearest you at: [https://europa.eu/european-union/contact\\_en](https://europa.eu/european-union/contact_en)

### **On the phone or by email**

Europe Direct is a service that answers your questions about the European Union. You can contact this service:

- by freephone: 00 800 6 7 8 9 10 11 (certain operators may charge for these calls),
- at the following standard number: +32 22999696, or
- by electronic mail via: [https://europa.eu/european-union/contact\\_en](https://europa.eu/european-union/contact_en)

## **FINDING INFORMATION ABOUT THE EU**

### **Online**

Information about the European Union in all the official languages of the EU is available on the Europa website at: [https://europa.eu/european-union/index\\_en](https://europa.eu/european-union/index_en)

### **EU publications**

You can download or order free and priced EU publications from EU Bookshop at: <https://publications.europa.eu/en/publications>. Multiple copies of free publications may be obtained by contacting Europe Direct or your local information centre (see [https://europa.eu/european-union/contact\\_en](https://europa.eu/european-union/contact_en)).

## The European Commission's science and knowledge service

### Joint Research Centre

#### JRC Mission

As the science and knowledge service of the European Commission, the Joint Research Centre's mission is to support EU policies with independent evidence throughout the whole policy cycle.



**EU Science Hub**  
[ec.europa.eu/jrc](https://ec.europa.eu/jrc)



@EU\_ScienceHub



EU Science Hub - Joint Research Centre



EU Science, Research and Innovation



EU Science Hub



Publications Office  
of the European Union

doi:10.2760/48622  
ISBN 978-92-76-55599-5